Technische Universität München

Lehrstuhl für Anorganische und Metallorganische Chemie

Metalloporphyrin-based Metal-Organic Frameworks as Multi-Functional Heterogeneous Catalysts

Konstantin Epp

Vollständiger Abdruck der von der Fakultät für Chemie der Technischen Universität München zur Erlangung des akademischen Grades eines

Doktors der Naturwissenschaften (Dr. rer. nat.)

genehmigten Dissertation.

Vorsitzender:		Prof. Dr. Job Boekhoven
Prüfende der Dissertation:	1.	Prof. Dr. Roland A. Fischer
	2.	Prof. Dr. Dirk De Vos

Die Dissertation wurde am 24.04.2019 bei der Technischen Universität München eingereicht und durch die Fakultät für Chemie am 16.05.2019 angenommen.

Eidesstattliche Erklärung

Ich erkläre an Eides statt, dass ich die bei der promotionsführenden Einrichtung bzw. Fakultät der Chemie der TUM zur Promotionsprüfung vorgelegte Arbeit mit dem Titel:

“Metalloporphyrin-based Metal-Organic Frameworks as Multi-Functional Heterogeneous Catalysts”

in der Fakultät für Chemie, Lehrstuhl für Anorganische und Metallorganische Chemie unter der Anleitung und Betreuung durch Prof. Dr. Roland A. Fischer ohne sonstige Hilfe erstellt und bei der Abfassung nur die gemäß § 6 Abs. 6 und 7 Satz 2 angegebenen Hilfsmittel benutzt habe.

(×) Ich habe keine Organisation eingeschaltet, die gegen Entgelt Betreuerinnen und Betreuer für die Anfertigung von Dissertationen sucht, oder die mir obliegenden Pflichten hinsichtlich der Prüfungsleistungen für mich ganz oder teilweise erledigt.

(×) Ich habe die Dissertation in dieser oder ähnlicher Form in keinem anderen Prüfungsverfahren als Prüfungsleistung vorgelegt.

( ) Die vollständige Dissertation wurde in ..... veröffentlicht. Die promotionsführende Einrichtung..... hat der Vorveröffentlichung zugestimmt.

(×) Ich habe den angestrebten Doktorgrad noch nicht erworben und bin nicht in einem früheren Promotionsverfahren für den angestrebten Doktorgrad endgültig gescheitert.

Die öffentlich zugängliche Promotionsordnung der TUM ist mir bekannt, insbesondere habe ich die Bedeutung von § 28 (Nichtigkeit der Promotion) und § 29 (Entzug des Doktorgrades) zur Kenntnis genommen. Ich bin mir der Konsequenzen einer falschen Eidesstattlichen Erklärung bewusst.

Mit der Aufnahme meiner personenbezogenen Daten in die Alumni-Datei bei der TUM bin ich einverstanden.

München, den 20.04.2019

Metalloporphyrin-based Metal-Organic Frameworks (MOFs) as Multi-Functional Heterogeneous Catalysts

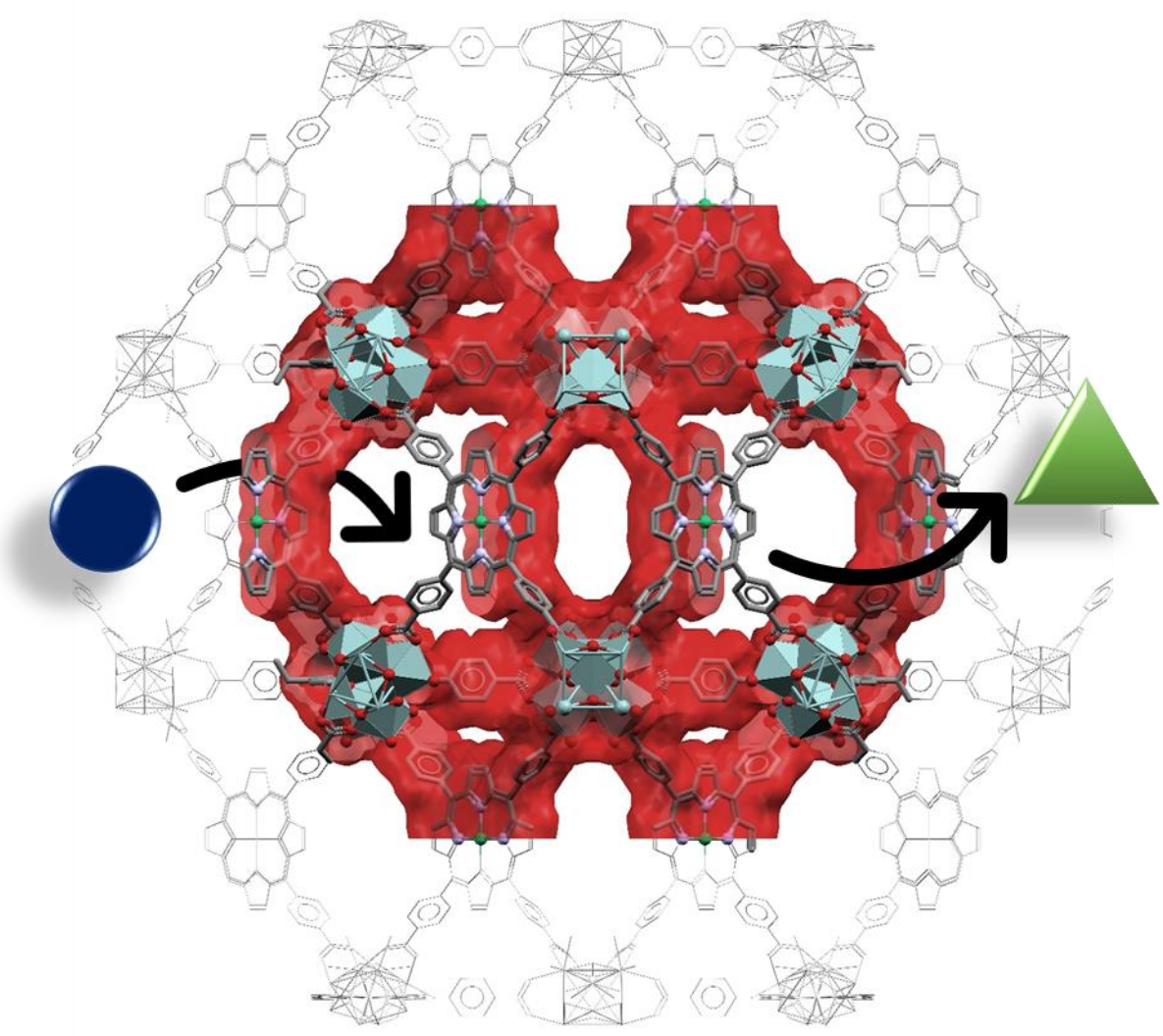

Dissertation

Konstantin Epp

Abstract:

In this work, zirconium containing metallo-porphyrin (MP)-based metal-organic frameworks (MOFs), PCN-224, PCN-222 (PCN = porous coordination polymer) and MOF-525 are tested as heterogeneous catalysts in selected Lewis-acid catalyzed reactions as well as biomimetic oxidation reactions. Moreover, these MP-MOFs are applied as potential multi-functional tandem catalysts. The intrinsic Lewis-acidity of the inorganic building units, namely, the Zr-oxo-clusters catalyzes the cyclic addition of carbon dioxide in epoxides and cyanosilylation of benzaldehyde in good yields and high selectivity. The catalytic activity in these reactions can be further improved by metalation of the organic porphyrin linkers due to the introduction of new Lewis-acid sites which contribute to the overall activity. The catalytic activity is derived from the underlying topology of the corresponding MP-MOF phase which depend on the Zr-oxo-cluster connectivity and amount of defects. Rhodium-porphyrin MOFs catalyze the cyclopropanation (CP) reaction of olefins with diazo-compounds as carbene transfer reagents in high yields and selectivities for a broad substrate scope of substituted styrenes and linear, cyclic olefins. Styrenes carrying amino and hydroxy groups show high diastereoselectivity due to confinement-derived substrate-catalyst interactions, which can be optimized by careful selection of suitable MP-MOF phases with appropriate Rh−Rh distances. PCN-222(Mn) show high biomimetic catalytic activity and selectivity in oxidation reactions using unfunctionalized hydrocarbon substrates and (alkyl)peroxides as oxygen transfer agents. Dioxygen is successfully employed as ‘green’ oxidant under static and dynamic experimental conditions. Multi-functional catalytic oxidation and Lewis-acid properties of abovementioned MP-MOFs are attractive for the design of tandem catalysts which are able to catalyze multiple reactions, thus, these materials are tested as potential tandem catalysts in the tandem oxidation of benzaldehyde / cyanosilylation and tandem epoxidation/ CO_2-insertion reaction. Desired products after two consecutive reaction are obtained in poor yield and low selectivity which is attributed to the blocking of active sites and incompatible reagents which drastically affects the reactivity and selectivity of the reaction. Therefore, the reactions require further optimization of reaction parameters and conditions.

Danksagung

In erster Linie gilt mein besonderer Dank meinem Doktorvater

Prof. Dr. Roland Augustinus Fischer

für seine Unterstützung als Betreuer, Motivator und Inspirator. Sie waren immer ansprechbar und interessiert an unserem sowohl menschlichen und wissenschaftlichen Wohlergehen. Sie haben mich gefordert und gefördert und haben immer das vorgelebt, was Sie von anderen verlangt haben. Fischer-Wörter wie „Frustrationstoleranz“ und „Transzendentes Denken“ haben sich eingebrannt und werden mich auch über das rein wissenschaftliche Hinaus begleiten. Ich bedanke mich für ihren Ehrgeiz, Passion und Herzblut. Vor allem ihre Rolle als Lehrer, ist so für mich einzigartig und sucht seinesgleichen. Obwohl Sie teilweise viel Gegenwind für Ihre innovativen Änderungen an den etwas verstaubten, klassischen Vorlesungen und Übungen von Studenten und manchem Kollegen bekommen haben, haben Sie sich nie davon beirren lassen und so wertvolle Impulse, gerade für die Studenten gesetzt. Sie haben mir ein fruchtbares Umfeld zur Verfügung gestellt, in dem man selbstständig forschen, wachsen und sich frei entwickeln konnte. Dafür bin ich dankbar.

Meiner Prüfungskommission danke ich für die bereitwillige und freundliche Übernahme des Koreferats.

Furthermore, I like to thank

Prof. Dr. Dirk De Vos

for your efforts on correcting my thesis and our paper, and your participation as second examiner for my defense. Additionally, I want to thank you for accepting me in your labs on totally short notice upon closure of the CRC. Thank you very much for your generous and well-organized support during my stay in Leuven. With your continuous help, guidance and great scientific contributions, I immediately felt like home in your labs and I am proud that I was part of your group.

Weiterhin möchte ich meinem Doktor „Bruder“

Julius Hornung

bedanken, für deine Freundschaft und Unterstützung, die im Wesentlichen dazu beigetragen haben schwierige Phasen durchzustehen, Rückschläge besser wegzustecken und Motivationstäler zu überbrücken. Als mein „Betreuer“ hast du als erster meine Ergebnisse diskutiert und wir haben zusammen über Probleme und Lösungen gebrütet. Deine Ratschläge und Unterstützung bei unzähligen Problemen haben maßgeblich zu dieser Arbeit beigetragen.

Insbesondere möchte ich mich bedanken bei / I am particularly thankful to

den Personen im **akademischen Mittelbau**, Dr. Christian Gemel für seine erfrischende sachliche und nüchterne Art, seine Betreuung in den AC Praktika in Bochum und in seiner Funktion als Vertreter von RAF und Ansprechpartner bei allerlei Problemen und Fragen. Dr. Mirza Cokoja, für seinen wissenschaftlichen Input, Hilfe beim Erstellen von Manuskripten und zahlreiches Feedback zu meiner Arbeit. Dr. Gabriele Raudaschl-Sieber, für Festkörper NMR Messungen und Hilfe bei unterschiedlichsten Fragen. Dr. Alexander Pöthig, Dr. Gregor Kieslich, Dr. Markus Drees, für ihr Interesse an meiner Arbeit und Unterstützung bei wissenschaftlichen Problemen und anregende Diskussionen in den Gruppenseminaren. Außerdem danke ich Prof. Richard Fischer für seine Unterstützung als mein Mentor.

Martin Schellerer, der mir als Ersatz-**Sekretär** bei zahlreichen bürokratischen und formellen Angelegenheiten geholfen hat und den anderen **hilfsbereiten Angestellten** der TUM, Jürgen Kudermann, Maria Matthews, Tobias Kubo und Rodica Dumitrescu, die durch ihre Arbeit im Hintergrund unsere Arbeit erst ermöglicht haben. Vielen Dank dafür.

Meinen Studenten, die ich im Rahmen von Forschungspraktika oder Abschlussarbeiten begleiten durfte: Maximilian Werny, Jonas Müller, Sebastian Ott, Daniel Henschel, Xiaoyu Zhou, Philip Böhm und Andreas Schmitt.

Dem **Deutschen Akademischen Austauschdienst** (DAAD) für die finanzielle Unterstützung meiner Masterarbeit in Valencia, Forschungspraktikum in Chicago und Kongressreisestipendium in Neuseeland.

Natürlich möchte ich auch unserer gesamten **AMC Gruppe** und den alten Recken der mittlerweile aufgelösten **AC2 Gruppe** für gemeinsame Momente beim brunchen, Ausflügen, Weihnachtsfeiern und der täglichen Arbeit im Labor danken. Insbesondere danke ich, Julius Hornung, Maximilian Muhr (Kunde), Patrizia Heiß (Sekretariat), Dr. Ragav Medishetty, Dr. Kerstin Freitag, Dr. Hung Banh, Dr. Andreas Schneemann, Dr. Jana Weßing, Dr. Daniel Peeters, Dr. Christoph Rösler, Dr. Wenhua Zhang, Dr. Maximilian Gebhardt, Dr. Philipp Altmann, Dr. Christian Jandl, Dr. Suttipong Wannapiboon, David Mayer, Pia Vervoorts, Anna-Lisa Semrau, Werner Heinz, Christian Schneider, Stefano Dissegna, Kathrin Kratzl, Zahid Hussain, Stefan Burger, Fabian Schmitt und Lena Staiger und für eine großartige, teils ausgelassene Gruppenatmosphäre und Zusammenhalt.

Natürlich danke ich auch der gesamten **Kühn Gruppe**, in der ich offen aufgenommen wurde als ich als erster Neuankömmling Asyl bekommen habe, vor allem danke ich Dr. Robert Reich und den anderen Dartslegenden und natürlich der systemrelevanten Dartscheibe. Unsere gemeinsamen Hüttensaufgelage unter Anleitung von Dr. Florian Groche werden mir in Gedächtnis bleiben (oder auch nicht). Für rege Teilnahme und viele gemeinsame Stunden im Kaffeeraum danke ich Panline Fischer, Flo der zweite Dyckhof Ben Hofmann, Dr. Anja

Lindhorst, Dr. Patrizia Wand, Dr. Mario Bitzer, Dr. Daniel Betz, Bruno Labbadia, Dr. Felix Kaiser, Sebastian Hölzl, Lorenz aus Tirol, Jens Oberkofler, Lilly, Andreas Hinterberger, Jonas Schlaginweit und Nadine Tappe. Auch den Schicksalsgenossen aus anderen AK's bin ich zu Dank verpflichtet: Theresa Ludwig, Sophia Stark, Manuel Kasper, Dr. Ruth Maas, Daniel Melzer und Sabine Frischhut.

I also like to thank the people in the **Dirk De Vos group (DDV)** at KU Leuven, especially, my people in "office Awesome" Patrick Tomkins, Koen Adriaensen, Matthias Van den Bergh and Mickaël Henrion. I will not forget our Fridays "Koffie-koeken", your great help with my broken netbook, your warm welcome and funny beer sessions in "the Baar". Moreover, I am thankfull to Bart Bueken for scientific discussions and support, Simon Smolders for patient and continuous support and assistance in the laboratory and the other group members Francisco García Cirujano, Carlos Marquez, Niels van Velthoven, Laurens Claes, Maxime Stalpaert, and Guangxia Fu for the nice group atmosphere and help in everyday problems. Additionally, I like to thank Annelies Vanvlasselaer for your great assistance with the bureaucracy, for providing coffee pads, stirring bars, syringe filters and many more stuff. Next to that, I like to thank the members from the **Rob Ameloot group**, especially, Dr. Priscilla Rocío-Bautista, Dr. Min Tu, Dr.Cesar Parra, Dr. Sabina Rodriguez Hermida, Dr. Max Lutz Tietze, Clement Achille, Alexander John Cruz, Dmitry Kravchenko, Benzheng Xia and Víctor Rubio-Giménez. Our lunch breaks in the "Alma" will be greatly missed and our political and scientific discussions and evenings at the "Oude Mark" will definitely not be forgotten.

Ich danke insbesondere meinen Eltern **Wladimir** und **Tatjana Epp** für eure Liebe, Fürsorge und Erziehung, die mich im Wesentlichen geprägt haben und zudem dem gemacht haben, der ich heute bin. Meinen Geschwistern **Wladimir, Olga, Elwira, Alexej, Peter** und **Katharina**. Ihr habt mich zusammen mit unseren Eltern am meisten geprägt; wir sind zusammen aufgewachsen und haben viel Freude und Schmerz geteilt und sowohl gute als auch schlechte Situationen zusammen gemeistert. Die familiäre mentale und finanzielle Unterstützung und euer Vertrauen ist der Grund, warum ich es bis hierher geschafft habe. Weiter danke ich meinen Verwandten, insbesondere **Tante Olga** und **Gerd**, die mich während des Studiums finanziell unterstützt haben und **Tante Sonja** und **Onkel Peter** für lebenslange Unterstützung und Rückhalt. Auch möchte ich mich bei meinen Cousins and Cousinen bedanken, besonders bei **Dimitri Epp**, der für mich wie ein Bruder ist.

Zuletzt bedanke ich mich bei meinem Bruder **Alexej Epp**. In meiner Rolle als großer Bruder musste ich natürlich ein Vorbild sein. Das hat mich stark motiviert das Studium gut zu absolvieren und durchzuziehen. Neben dem Persönlichen, hast du dadurch viel zu meiner Arbeit beigetragen. Es war mir eine große Ehre, dass dich als meinen Bruder zu haben. Du wirst uns immer in Erinnerung bleiben.

Hätt ich des Himmels reichbestickte Tücher,
bestickt aus Golden- und aus Silberlicht,
die dunklen, die blauen und die hellen Tücher,
aus Nacht, aus Tag und aus der Dämmerung,
legt ich die Tücher dir zu Füßen.
Doch ich bin arm und habe nichts als Träume,
so leg ich meine Träume dir zu Füßen.
Tritt leise, denn du trittst auf meine Träume.

William Butler Yeats

Für meinen Bruder Alexej Epp

Abbreviations

ALD	Atomic layer deposition
Bdc^{2-}	1,4-benzenedicarboxylate
BET	Brunauer, Emmett and Teller
BJH	Barrett-Joyner-Halenda
$Bpdc^{2-}$	1,1‘-biphenyl 4,4‘-dicarboxylate
Btc^{3-}	Benzene-1,3,5-tricarboxylate
CC	Coordination compound
CP	Cyclopropanation
CP	Coordination polymer
$DCPDBPP^{2-}$	5,15-bis(3,5-dicarboxyphenyl)-10,20-bis(2,6-dibromophenyl)porphyrinate
DMF	*N*,*N*-Dimethylformamide
dr	Diastereomeric ratio
DNA	Deoxyribonucleic acid
ee	Enantiomeric excess
H_2-Salen	Bis(salicyliden)ethylendiamin
HKUST	Hong Kong University of Science and Technology
IR	Infrared
IUPAC	International union of pure and applied chemistry
MIL	Matériaux de l'Institut Lavoisier
MMPF	Metal–metalloporphyrin frameworks
MOF	Metal-organic framework
MP	Metalloporphyrin
MPV	Meerwein–Ponndorf–Verley
NADPH	Nicotinamide adenine dinucleotide phosphate
NMR	Nuclear magnetic resonance
NP	Nanoparticle
NU	Northwestern University

PCN	Porous coordination network
PCP	Porous coordination polymer
PIZA	Porphyrinic Illinois zeolite analogue
PSM	Post synthetic modification
PW	Paddle wheel
PXRD	Powder X-ray diffraction
RPM	Robust porphyrinic materials
SA	Surface area
SDA	Structure directing agent
TATB	4,4′,4″-*s*-triazine-2,4,6-triyl-tribenzoate
$TCPP^{4-}$	5,10,15,20-tetrakis(4-carboxyphenyl)porphyrin
TGA	Thermogravimetric analysis
$Tpdc^{2-}$	p-terphenyl 4,4″-dicarboxylate
TPP	5,10,15,20-tetraphenylporphyrin
UiO	University of Oslo
ZJU	Zhejiang University

Table of content

1 Motivation

Nature provides an enormous pool of special and complex catalytic systems, which are known as enzymes. One important class are the metalloporphyrin (MP) based enzymes. The sophisticated environment of the enzymatic pocket protects the catalytically active metal-ion center and allows high catalytic activities and more importantly, an unmatched degree of substrate selectivity. These remarkable properties are an inspiration for the development of artificial MP based catalysts, which ideally, would mimic the behavior of the natural enzymes.

In the last four decades, a vast number of highly active, molecular MPs was developed, however, self-oxidation and the formation oxo-dimers in solution remained a major problem due to irreversible catalyst deactivation. Consecutively, new generations of MPs decorated with bulky and sterically demanding groups were developed, providing structural stability and improved catalyst lifetime combined with increased selectivity of the reaction. However, these MPs require sophisticated synthetic protocols and the obtained yields after extensive purification are very low (often < 1%) hindering their applicability. As another strategy to prevent their deactivation MPs were heterogenized on supports, which on the one hand increased their lifetime but on the other hand was accompanied with a loss in catalytic activity. The question rises how these challenges can be faced and how is it possible to design stable materials without compromising high catalytic activity.

In this context, the discovery of metal-organic frameworks (MOFs) offered a great chance to design self-supported MP based catalysts with improved properties. MPs were successfully used as organic building blocks; combined with appropriate metal-ions or clusters, various MP-MOFs can be constructed. This rational synthesis using well defined building blocks makes it more straight forward to access novel MP-MOF structures. Due to the high crystallinity of these materials, the understanding of the local environment of the active sites within the MOF matrix is clearer. Consecutively, this knowledge engenders computational modeling which is critical for the deeper understanding of binding modi and calculation of possible intermediates. The obtained MP-MOFs exhibit isolated, spatially distributed, catalytically active MP-sites, which ideally, act as sites single-site-catalysts. The high porosity of the materials allows mass transport and helps to overcome diffusion limitations, which is a typical problem in heterogeneous catalysis. More importantly, by incorporation of MPs into the rigid framework, their deactivation by the formation of oxo-dimers is inhibited, pathing the way to robust heterogeneous catalysts.

In a way the MOF can be seen as some sort of “pocket” itself; similar as the enzymatic pocket, most of the internal MP-sites are protected by the MOF matrix increasing the catalyst lifetime. Introduction of functional groups i.e. by the decoration of the auxiliary *meso*-arylsubstituents

with electron-withdrawing halogen atoms on the hand, influences the electronic state of the inner metal core. On the other hand, these groups make the MP more hydrophobic, thus, the pore channels may favor non-polar substrates due to positive hydrophobic-hydrophobic interactions and disfavor more polar substrates by negative hydrophobic-hydrophilic interactions. The abovementioned tailorability of MOFs enables the precise manipulation of their properties by introduction of functional groups on the porphyrinic backbone i.e. enhanced product selectivity.

Further, the MOF matrix itself may provide influence on the stereochemistry due to the pore geometry of the pore channels / cavities and the resulting confinement effects. Different MP-MOF phases built from same inorganic and organic building units can be synthesized by the adjustment of reaction parameters like solvent, modulator, temperature and reaction time. As a result, the obtained phases may differ in topology, pore size and geometry but other chemo-physical properties are mostly unaffected or can be tailored, hence, good comparability is given. This allows the study of pore confinement effects and their impact on stereo-, size- and shape selectivity of catalyzed reactions, which is crucial to produce pharmaceuticals, flavors and fine chemicals.

The objective to investigate stereocontrol using MP-MOFs was tackled in the cyclopropanation (CP) reaction under Zr-MOFs(MP) catalysts. Therein, smaller pore sized Rh-porphyrin MOFs did show strong confinement effects using coordinating substrates, which was translated into very high diastereoselectivity. Contrary, Rh-porphyrin MOF with larger pores and larger Rh−Rh distances did show less high diastereoselectivity with coordinating substrates, indicating that stereoselectivity is dependent on the topology and the pore confinement of the MOF.

Another focus of this thesis was to study different Zr-MOFs(MP) systems on how connectivity and effect of incorporated metals influences the Lewis acid catalytic activity. This was tested in the CO_2/epoxide coupling reaction, which is catalyzed by Lewis acids. It was found that in this dual-catalysts connectivity, the nature of used metal, and the degree of defects strongly influence the overall catalytic activity. Moreover, the abundance and accessibility of Zr(IV) and/or Mn(III)/Zn(II) sites can be independently adjusted, offering great control of the number of active sites.

The tailorability and diversity from MPs as well as MOFs, principally enables the fabrication of multi-functional catalysts, as demonstrated in the abovementioned Zr-MOFs(MP). These systems consist out of Zr_6-oxo-clusters which do provide Lewis acidity, while metalloporphyrins -in dependence of the incorporated metal- do provide Lewis acidity as well as oxidation activity. So, the question rises, for what kind of reactions these bi-functional catalysts can be used? Can these materials perform multi-step, tandem-like reactions and if yes, what are appropriate catalytic conditions for such reactions?

Motivated by these questions, tandem reactions taking advantage of (1) Lewis acid and (2) MP-sites with catalytic oxidation capabilities were examined. Dual Zr-MOF(Mn) system was investigated in the one-pot epoxidation/CO_2-insertion reaction to produce cyclic carbonates and in the one-pot oxidation/cyanosilylation for the production cyanohydrin derivatives.

2 Introduction

2.1 Homogeneous metalloporphyrins as catalysts

Porphyrins are a class of complex heterocyclic organic compounds. The name "porphyrin" is derived from the Greek word πορφύρα (*porphyra*), meaning *purple*. Due to their extended highly conjugated π-system, they show high absorbance in the visible light region which is the reason for their usually intense colors. The structure of porpyhine, -the simplest porphyrin- is composed out of four pyrrole molecules connected by α carbon atoms via methine bridges. Porphins can be readily substituted at the *meso*- or *β*-positions at the backbone, usually by functionalized alkyl-groups and are termed porphyrins. The nomenclature of these substituted compounds is depicted in Figure 1.

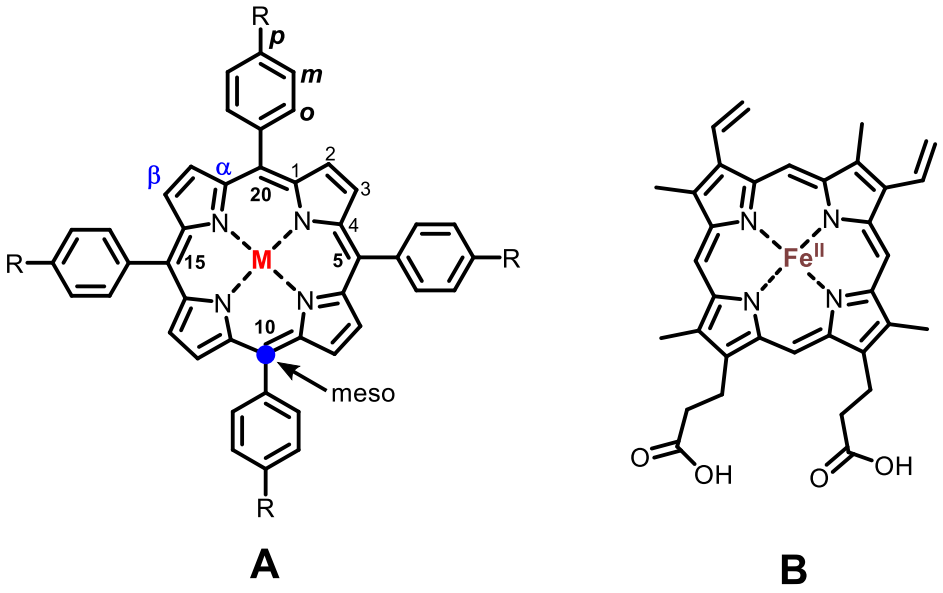

Figure 1. A: Substituted tetraaryl-metalloporphyrin unit with the corresponding nomenclature. B: Heme protein with complexated Fe^{II} and its protoporphyrin IX unit.

In nature, the metalloporphyrin (MP) unit plays a crucial role in fundamental processes, i. e. the heme blood protein (Figure 1, B) which binds dioxygen via Fe^{II}, and chlorophyll, a Mg^{2+}-based porphyrin responsible for the absorption of sun-light to produce sugars via photosynthesis. It's unique structural composition allows important functionality. First, MPs have high thermal (~ 400 °C) and, more importantly, excellent metal coordination stability which is reasoned by the macrocyclic chelation effect of the aromatic *N*-donor ligands.[1] Complexation is possible for almost every transition metal (TM) and is nearly irreversible in many cases, only be undone by applying harsh acidic conditions.[2] This is beneficial in terms of catalyst lifetime and, especially, to metal elimination (leaching) which is important in the production of drugs and

pharmaceuticals, where metal contamination is highly undesired. Second, since MPs are planar *cis*-coordinated by the tetrapyrrole core, further *cis*-coordination – which is requisite in many catalytic processes- is not possible. Therefore, catalytic site reactions involving the mentioned *cis*-coordination step are inhibited pathing the way to a more selective reactions.[1] Third, the tunability of MPs gives rise to alter their physical and chemical properties. Systematic tuning allows the introduction of peripheral substituents carrying varied electronic, steric, and conformational environments on the aromatic ring structure of the porphyrin. Since the porphyrin ligand can be readily metalated with almost every TM, altered functionality can be introduced by the choice of different metals and same metal ions but with altered oxidation states. This allows changes in chemical reactivity and at the same time, let the coordination mode of the metal unaffected, due to the rigid ligand environment.[1] Fourth, compared to often extremely complex MP-based protein superstructures used by nature containing large enzyme pockets, molecular, artificial MPs bearing simple structures are more easy to study by means of computational modeling. However, MPs might exhibit poor structural stability due to self-oxidation and dimerization paired with difficult recyclability in homogeneous reaction conditions. A simple solution would be their heterogenization. Reported heterogenization methods include their immobilization onto inorganic supports such as silica gel,[3, 4] molecular sieves,[5] zeolites[6, 7] and many more.[8] The obtained supported MP structures provide enhanced structural stability and allow recycling. However, the precise control of encapsulation and the distribution of catalytically active MP units within the respective matrices is challenging.

Homogeneous porphyrin catalysts are mainly being used in biomimetic (asymmetric) oxidations of hydrocarbons and epoxidation of olefins.[9] Other reactions involve C-H Bond halogenations,[10, 11] oxidative degradation of Lignin[12, 13] and organic pollutants[14] as well as DNA cleavage.[9] Next to the broad range of oxidative reactions, MPs are also being used in carbene transfer reactions *e.g.* in the cyclopropanation reaction.[15] Along with other Lewis acid mediated reactions, in example the CO_2/epoxide coupling for the production of cyclic carbonates,[16] in the following selected examples demonstrating the catalytic activity of MPs are discussed.

2.1.1 Biomimetic oxidation catalysis

MPs are integral parts of natural enzymes and i.e. responsible to reversibly bind dioxygen. One important enzyme class is the cytochrome P-450 (CYP) family, a heme protein which include a Fe^{II}-center discovered by Omura and Sato in 1962.[17] It is extensively used in nature to perform a broad range of catalytic oxidations including oxidation of alcohols, aldehydes and nitriles, hydroxylation, epoxidation, sulfoxidation, *N*-oxygenation, dehalogenation etc. with unmatched catalytic activity and selectivity (Figure 2).

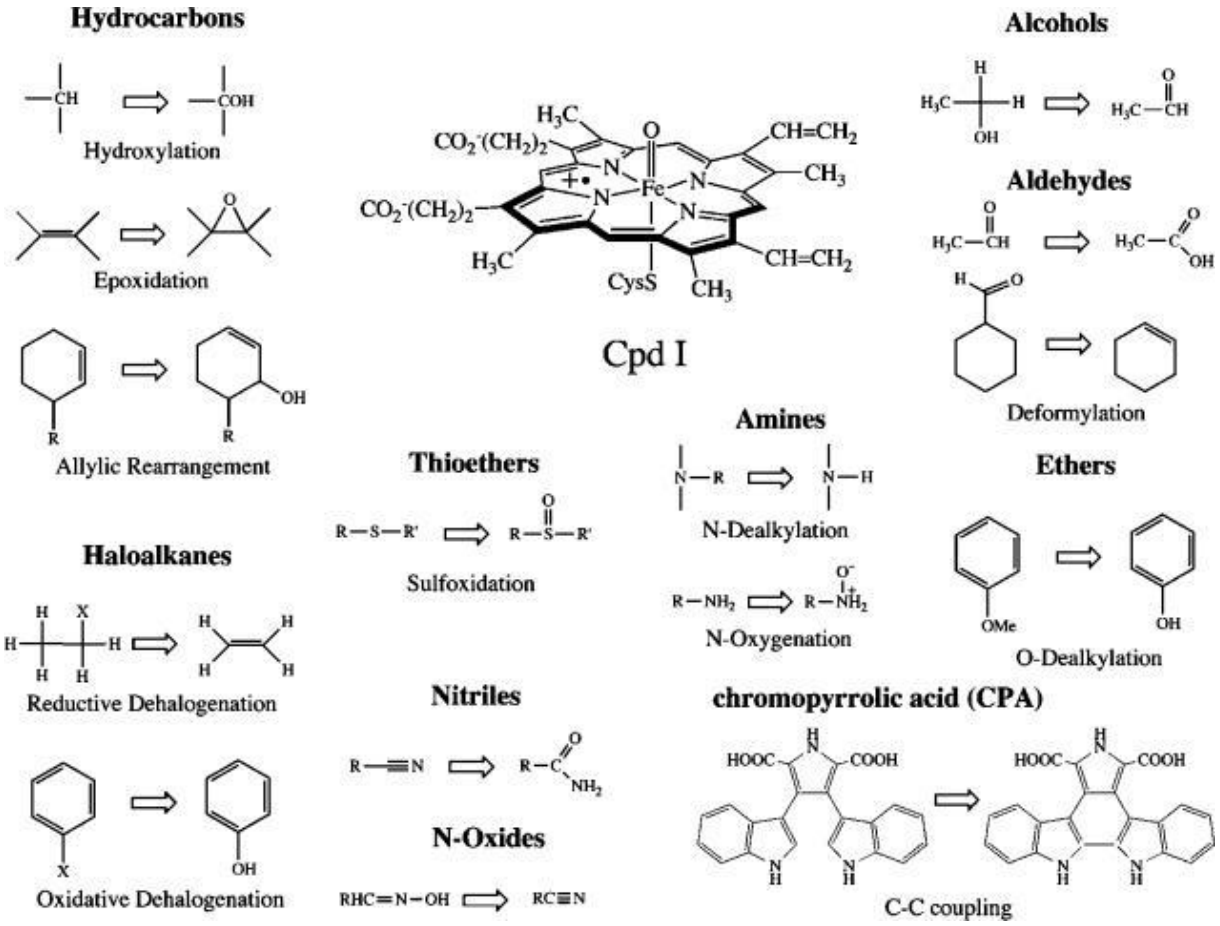

Figure 2. Scope of chemical transformations catalyzed by P450s, shown along with the putative active species, compound I (Cpd I). Reprinted with permission from ref [18]. Copyright 2010 American Chemical Society.

Inspired by this fascinating enzyme, scientists started to develop artificial, so-called biomimetic catalysts which are supposed to show similar catalytic reactivity as the natural enzyme. Mechanistically, the most frequent reaction type is the insertion of one oxygen-atom into organic molecules, *e.g.* in the C-H hydroxylation, sulfoxidation and C=C epoxidation, whereby the other O-atom of dioxygen is reduced to water (Scheme 1). Hence, the name "*mono*oxygenase" is given to this enzyme, in contrast to other enzymes which are able to transfer both oxygen atoms.[18]

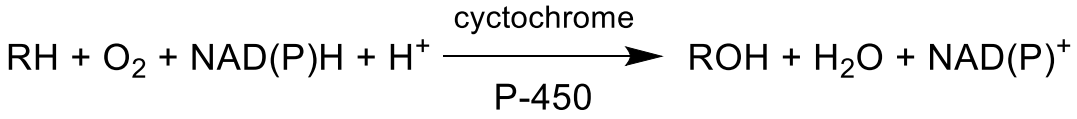

Scheme 1. General reaction scheme of the oxidation catalyzed by the natural enzyme cytochrome P-450 with nicotinamide adenine dinucleotide phosphate (NADPH) as co-factor using dioxygen as oxidant.

The most common oxidation reaction catalyzed by MPs is the epoxidation of olefins, which is a reaction greatly used in organic synthesis.[9] Relevant industrial applications are the direct epoxidation of ethylene using O_2 over Ag-catalysts or the TM-catalyzed epoxidation of olefins by alkylhydroperoxides in the *Halcon process*™ (propene epoxidation with ^{t}BuOOH and a molybdenum catalyst).[19] In this context, MP-catalyzed epoxidation might have some advantages compared to other catalysts classes: (i) MPs tolerate a large variety of oxidants (iodosylbenzene, hypochlorite, organic or inorganic peroxides, molecular oxygen, ozone etc), (ii) a broad range of reaction conditions can be used (soluble or supported MPs and mono- and biphasic systems), and (iii) their great synthetical tunability and incorporation of functional and reactive groups, principally, engenders shape-selective and asymmetric epoxidations.[9, 20]

In an early work Groves et al. reported on olefin epoxidations and alkane hydroxylations using iodosylbenzene as oxygen atom donor under TPP(FeCl) (TPP = 5,10,15,20-tetraphenylporphyrin) catalyst in 1979.[21] Conversion of cyclohexene mainly gave cyclohexene oxide (yield = 55 %), but also the allylic oxidation product cyclohexanol was observed (yield = 15 %). Interestingly, the reaction of *cis* and *trans*-stilbenes proceeded diastereoselective, since the racemate was converted to exclusively *cis*-stilbene oxide as product. However, the catalyst degraded upon the applied reaction conditions, which is an intrinsic problem of MPs, since they may form oxo-dimers via self-oxidation.[22] Nevertheless, this remarkable example was the first demonstration that artificial, biomimetic MPs can utilize an *exogenous* oxygen source in the absence of NADPH and dioxygen which are the most prominently used systems in biology (Scheme 1). This "domestication" of the biological P-450 heme enzymes by the use of bio-inspired, artificial heme-like MPs was a true milestone opening the toolbox for various oxidizing agents and even more sophisticated MPs and marked the beginning for a plethora of further studies. Further work reported by Groves et al. on Cr(III) metalated TPP analogs showed similar activity but with altered selectivity towards the allylic oxidation products.[19] Also TPP(MnCl) was active in the epoxidation of cyclohexene revealing catalytic activity in the same order of magnitude, but with loss of stereoselectivity.[23, 24] This was explained with an prolonged life-time of the carbon radical which allowed the isomerization via C-C bond rotation. These examples demonstrate that various TMs can be used, effecting the activity and selectivity of the reaction, thus, enabling certain control over the reaction. In order to improve the poor structural stability of the so-called "fist-generation porphyrins" towards *meso*-oxidation (destruction) and μ-oxo dimer formation, Chang et al. reported on the use of fluorinated porphyrins such as Fe-tetra(pentafluoropheny1)porphyrin chloride which

significantly improved their stability.[25] Moreover, the introduction of highly electronegative groups such as F^- and Cl^- at the *meso*-aryl-substituents leads to the reduction of electron density of the incorporated TM ("second-generation MPs"), thus, forming more electrophilic metal-oxo intermediates (more Lewis-acidic). Trayler et al. used Fe-tetra(2,6-dichlorophenyl)porphyrins in the epoxidation of norbornene and indeed, the improved structural stability allowed turnover numbers (TONs) up to 10.000 in 20 min of reaction.[26] Other chiral Fe-porphyrin epoxidation catalysts are reviewed by Gopalaiah.[27] The so-called "third-generation MPs" do have additional halogen substituents at the *β*-positions, which basically extends the idea of the electron withdrawing effect on the central metal ion. One example is the highly perfluorinated "teflon ligand" *meso*-tetra(pentafluorophenyl)-*β*-octafluoroporphyrin (contains 28 F-atoms) developed by Shinshi and Manabu and applied in the hydroxylation of benzene to phenol by the use of hydrogen peroxide.[28] Besides the electronic effect, one have also to consider the altered hydrophobicity of the porphyrin ligand environment which is created around the catalytically active TM-center. Ideally, it favors the entrance of non-polar educts (alkanes, alkenes, aromatics) via hydrophobic interactions and at the same time prevents molecular contacts of more polar reaction products due to unfavorable hydrophilic-hydrophobic interactions. To mimic this fascinating enzyme-like pocket which is absolutely crucial regarding (enantio)selectivity and activity, much attention was given to the MP-pocket engineering for the design of highly selective, biomimetic oxidation catalysts.

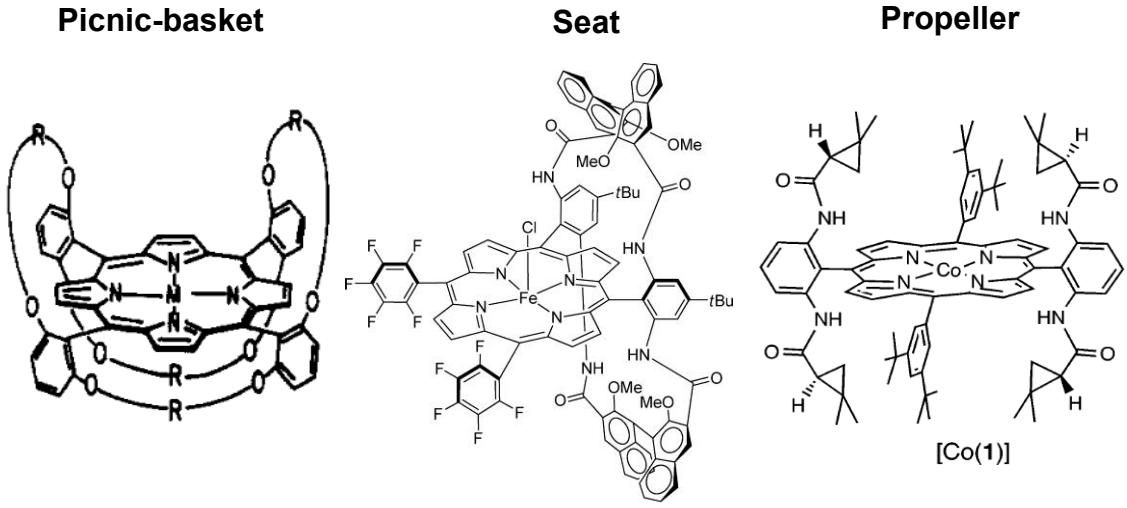

Figure 3. Selected examples of the porphyrin-pocket engineering, resulting in "picnic-basket",[29] "seat"[30] and "propeller"[31] shaped porphyrin structures. Ref. [29] was reproduced with permission by Elsevier Ltd. Copyright © 1999. Ref. [30] was reproduced with permission by Elsevier Science Ltd. Copyright © 2000. Ref. [31] was reprinted with permission from Y. Chen, J. V. Ruppel, X. P. Zhang, J. Am. Chem. Soc. 2007, 129, 12074-12075. Copyright (2007) American Chemical Society.

The porphyrin-pocket engineering produced a vast of fascinating architectures: Gross et al. designed "picnic-baskets" MPs, whereby the aryl-substituents are interlinked.[29] Kodadek et al. reported on "chiral wall"[32] and "chiral fortress" structures, wherein the central metal ion is protected by large substituents.[33] Halterman introduced even bulkier, chiral anthracene groups.[34] Zhang and co-workers reported on crowed, chiral "propeller-like" MP structures.[31]

Collman et al. and others introduced “totem” shaped bis-binaphthyl-substituted porphyrins.[35, 36] Furthermore, Rose et al. developed “seat” shaped chiral Fe-porphyrins.[30] Most of these structures exhibit extensive sterical protection of the inner TM-core and more importantly, chiral ligand environment which can induce the transfer of chiral information onto substrate molecules. So, it is not surprising that TONs > 10.000 h^{-1} with enantiomeric excess (*ee*) up to 97 % can be achieved by these highly sophisticated, functionalized MPs.[37]

These selected examples highlight the impact and important role of MP-based catalytic systems in the shown (ep)oxidation and hydroxylation reactions. In the difficult epoxidation of terminal olefins, they give better *ee* values compared to other catalytic systems such as the Mn(salen) catalysts. Nevertheless, several challenges and intrinsic limitations remain. First, the good turnover numbers are highly restricted to reactions utilizing iodosylbenzene as oxidant which has poor atom economy and only ~8 % O-efficiency. Thus, other oxidant classes with improved environmental fingerprint and less hazardous constrains such as (alkyl)peroxides, O_2/O_3 and the industrially more relevant NaOCl need more attention. Secondly, the sophisticated porphyrin architectures obtained by porphyrin engineering are synthetically complex, challenging and low-yielding. Consecutively, more easy-to-synthesize porphyrins are required.[20] Hence, their scope towards applications seems to be restricted to the production of expensive drugs, pharmaceuticals and fine-chemicals.

2.1.2 Lewis acid mediated carbene transfer

In contrast to the oxene transfer, as demonstrated by the biomimetic olefin epoxidation and alkane and aromatic hydroxylation reactions, the carbene transfer is not known in biologic systems.[38] The utilization of artificial MPs is an example for establishing new C-C bonds via carbene transfer, exemplary shown in the catalyzed reaction to yield cyclopropanes (Figure 4).

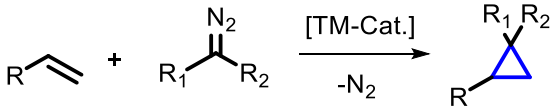

Figure 4. General reaction scheme of the TM-catalyzed cyclopropanation of olefins using diazo esters as carbene sources to give the cyclopropane unit (highlighted in blue).

This example shows that the study of the structure and mechanisms of fundamental biological enzyme systems is absolutely key for the understanding of how catalytically active sites work. Hence, it allows to transfer this knowledge onto other catalytic reactions which do not have any biological counterpart as shown for the carbene transfer.[38] Nowadays it is established that MPs catalyze group transfer reactions such as carbene (alkylation) and nitrene (amination) C-H insertions to form new C-C and C-N bonds, respectively.[1] Cyclopropanation (CP) is a well-known C–H alkylation reaction, usually mediated by diazo reagents as carbene sources. Cyclopropanes are important synthetic targets and are used as pharmaceuticals, natural products

and antibiotics.[39] The specific reactivity of the strained three-membered ring system and its ability to induce conformational constraints on otherwise flexible acyclic chains is an absolutely key feature of this structural building block.[40-42] The TM-catalyzed mechanism involves the catalytical decomposition of the diazo reagent by the release of dinitrogen (Figure 5).

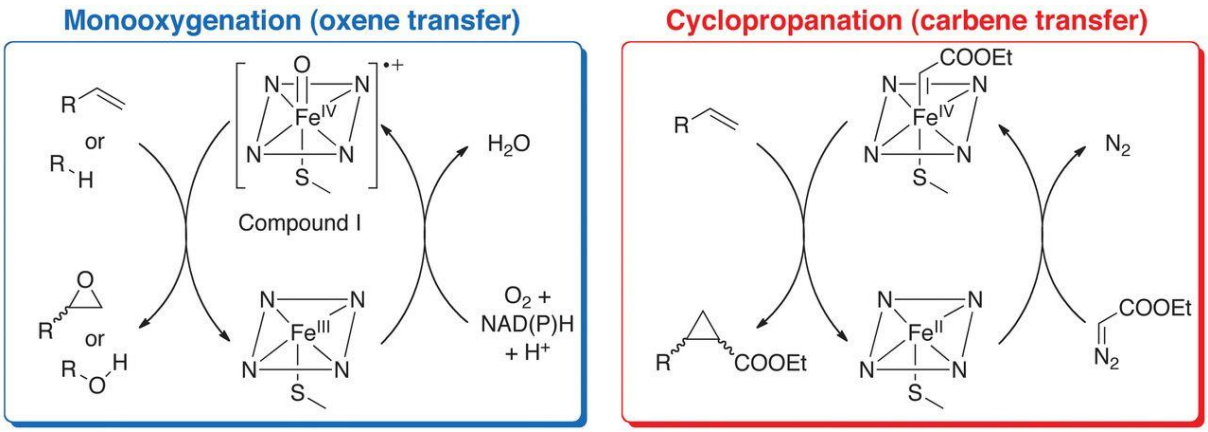

Figure 5. Comparison between monooxygenase activity catalyzed by the high-valent ferryl porphyrin radical intermediate (left) (compound I) and the artificial mode of formal carbene transfer activity of cytochrome P450s, using diazo reagents as carbene precursors (right).[38] From P. S. Coelho, E. M. Brustad, A. Kannan, F. H. Arnold, *Science* 2013, *339*, 307-310. Reprinted with permission from AAAS.

The resulting intermediate carbene species is transferred onto given olefinic substrates forming the typical cyclopropane unit. A myriad of MPs (M = Fe(II,III),[35, 43-45] Co(II),[31, 46, 47] Rh(III),[33, 47-49] Ru(II),[50] Ir(III),[47, 51] Os(III)[52] and others catalyzes the CP of olefins. As the evolution of MP structures used in biomimetic stereoselective oxidation reactions was systematically developed, MP structures applied in CP catalysis equally evolved. Hence, both reactions require similar pocket-design in order to perform stereoselective reactions. The auxiliary substituents were functionalized with chiral and sterically demanding groups which creates a pocket for incoming substrates. The specific pocket environment allows certain substrate specifity and high catalytic turnovers and more importantly, diastereoselective and enantioselective chemical transformations. One remarkable example was reported by Gallo and co-workers: Their chiral "totem" Fe(III)-porphyrin catalyst, Fe(**2**)(OMe), with C_2-symmetry is one of the most active reported MPs in the cyclopropanation reaction exhibiting TOFs > 120.000 h^{-1} and *ee*'s up to 97 %.[35] The non-innocent auxiliary substituents at the porphyrin skeleton provide an enzyme-like pocket with complex multi-functionality, namely, (i) high catalytic activity and diazo activation by the Fe(III) in the tetrapyrrolic core of the totem structure (ii) induction of trans-diastereoselectivity by the C_2 symmetrical skeleton, and most importantly, (iii) enantiocontrol via the chiral hat (Figure 6).[53]

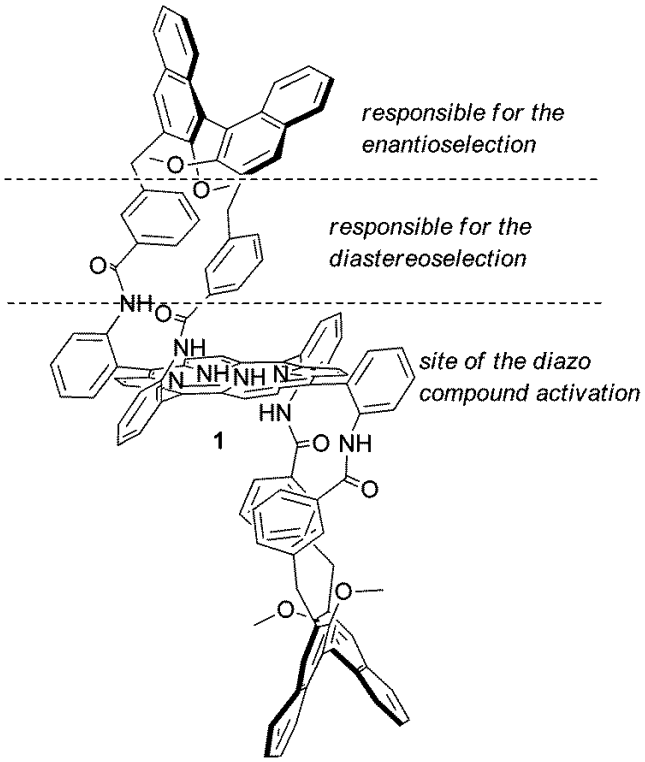

Figure 6. Structural complexity in "totem" porphyrin. Different structural components of bis-binaphthyl functionalized porphyrin influence the enantio- and stereoselectivity. Reproduced from ref.[53] with permission from Royal Society of Chemistry.

2.1.2.1 Other Lewis acidic reactions using metalloporphyrin catalysts

MPs principally provide Lewis acidic catalytic activity due to their coordinated metal ions inside the tetrapyrrole core. Therefore, they have also been used as Lewis acid catalysts in the CO_2/epoxide coupling to produce cyclic carbonates (Scheme 2). This is a relevant reaction for using CO_2 as a cheap and sustainable carbon feedstock for the transformation into value-added chemicals (CO_2-fixation).[54-56]

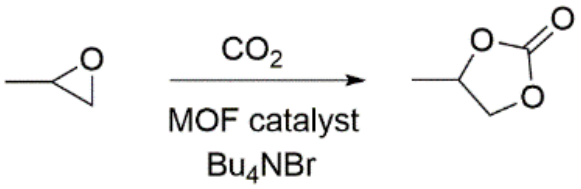

Scheme 2. Catalytic reaction scheme of cycloaddition of propylene oxide with CO_2 using MOFs as heterogeneous catalyst and Bu_4NBr as homogeneous co-catalyst.

The reaction is catalyzed by a (metal) Lewis acid (epoxide activation) and by a nucleophile – typically tetraalkylammonium halides – as the co-catalyst (epoxide ring opening).[57, 58] Many materials are known to catalyze this reaction including metal oxides,[59] transition metal complexes,[60-62] ionic liquids[63, 64] and other organocatalysts.[65] Aida and Inoue were the first to use MPs in this reaction, namely, Al-TPP.[15] Jing et al. extended their work utilizing TPP(M)

catalysts (TPP = tetraphenylporphyrin; M = Mg(II), Al(III), Sn(II) and Sn(IV)) reaching TONs and TOFs up to 3972 and 794 h^{-1}, respectively.[16] Interestingly, when these porphyrins are metalated with ions of stronger Lewis acidity, they show higher catalytic activity (Al(III) > Mg(II) > Sn(IV) > Sn(II)), highlighting that these catalytic systems can readily be tuned by simply using other TMs. One remarkable example was reported by Sakai and co-workers.[66] In their work the homogeneous co-catalyst quaternary ammonium bromide was immobilized via covalent attachment on the meso-substituents of the porphyrin skeleton, demonstrating again the great tuneability of MPs. Hence, the bi-functional system of Mg(II)-porphyrin and grafted co-cat. exhibit outstanding catalytic activity. Catalytic amounts (0.0008 mol%) of Mg(II)-porphyrin gave high yields with a TON of 103.000 and a TOF of 12.000 h^{-1}, respectively.[66] Other reactions using MPs include the Ru-porphyrin catalyzed alkylation of indoles with tertiary amines by oxidation of a sp^3 C-H bond,[67] enantioselective Cr-porphyrin catalyzed hetero-Diels–Alder reaction of aliphatic, aromatic, and heteroaromatic aldehydes.[68]

Summarized, biomimetic MPs are versatile catalysts which can provide excellent catalytic activity. Due to their great tunability MPs are easy to functionalize with *e.g*. chiral groups and thus, can be used in enantioselective epoxidation, hydroxylation and Lewis-acid mediated carbene transfer reactions. As previously described, one major drawback of MPs is their deactivation behavior due to self-oxidation and the formation of dimers. This problem was addressed by the heterogenization of (porous) supports. While this approach indeed improves the catalysts lifetime, the heterogenization or grafting results in the formation of a quite complex MP@support composite material which structural composition is less good defined. Moreover, often the exact location and arrangement of the MPs within the support matrix is difficult to elaborate with standard characterization techniques. Thus, the chemical environment of the MPs which is crucial for the (chemo)selectivity remains unknown making it more difficult for targeted tailoring and manipulation. This aspect is of key importance in the context of rational design of catalysts. Most heterogeneous catalysts are highly complex systems, where many different catalytic sites provide different types of reactivity. Often it is difficult to understand the nature of the catalytically active site, because only a small fraction of special sites, namely, terrace, steps, and kinks are active. One recent approach to reduce the complexity is the design of so called ‘single-site-catalysts’.[69] Ideally, these catalysts are built from only one type of catalytic sites, allowing rational design and providing great control of the nature and distribution of catalytic sites.

Next to the grafting of molecular MPs onto surfaces to design heterogeneous MP-catalysts, an alternative route is their utilization as structural building blocks in the construction of poly-dimensional network compounds. One major advantage when compared to amorphous compounds is that in crystalline networks, the crystallographic positions of the MPs are well-defined allowing rational design and control of the arrangement of the active MP sites. Moreover, the crystallinity allows the easy structural elucidation using standard powder X-ray

diffraction techniques. Historically, one of the first examples using porphyrins as organic building blocks in combination with Cd(II) and Cu(I)-ions for the construction of microporous 3D networks 'infinite structures', were pioneered by Robson et al. in 1991[70] and 1994,[71] respectively. These fascinating architectures, however, suffer from framework collapse and loss of porosity upon solvent removal. Generally, the structural stability depends on careful selection of appropriate inorganic metal-ion clusters in combination with organic multi-dentate (carboxylate-based) porphyrin ligands. As one of the first, Yaghi et al. paved the way to a novel class of hybrid organic/inorganic coordination polymers, namely, metal-organic frameworks (MOFs) which will be discussed in the next chapter.

2.2 Metal-organic frameworks (MOFs)

Porosity is an important property found in nature, in example the lungs in the human body are the primary organs of the respiratory system, which main function is to "extract" the gas (oxygen) from air into the blood system. This exchange rates dependent on the surface area of the air-blood interface. Therefore, the lungs contain approximately 2.400 km of airways and 300 to 500 million alveoli which increase this contact area facilitating the uptake of oxygen. In this context, the artificial development of materials which do exhibit high surface areas is of great interest, since the property of porosity may play a crucial role also in other areas.

In the mid-1990s there were basically only two relevant types of porous materials known, namely, carbon-based and inorganic materials.[72] Those microporous inorganic materials, also known as zeolites, are crystalline solids with the general formula $M^{n+}_{x/n}[(AlO_2)_x(SiO_2)_y]^{x-} \cdot w\ H_2O$ (M = metal) with ≥ 200 different known different structures.[73] The two main subclasses of zeolites are aluminosilicates or aluminophosphates which are widely used in industry as heterogeneous catalysts and adsorbent materials. The advantages are their exceptionally high thermal (T > 1000 °C) and chemical stability. On the other hand, the discovery of novel zeolites is intrinsically difficult due to their purely inorganic structure and limited number of possible tetrahedral building blocks. Typically, only the $[SiO_4]^{-4}$ and $[AlO_4]^{4-}$ are available as building units. Basically, the variety rises from different topologies of linking tetrahedra, which is induced by the utilization of structure directing agents (SDAs), the so-called templates.[74]

In the end of the 90's, another family of porous materials were discovered: Metal-organic frameworks (MOFs). They belong to the material class of coordination compounds (CCs). Briefly, the term 'coordination compound' (CC) is defined as any compound that contains a coordination entity, whereas a 'coordination entity' can be described as an ion or neutral molecule that is composed of a central atom, usually that of a metal, to which is attached a surrounding array of atoms or groups of atoms, each of which is called ligands.[75] One important sub-class are coordination polymers (CPs) which are known since the early 1960s[76] (Werner-type coordination complexes) and can be described as infinite one-, two-, three-

dimensional (1D, 2D and 3D) arrangements of molecules in space, or in other words following the recommendation of international union of pure and applied chemistry (IUPAC), a CP is;

“A coordination compound with repeating coordination entities extending in 1, 2, or 3 dimensions.”

Notably, CPs do not need to be crystalline or porous by definition, in fact only a fraction of CPs exhibit (permanent) porosity.[77] Kitagawa et al. introduced the term “porous coordination polymers” (PCPs),[72, 78] which in literature is used as a synonym to the term ‘MOFs’. In the last two decades, this sub-class of inorganic/organic materials achieved a lot of attention. From a more mathematically point of view, the term “framework” or “network” can be defined as the interconnection of vertices (nodes) with edges (derived from graph theory).[79] The resulting frameworks can extend 1D (linear rods/chains), 2D (layers, planes) or 3D (MOFs) structures.

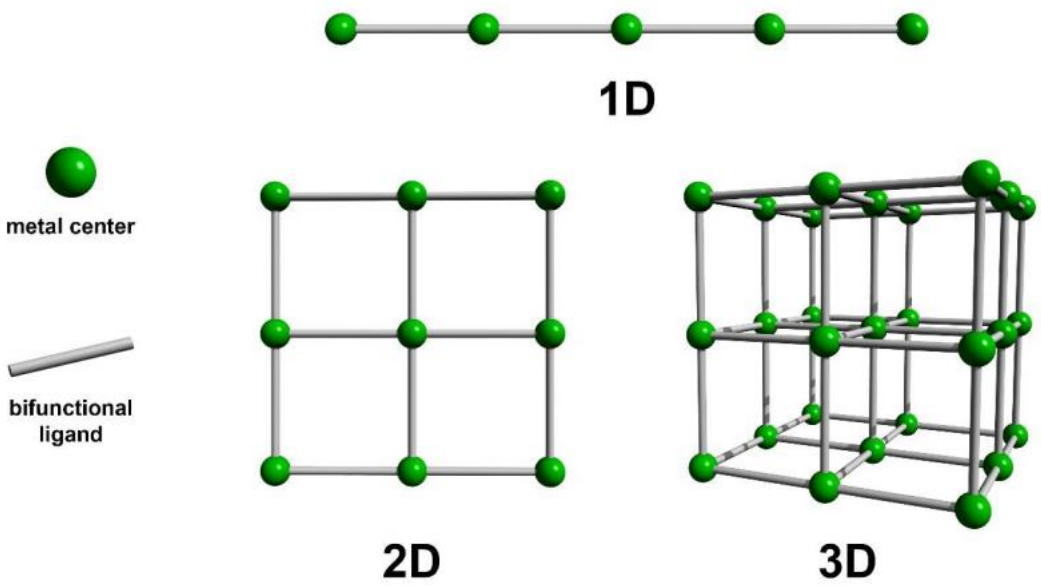

Scheme 3. Adapted simplified scheme of 1, 2 and 3 dimensional framework structures, composed by metal-ions linked by linkers.[80]

MOFs are built from inorganic building units, usually, metal ions or oxo-clusters which are linked by polytopic organic (carboxylate) linkers, forming poly-dimensional networks with well-defined pores.[81] Their high porosity, crystallinity and their tolerance towards the implementation of different functional groups and the precise tailoring of their structure and topology are giving rise for MOFs to play a part in numerous potential applications such as heterogeneous catalysis,[82, 83] sensors,[84-86] semiconductors,[87] adsorption,[88-90] and others.[91] Mechanistically, MOFs are formed by the self-assembly of metal-ions also known as secondary building units (SBUs), and conformationally restrained (‘stiff’), often aromatic organic linkers, via a crystallization based process under solvo-thermal conditions. More flexible, non-stiff linkers would dramatically decrease the structural stability of the framework due to more degrees of freedom and rotation. Moreover, the use of aromatic linkers engenders chemical

stability, since "inert" aromats do have poor reactivity and are less prone to oxidation compared to aliphatic-based linkers, providing additional stability to the framework. Different from zeolites, organic linkers can be easy functionalized -even post-synthetically- offering a great chemical diversity. Additionally, the manifoldness also arises from the large toolbox of possible SBUs (connectors) and linkers, which can be recombined in almost infinite possible permutations. The metal containing SBU, which is associated as a connector exhibits different numbers of possible connectivities in the range from 2-12 (Figure 7). Furthermore, also the linker is able to form multitopic connectivities sites. As a matter of fact, this multitopic binding and various connectivities for both building units create plenty of opportunities for the targeted synthesis of desired framework geometries and topologies.

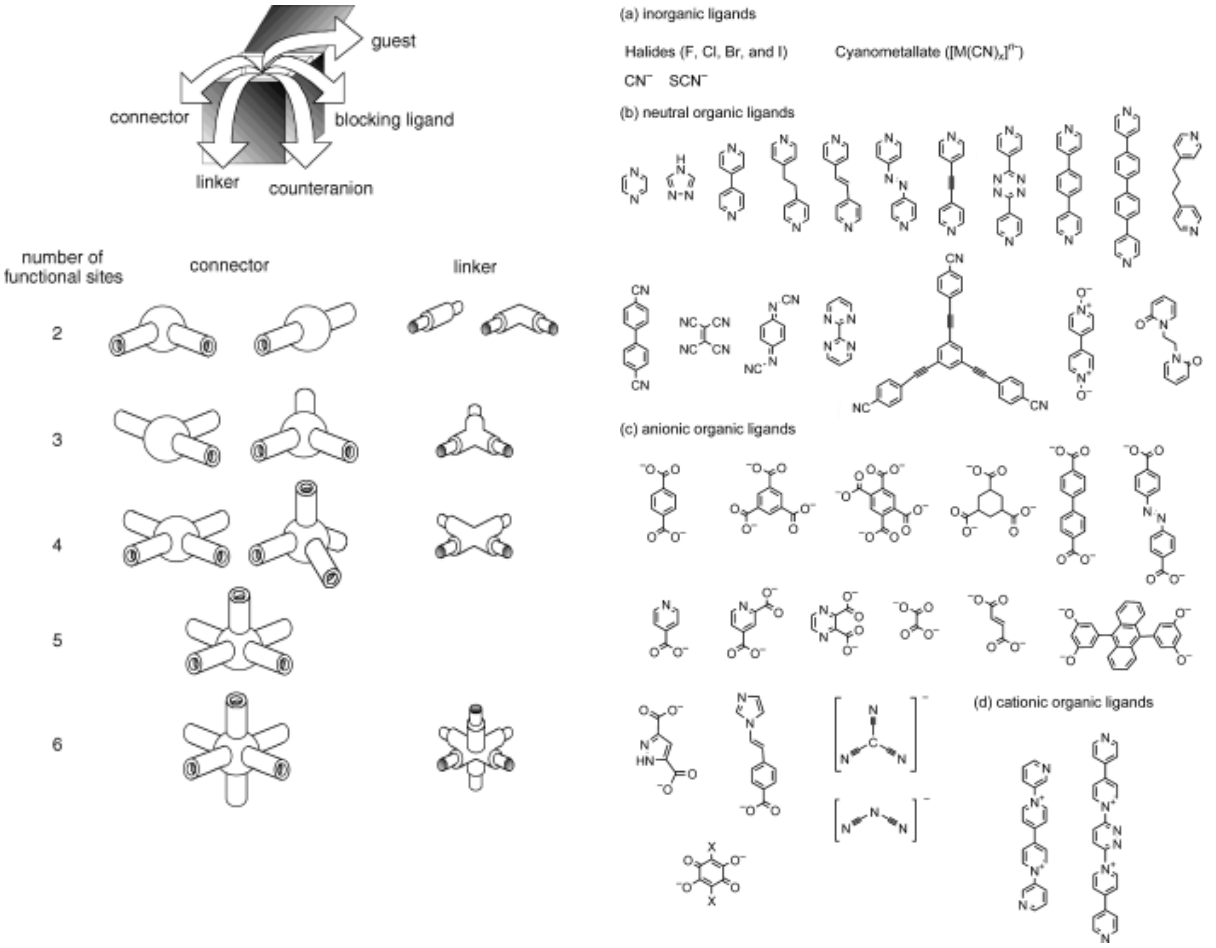

Figure 7. Illustration of selected examples of different possible numbers of functions sites of the metal containing SBU (connector) as well as the linkers with their different binding geometries (linear, tri-, tetra-, penta- and hexatopic connectivity) (left). The classification of the linkers in inorganic (a), neutral (b), anionic (c) and cationic (d.) is displayed in the right part of the Figure.[72] Copyright © 2004 WILEY-VCH Verlag GmbH & Co. KGaA, Weinheim.

Based on their stability and chemo-physical properties, MOFs are categorized into three different generations: 1st; 2nd and 3rd generation of MOFs. The first generation describes MOFs which are only stable as long as they contain clathrates, which are defined as trapped solvent

molecules and counter-anions originated from solvo-thermal synthesis. Usually, the clathrates provide some sort of directing or stabilizing effect on the framework. When those guest molecules inside of the framework are removed, f.e. by thermal activation or drying, the underlying framework collapses and is irreversibly destroyed. The second generation characterizes more stable MOFs which consists out of a rigid assembly of building blocks and do not collapse upon solvent removal, demonstrating permanent porosity. The third generation represents MOFs which embody a more flexible and dynamic structure and show responsive structural behavior upon external stimuli, such as temperature, UV-light and type of the adsorbed solvents. This reversible single crystal to single crystal transformations, are known as "breathing behavior". Therefore, these MOFs were named 'soft crystals', in the sense that they exhibit a certain degree of flexibility within a very rigid and stiff coordination environment.[92]

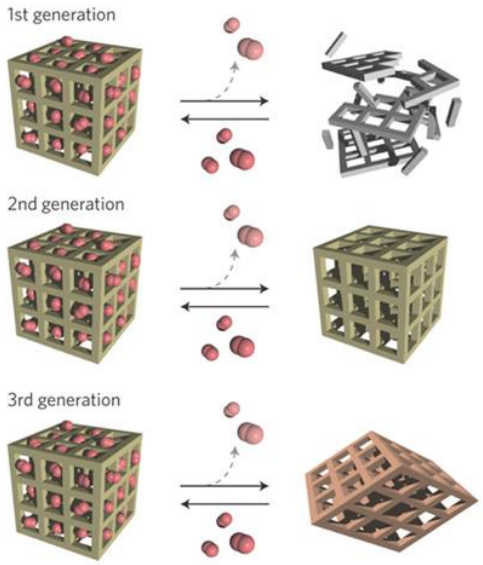

Figure 8. Classification of MOFs into three categories based on their structural stability. The first-generation materials collapse on guest removal. The second-generation materials have robust and rigid frameworks and are stable when the solvent molecules are removed. The third-generation materials reveal a flexible and dynamic structure, which transforms upon the removal of guest molecules.[92] Reprinted from *Nat. Chem.* 2009, *1*, 695, with permission from Macmillan Publishers Limited, Copyright © 2009.

One of the first MOFs, known as MOF-5, $[Zn_4O(bdc)_3]_n$ (bdc^{2-} = benzene-1,4-dicarboxylate), was introduced in 1999 by Yaghi et al.[81] The network consists out of ZnO_4 -tetrahedrons as SBUs, which are connected at each edge with a bdc linkers, forming a cubic structure. The microporous solid exhibits a calculated pore volume of 0.61-0.54 cm^3 and a large BET-surface area of 3800 m^2/g. Notably, MOF-5 was one of the first reported structures, which was stable in absence of guest molecules, so it can be associated as a MOF of the 2nd generation (Figure 8). Another prototypic MOF is HKUST-1 (Hong Kong University of Science and Technology), which is constructed from Cu-dimer based paddlewheels (PWs) linked by tritopic carboxylate btc^{3-} (btc^{3-} = benzene-1,3,5-tricarboxylate) linkers.[93] Interestingly, the axial positions at the Cu-PWs which usually are occupied by water molecules can be removed thermally. This special feature opens the possibility to obtain coordinatively unsaturated sites (CUSs) which might

participate as reactive sites for catalysis or adsorption. Other well-known MOF systems are the MIL-series (MIL = Matériaux de l'Institut Lavoisier),[94] *e.g.* MIL-53, a nanoporous, flexible MOF $[M(OH)(bdc)]_n$ ($M = Al^{3+}$, Cr^{3+}) built from $[M(OH)]_n$ rods connected by bdc^{2-} linkers. The metal-benzenecarboxylate MOFs exhibit BET surface areas of 1100 m^2/g and show a hydrogen storage capacity of 3.8 and 3.1 wt.%, respectively.[94] Through the highly flexible structure it was the first reported MOF showing "breathing behavior". As above mentioned, the huge variety of MOFs arises from the great diversity of available structural buildings blocks, the inorganic SBUs in combination with multi-dentate organic linkers. Some typical SBUs and their corresponding frameworks are shown in Figure 9.

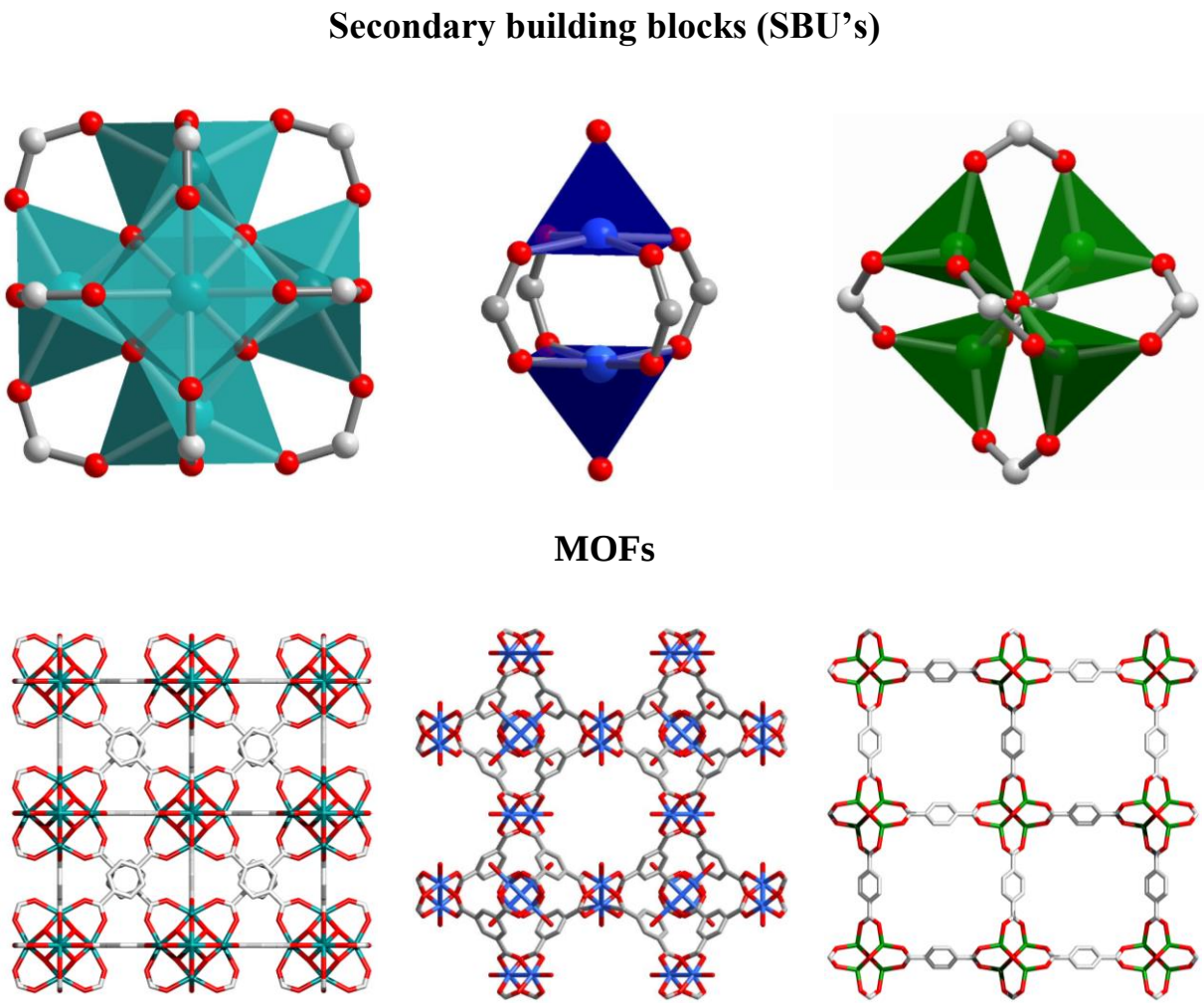

Figure 9. Simplified SBU's (top) in polyhedral design used in the construction of the corresponding MOFs (down). From left to right: Dodecanuclear Zr_6-oxo-cluster $[Zr_6O_4(OH)_4(CO_2)_6]$ → UiO-66, Dinuclear Cu_2-paddle-wheel $Cu_2(CO_2)_4(H_2O)_2$ → HKUST-1 and tetranuclear $Zn_4O(CO_2)_6$ → MOF-5, respectively.

2.3 Zr-based MOFs

Zirconium is a relatively rare transition metal atom found on earth, however, it is more abundant than copper.[95] Among the large growing field of MOFs, Zr-based MOFs are of special interest because of their robustness, thermal and chemical stability, low toxicity as well as tolerance to the incorporation of functional groups.[96, 97] Moreover, Zr is highly resistant to corrosion and has a high affinity for hard oxygen donor ligands, pathing the way to Zr-carboxylate based MOFs. In the decade from 2008-2018, 675 papers have been published dealing with Zr-MOFs and over 211 novel Zr-MOF structures were reported, showing the rapidly growing interest in the discovery of novel Zr-MOFs (Figure 10).[98, 99]

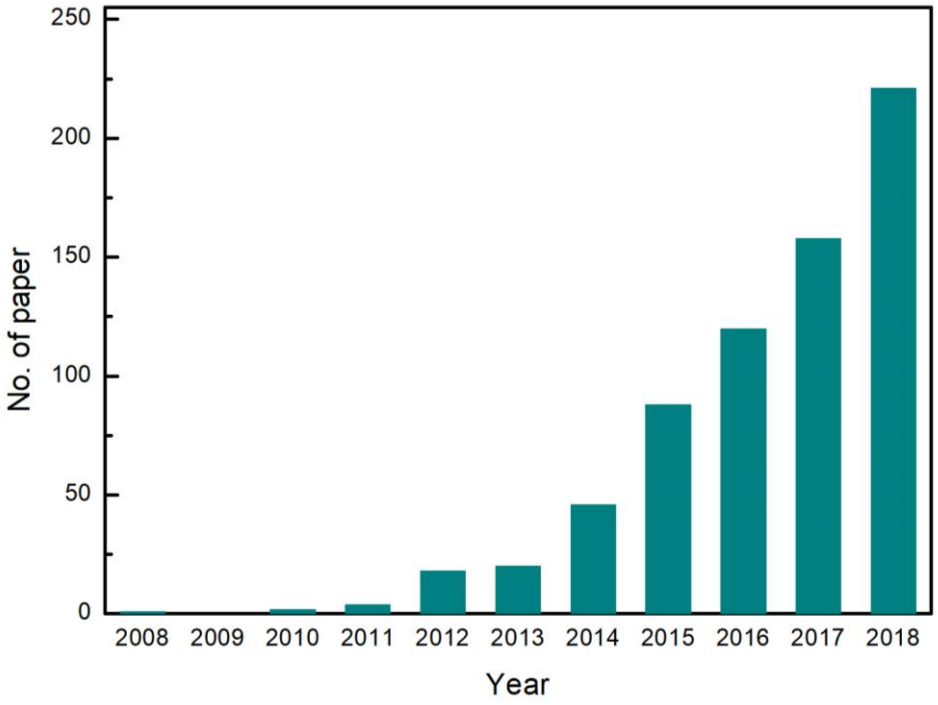

Figure 10. Number of papers published with the search terms 'Zr *MOF' found in the Web of Science database up to the year 2018 (date of access: 18.04.19).

Stability wise, a MOF can be compared to a chain, which metaphorically can be seen as a polymer of self-repeating link-monomers: The overall stability is limited by the weakest parts (bonds) present in their structure, because they are most prone to disintegration. Transferred to MOFs, the weakest parts often are the chemical bonds between inorganic SBU and organic linkers. Following the concept of hard and soft (Lewis) acids and bases theory (HSAB), Zr^{4+} is regarded as a hard Lewis acid, while O^{2-} is a relatively hard Lewis base.[100] The good match regarding size and charge results in the formation of strong Zr-O coordination bonds,[1] which do provide exceptional stability to the framework. Consecutively, the group(IV) transition

[1] The Zr-O bonds, in parts can be seen as relatively strong coordination bonds, however, a significant ionic contribution coming from coulomb interactions of the highly polarized Zr^{4+}- and O^{2-}- ions is expected.

metal (TM) SBUs with high oxidation states Zr_6^{4+}, Ti_6^{4+} and Hf_6^{4+} (UiO-type series) together with $M(III)_3O$-type (M(III) = Fe, Cr, Al; MIL-x series) SBU's can be classified as *hard* Lewis acidic metal-ion nodes, whether SBU's constructed from TM^{2+} (TM's = Zn, Cu, Co, Cd, Mn, Ni) can be considered as *soft* Lewis acidic metal-ion nodes.[101]

Ditopic carboxylate linker MOFs

The first reported Zr-MOF, UiO-66 (UiO = University of Oslo), was introduced in 2008 by Lillerud and co-workers.[96] It is built from octahedral Zr_6-oxo-clusters, which are bridged by ditopic 1,4-benzenedicarboxylate (bdc^{2-}) linkers. In the abovementioned UiO-66, the Zr-oxo-clusters serve as SBUs with a formula known as $[Zr_6(\mu_3\text{-}O)_4(\mu_3\text{-}OH)_4]^{12+}$, whereas six bdc^{2-} linkers compensate the charge. Overall a sum formula of $[Zr_6(\mu_3\text{-}O)_4(\mu_3\text{-}OH)_4(bdc)_6]_n$ is obtained. The Zr^{4+} ions are arranged octahedrally while in the middle of each triangular face, O^{2-} or OH^- is located alternatively, bridging in a μ_3-fashion. This coordination mode leads to triangular pore opening windows with a diameter of 6 Å with respect to the largest spherical compound being able to enter the pore. UiO-66 shows permanent microporosity with a Langmuir surface area of 1187 m^2/g. Compared to other SBU's such as the copper paddle-wheel $Cu_2(OH)_2(CO_2)_4$ from HKUST-1,[102] the tetrahedral $Zn_4O(CO_2)_6$ from MOF-5,[103] and the six-connected $Cr_3O(OH)_3(CO_2)_6$ from MIL-88,[104] the Zr_6-oxo-cluster SBU demonstrates unique structural flexibility. Interestingly, the inner Z_6-core shows reversible dehydroxylation upon activation at elevated temperatures (T > 300 °C, Figure 11). Thus, the $Zr_6O_4(OH)_4$ unit reorganizes itself with slight geometrical changes in symmetry (from T_d to D_{3d}), resulting in the formation of a distorted Zr_6O_6 cluster.[105] This remarkable flexibility allows the preservation of the structural integrity of the SBU upon external stimuli providing stability to the framework without facing collapse.

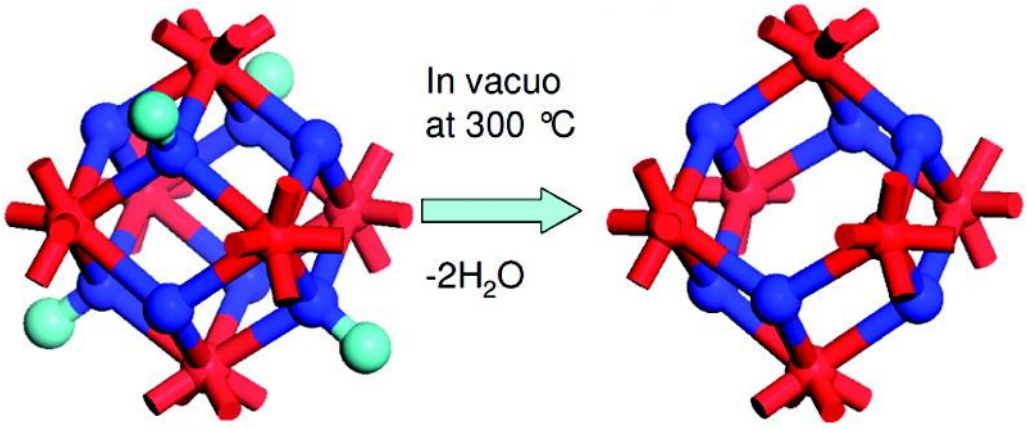

Figure 11. Representation of the geometrical reorganization of the Zr_6-oxo-cluster induced by the dehydroxylation upon thermal treatment.[105] Zr: red, O: blue and H: cyan. Adapted with permission from L. Valenzano, B. Civalleri, S. Chavan, S. Bordiga, M. H. Nilsen, S. Jakobsen, K. P. Lillerud, C. Lamberti, *Chem. Mater.* 2011, *23*, 1700-1718. Copyright (2011) American Chemical Society.

In this regard it is not surprising that UiO-66 shows advanced thermal stability, which was demonstrated by TGA showing a decomposition temperature ~500 °C while most non Zr-

MOFs are only stable up to ≤ 400 °C. Additionally, UiO-66 shows good chemical stability towards water, organic solvents and acids was well as mechanical stability upon treatment with pressure up to 10.000 kg/cm^2.[96] All these properties makes UiO-66 one of the most studied MOF systems so far. However, one intrinsic problem is the small trigonal pore opening window of about 6 Å, which hinders its application *e.g.* in catalysis, due to diffusion limitations. Applying the design principles of isoreticular expansion, enlargement of the linker by using bpdc^{2-} (1,1'-biphenyl 4,4'-dicarboxylate) and tpdc^{2-} (p-terphenyl 4,4″-dicarboxylate) yields UiO-67 and UiO-68, respectively (Figure 12). The larger linkers lead to increase of the pore width to 8 Å and 10 Å, as well as enhancement of the BET surface area to 3000 and 4170 m^2/g, respectively.[96] The obtained 'expanded' analogs of UiO-66, UiO-67 and UiO-68 indeed exhibit larger pore dimensions, while preserving the net topology (ftw) of UiO-66. This might be interesting, because it enables the possibility to embed *e.g.* nanoparticles or other guests into the MOF matrix, resulting in metal@MOF systems which can be applied in catalysis.[106] In contrast to the initial reports of Lillerud et al. in 2008, UiO-67/68 were found to be partly unstable in water which was attributed to linker hydrolysis.

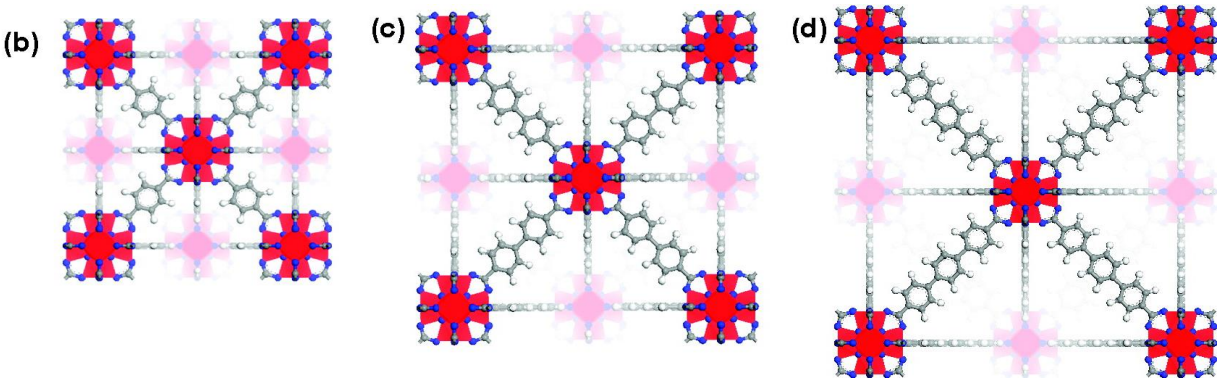

Figure 12. (b) Zr−MOF with 1,4-benzene-dicarboxylate (bdc^{2-}) as linker, UiO-66, (c) Zr−MOF with 4,4′ biphenyl-dicarboxylate (bpdc^{2-}) as linker, UiO-67, (d) Zr−MOF with terphenyl dicarboxylate (tpdec^{2-}) as linker, UiO-68 (Zr, red; O, blue; C, grey; H, white).[96] Reprinted with permission from American Chemical Society (Copyright 2008).

Disintegration of linkers was ascribed to clustering of water molecules close to the Zr_6-oxo-clusters and rotational effects of the extended linkers.[107-109] In UiO-67/68 the linkers are twisted which creates additional steric tension which may facilitate the attack of water leading to hydrolysis of the respective linkers. Additionally, isoreticular expansion may favor catenation and/or interpenetration due to the extended pore dimensions.[110] These findings demonstrate that the isoreticular synthesis which is used to access new MOFs with novel (improved) tailored properties such pore size is a multi-facetted challenge and by far not straight forward. Small changes *e.g.* solubility issues of slightly more non-polar linkers may lead to formation of amorphous product, or as demonstrated in this case, to drastic changes in topological aspects such as linker distortion tension obtained in extended MOFs, namely, the hydrolytic instability of UiO-67.

Tritopic carboxylate linker MOFs

To tackle the problem of small pore sizes, pore dimensions might also be tailored either by topology guided synthesis[99, 111] or be by the degree of connectivity of the respective Zr_6-SUBs. While the NU-110x series and UiO-typed MOFs exhibit the highest possible Zr-oxo-cluster connectivities of 12 (up to now), lower connected Zr-MOFs may offer the advantage to have less sterical hindrance due to less linker density per Zr-oxo-cluster. One example of Zr-MOFs built from tritopic linkers is MOF-808, which is constructed from Zr_6-oxo-clusters interconnected by six tritopic benzene-1,3,5-tricarboxylate (btc^{3-}) linkers containing large adamantane-shaped pores with a pore aperture of 14 Å.[112] Despite the relatively small linker sizes which are very similar to terephthalate linkers used in UiO-66, the pore opening is quite large which can be explained by the altered shape of the pore opening geometry. In UiO-66 the tetra- and octahedral pore cages suffer from small triangular pore opening windows, whereas in MOF-808 the shape of the pore opening is adamantane-like and thus, better accessible. Hence, MOF-808 is more interesting regarding applications in catalysis where large substrates are used, demonstrated in the Meerwein–Ponndorf–Verley reduction (MPV) which is catalyzed by the Lewis acidic Zr_6-oxo-cluster sites.[113] Another remarkable tritopic Zr-MOF which is built from 4,4′,4″-*s*-triazine-2,4,6-triyl-tribenzoate (TATB) linkers, is PCN-777.[114] Due to the extended linkers it features large ~3.1 nm mesopores. Lately, the multidentate linker library was broadened by the utilization of large tetradentate carboxylate linkers. Due to the huge numbers of reported Zr-MOFs only few selected examples are described here. A detailed table containing all Zr-MOFs can be found here.[98]

2.3.1 Porphyrin-based MOFs and their catalytic applications

The well-known homogeneous catalytic capabilities of MPs, especially for oxidation reactions, makes them promising targets for applications as heterogeneous (biomimetic) catalysts.[115] The incorporation of functionalized planar MPs as organic struts gives rise to free redox sites that display catalytic properties.[115] This, combined with the inherent Lewis-acidity of the metal atoms of the SBUs, ideally, gives rise to so-called tandem catalysis. Herein, the two most prominent, oxidation and Lewis acid catalyzed reaction types will be discussed (the aspect of photocatalysis is not included due to its limited relevance for this work).

Oxidation catalysis

In the early 90's Robson and co-workers pioneered network structures which were built from the self-assembly of porphyrins and metal-clusters.[70, 71] However, these microporous solids lack of structural stability since they undergo collapse and loss of porosity upon solvent removal. Therein, Cu(I) and Cd(II) ions were combined with porphyrins containing neutral N-donor ligands (pyridyl), which contrasts with the strong, highly polarized Zr-O bonds formed by negatively charged carboxylates with Zr(IV) found in Zr-based MOFs (see chapter 2.3).

Consecutively, low metal oxidation states and neutral ligand donors form relatively weak metal-ligand bonds which is the main reason for the structural instability of the first-generation of porphyrin solids. Many tetra-pyridylporphyrin based MOF structures have been reported in the past two decades,[116] however, these MOFs are excluded here due to their intrinsic structural instability. Suslick et al. extended this work and reported the discovery of PIZA-1 (PIZA = porphyrinic Illinois zeolite analogue) in 2002 (Figure 13).[117] In this structure, carboxylate-based (instead of pyridyl-based) TCPP(Co) linkers are coordinated in three dimensions to linear trinuclear cobalt(II) nodes. In the context of HSAB theory this example displays a better match in regards of charge and ionic radii of Co^{2+} and O^{2-} which favors the formation of stronger, more polarized metal-ligand bonds. The resulting microporous MOF, along with other structurally similar networks of the PIZA family[118], shows significantly improved stability. It retains its porosity after solvent removal and displays also thermal stability up to ~375 °C, thus, the authors described them as 'robust microporous solids'. PIZA-3 contains trinuclear Mn(II)-clusters which are linked by catalytically active TCPP(MnCl) carboxylate struts spanning a 3D porous network.[118] This was the first example of a porphyrin 3D MOF which was applied as a oxidation heterogeneous catalyst. It was used as oxidation catalyst in moderate to good yields for the hydroxylation of a variety of linear and cyclic alkanes (yields up to 47 %) and the epoxidation of cyclic alkenes (yields up to 74 %) using iodosylbenzene as the oxygen source and imidazole as co-catalyst. Interestingly, similar yields in comparison to other homogeneous Mn-porphyrins were obtained, showing that heterogenized porphyrins can principally compete with their homogeneous analogs.[22] The results from this work demonstrate the feasibility of carboxylate-based porphyrins as building blocks for the rational construction of functional porous solids and encompassed the way to new porphyrin-based MOFs. There are numerous examples of other (metallo)porphyrin-based materials including 1D and 2D coordination polymers,[119, 120] MOFs based on metal-oxides SBU's,[121] Lanthanides SBU's[122], Cu_2[123]- and Zn_2[124]- and Co_2- paddle-wheel (pillard) type SBUs's[125, 126], 3D tecton structures[127] and others known in literature.[128] In the following few representative examples are shown which demonstrate the scope of porphyrin-based MOFs as oxidation catalysts.

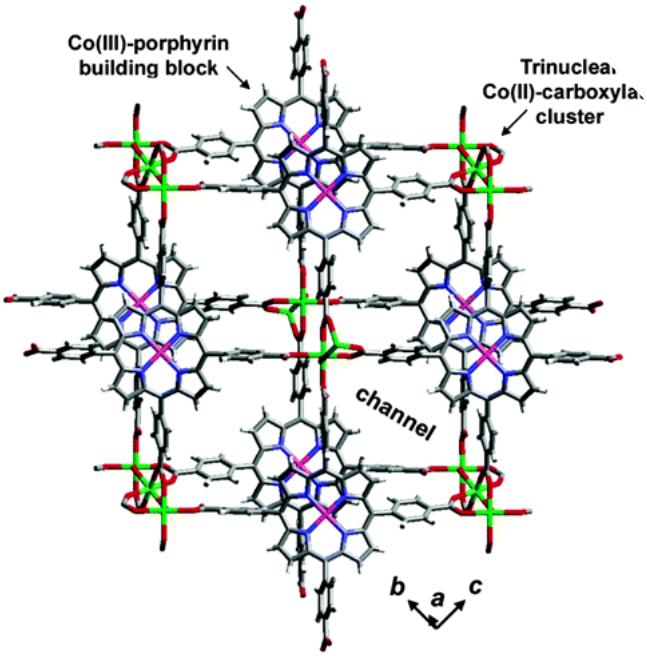

Figure 13. Structure of the PIZA-1 network as viewed along the *a* axis (grey coloring indicates C, red O, blue N, green Co(II) ions in trinuclear clusters, purple TCPP(Co(III)) ions).[117] Reprinted with permission from Nature Publishing Group (Copyright 2002).

Hupp et al. reported on a series robust porphyrinic materials (RPMs) constructed from Zn ions and Zn/Mn-porphyrin units, generally features large channels and thus readily accessible active sites.[129] The Mn-sample was used in the oxidation of cyclohexane proceeded in moderate 20 % yield (1 mol % catalyst) to give a mixture of cyclohexanol and cyclohexanone with good selectivities of 83:17 alcohol/ketone, outperforming homogeneous 5,10,15,20-tetrakis(pentafluoro-phenyl)porphyrin-Mn(Cl). Another example includes the family of metal–metalloporphyrin frameworks (MMPF-x). While MMPF-2, MMPF-3 and MMPF-5(Co) do catalyze the epoxidation of stilbene, MMPF-6 possesses peroxidase activity.[115] The most active epoxidation catalyst, MMPF-3, consists of Co-porphyrins that connect di-nuclear Co-paddlewheel SBUs. Its catalytic activity was found to be superior when compared to its homogeneous Co-porphyrin analog Co(DCPDBPP) ($DCPDBPP^{2-}$ = 5,15-bis(3,5-dicarboxyphenyl)-10,20-bis(2,6-dibromophenyl)porphyrinate).[130] MMPF-3 catalyst showed excellent conversion in the epoxidation of *trans*-stilbene to the epoxide of ~96% and 87% yield, using *tert*-butyl hydroperoxide as oxidant. A MP-MOF displaying size- and shape-selectivity in oxidation catalysis was reported by Wu et al.[131] ZJU-18 (ZJU = Zhejiang University) exhibits highly efficient and selective oxidation of ethylbenzene to acetophenone in quantitative yield. It is based on the octatopic Mn(III)Cl-5,10,15,20-tetrakis(3,5-biscarboxylphenyl)-porphyrin linker and two secondary building units in the form of bi-nuclear $Mn_2(COO)_4$ and trinuclear $Mn_3(COO)_4(\mu\text{-}H_2O)_2$ clusters (Figure 14). Due to its high activity, it was also applied for the oxidation of long-chain alkyl-benzenes, wherein it was observed that conversion decreased with increasing alkyl chain length. Supported by experiments with other substrates,

it was found that larger hydrocarbons are preferentially catalyzed on the surface of the MOF, while smaller molecules may also undergo conversion inside the pores.[131]

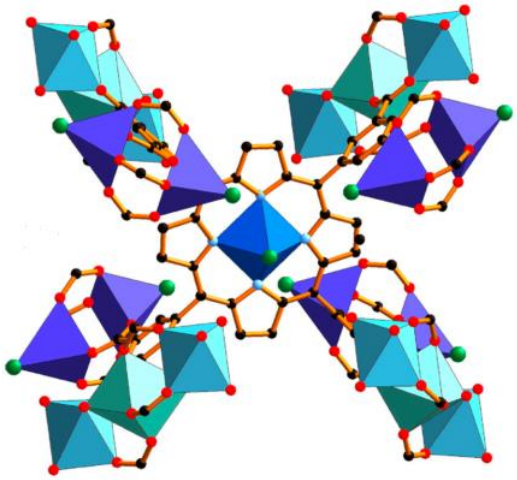

Figure 14. Mn-porphyrin ligand connected to binuclear $Mn_2(COO)_4$ and trinuclear $Mn_3(COO)_4(\mu\text{-}H_2O)_2$ SBUs in the crystal structure of ZJU-18 (black coloring indicates C, red O, light blue N, green Cl, Mn-centered polyhedra are shown in different shades of blue).[131] Reprinted with permission from American Chemical Society (Copyright 2012).

In Scheme 4 other *N*- and *O*-donor porphyrin linkers can be found which were used for the construction MOF structures, showing the huge variety of available organic porphyrin building blocks.

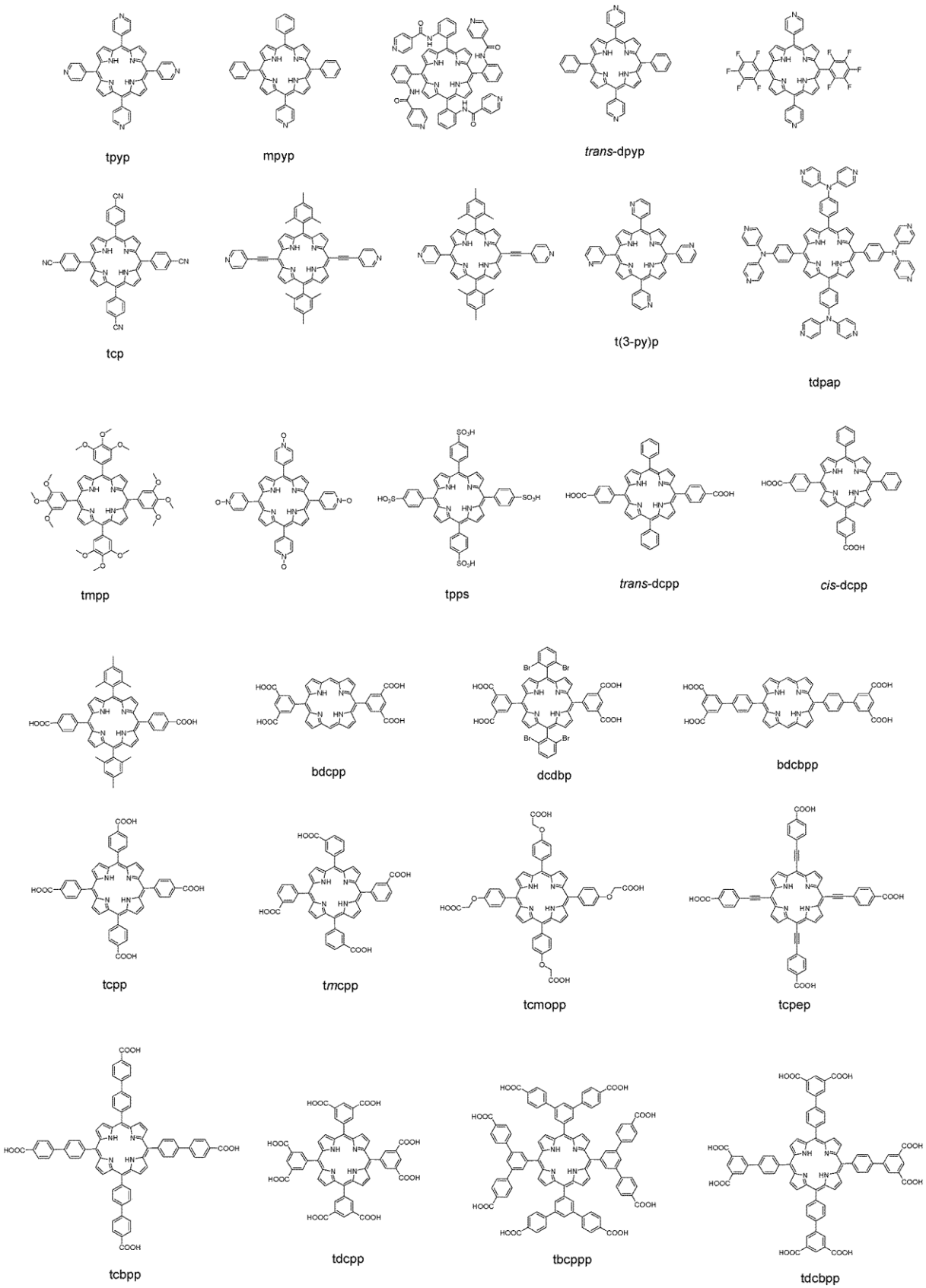

Scheme 4. Porphyrin ligands used in the construction of porphyrinic frameworks (tpyp = 5,10,15,20-tetrakis(4-pyridyl)porphine; mpyp = 5-monopyridyl-10,15,20-triphenylphorphinea; trans-dpyp = 5,15-dipyridyl-10,20-diphenylporphine; tcp = 5,10,15,20-tetrakis(4-cyanophenyl)porphine; t(3-py)p = 5,10,15,20-tetrakis(3-pyridyl)porphine; tdpap = 5,10,15,20-tetrakis(4,4′-dipyridylaminophenylene)porphine; tmpp = 5,10,15,20-tetrakis(3,4,5-trimethoxyphenyl)porphine; tpps = tetrakis(4-sulfonatophenyl)porphine; trans-dcpp = 5,15-di(4-

carboxyphenyl)-10,20-diphenylporphine; cis-dcpp = 5,10-di(4-carboxyphenyl)-15,20-diphenylporphine; bdcpp = 5,15-bis(3,5-dicarboxyphenyl)porphine; dcdbp = 5,15-bis(3,5-dicarboxyphenyl)-10,20-bis(2,6-dibromophenyl)porphine; bdcbpp = 5,15-bis(3,5-dicarboxybiphenyl)porphine; tcpp = 5,10,15,20-tetrakis(4-carboxyphenyl)porphine; tmcpp = 5,10,15,20-tetrakis(m-carboxyphenyl)porphine; tcmopp = 5,10,15,20-tetrakis[4-(carboxymethyleneoxy)phenyl]porphine; tcpep = 5,10,15,20-tetrakis(4-carboxyphenyl)ethynylporphine; tcbpp = 5,10,15,20-tetrakis(4-carboxybiphenyl)porphine; tdcpp = 5,10,15,20-tetrakis(3,5-dicarboxyphenyl)porphine; tbcppp = 5,10,15,20-tetrakis[3,5-bis(4-carboxyphenyl)phenyl]porphine; tdcbpp = 5,10,15,20-tetrakis(3,5-dicarboxybiphenyl)porphine).[132] Published with permission from Royal Society of Chemistry (Great Britain), Copyright 2014.

Lewis-acid catalysis

Next to the discussed biomimetic oxene and carbene group transfer reactions which are by far the most investigated systems, "classical" non-biomimetic Lewis acid catalysis is much less explored. Hence, only few papers are reported on porphyrin MOFs.

Hupp et al. reported on an acyl transfer reaction between *N*-acetylimidazole and 3-pyridylcarbinol, catalyzed by of ZnPO-MOF, a MOF containing Zn-porphyrin linkers.[133] The Lewis acidic Zn metal centers interact with the Lewis basic nitrogen atoms of the respective educts and thus facilitate the nucleophilic addition of the hydroxyl-group to the acyl-function.[133]

The Ma group applied MMPF-9 catalyst, which is built from octatopic Cu-tetrakis(3,5-dicarboxybiphenyl)porphine linkers bridging Cu_2-paddle-wheel (PW) moieties in the chemical fixation of CO_2 to form carbonates under ambient conditions with a yield of 87 % over 48 h.[134] It is believed, that the di-nuclear Cu-PW SBU's as well as the Cu-porphyrin likers contribute to the overall catalytic activity, however, no non-metalated MMPF-9 reference catalyst was reported which would show the separated catalytic contribution coming from the Cu_2-PW's.[134]

Jiang and co-workers reported on a chiral MOF (ps-CMOF) constructed from Cd-porphyrin and chiral Ni-salen mixed-linkers and Cd-paddlewheel SBUs, which served as an effective heterogeneous catalyst for the asymmetric cyanosilylation of aldehydes.[135] Cyanosilylation of benzaldehyde and other aldehydes with electron-donating or electron-withdrawing groups gave conversions of 81–96% and moderate to good enantioselectivities (55–98% ee's).[135] Similar results were obtained by Ma et al., whereby a large variety of benzaldehyde derivatives with electron-withdrawing (−Cl, −CN, and – NO_2) and -donating groups (−Me, −Et, and −OMe) were selected as substrates using a Cd-porphyrin MOF as heterogeneous catalyst.[136] Moreover, the catalyst was used in the Knoevenagel condensation employing benzaldehyde derivatives with malononitrile as substrates. Homogeneous Cd-porphyrin reveal slightly higher catalytic activity (99 vs 95 % yield after 1 h).[136]

2.3.2 Catalytic scope of porphyrin-MOFs PCN-222/224 and MOF-525

Lately, also porphyrin-based Zr-MOFs were reported. Generally, non-metalated porphyrin linkers are obtained by a facile 2-step synthesis and even are commercially available to

relatively reasonable prices (1 g = 108 €, 97 % purity, TCI Chemicals, Product Number A 5015, 20.10.18). Their metalated analogs are synthesized with an additional metalation step. In 2012 and 2013, three different Zr-porpyhrin phases constructed from same the building blocks, (1) stable inorganic Zr_6-oxo-clusters and (2) organic tetratopic (metallo)porphyrin linkers were reported (Figure 15).[137-139] Zr_6-oxo-clusters present in PCN-224, PCN-222 and MOF-525 exhibit altered linker connectivities of 6, 8 and 12 resulting in different linker densities and different pore environments (topologies). While MOF-525 and PCN-224 crystallize in the cubic space group and contain ~2 nm micropores, PCN-222 consists out of large hexagonal mesoporous 3D channels of ~3 nm in diameter and small trigonal micropores with a pore width of 1.3 nm. Similar to described to other Zr-based MOFs, these phases all show high chemically and thermal stability and thus, are suitable candidates for catalytic tests.

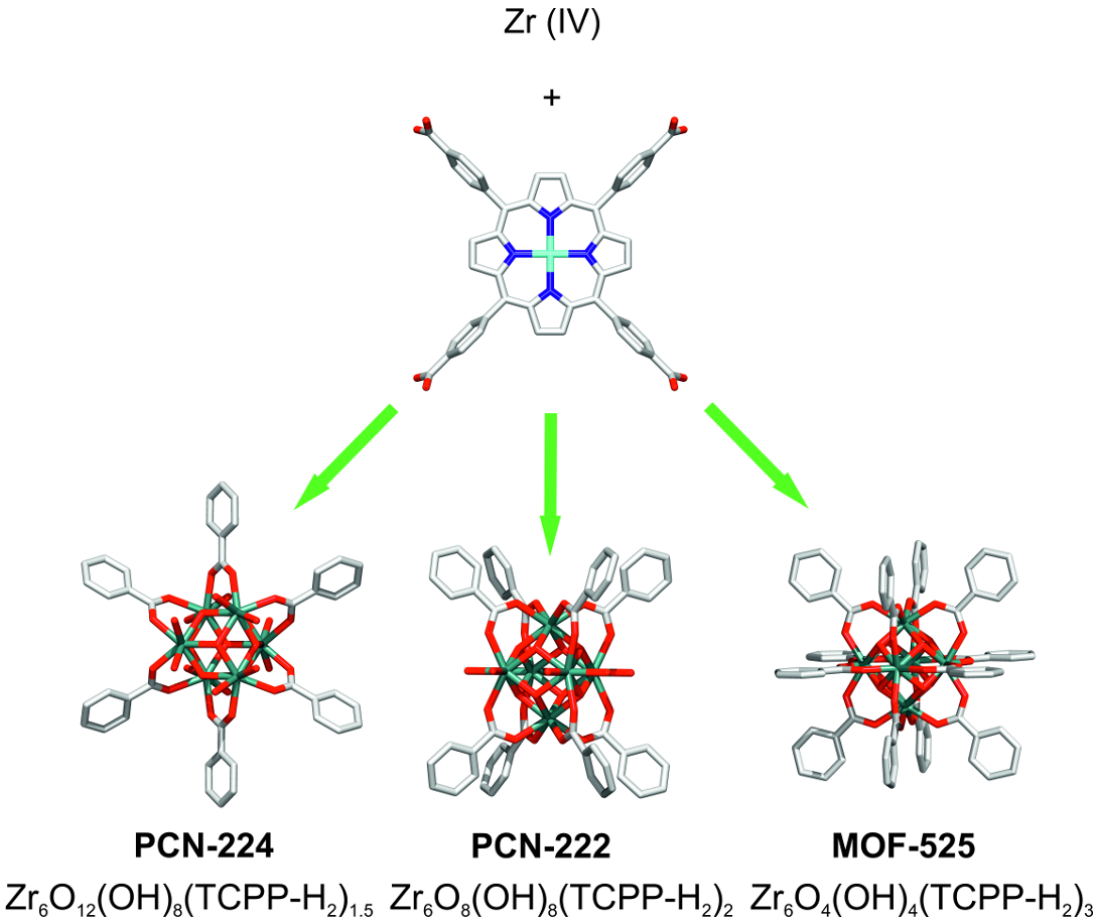

Figure 15. Representation of the three Zr-oxo-cluster based MOFs of different node connectivity selected for this study: PCN-224 with 6 linkers (L6), PCN-222 with 8 linkers (L8) and MOF-525 with 12 linkers (L12) per Zr_6-node, respectively. M-TCPP = 5,10,15,20-tetrakis(4-carboxylatephenyl)-porphyrin (M = metal).[140] Reprinted with permission from Wiley-VCH Verlag GmbH & Co. KGaA, Weinheim, 2018.

Biomimetic oxidation reactions

Since molecular Fe-porphyrins are used as artificial enzymes in biomimetic reactions, solid PCN-222(Fe) was tested accordingly. It shows peroxidase-like activity as demonstrated by Zhou et al. in the oxidation of pyrogallol, 3,3,5,5-tetramethylbenzidine, and o-phenylenediamine, which are considered as model substrates to characterize the catalytic performance of heme-like enzyme mimics,[138] as also independently shown by Ma et al. (Figure 16).[141]

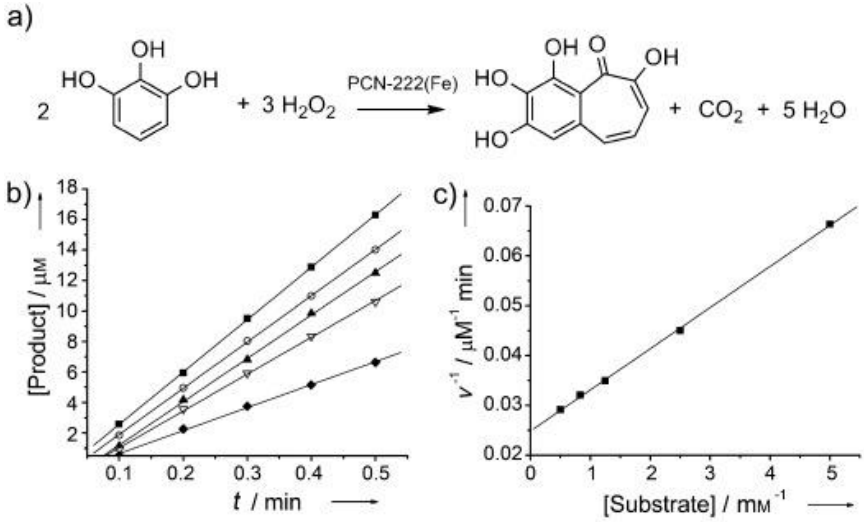

Figure 16. Adapted from.[138] Peroxidase-like oxidation reaction of pyrogallol catalyzed by PCN-222(Fe), in which pyrogallol is oxidized to purpurogallin by hydrogen peroxide. b) The initial pyrogallol oxidation profile catalyzed by PCN-222(Fe) (2.5 µM active site equivalent); the concentrations of pyrogallol shown are 0.2 mM (⧫), 0.4 mM (▾), 0.8 mM (▴), 1.2 mM (○), and 2.0 mM (▪). c) Lineweaver–Burk plot of the pyrogallol oxidation catalyzed by PCN-222(Fe). Copyright © 2015 WILEY-VCH Verlag GmbH & Co. KGaA, Weinheim.

The integration of a high density of isolated catalytic Fe-centers, large open channels paired with high chemical stability of PCN-222(Fe) broadens the path for the design of artificial heme-like enzymes.

In 2015 porphyrin MOFs had been applied as oxidation catalysts employing O_2 as oxidant. Bouchard et al. reported MOF-525(Mn) as catalyst in the epoxidation of styrene and found a remarkable conversion of 99 % and a selectivity of 82 % towards styrene epoxide at rt (Figure 17).[142] The use of molecular oxygen encompasses the way to more green oxidizing agents and the operation of catalytic tests under more industrial relevant conditions. Moreover, MOF-525(Mn) catalyst was found to be stable after six cycles of reaction. Comparison to homogeneous Mn-porphyrin catalyst show slightly decreased catalytic activity (82 to 97 %), however, heterogeneous MOF-525(Mn) catalyst could be separated by facile filtration and re-used up to six additional catalytic cycles without disintegration of the framework which was indicated by PXRD.[142]

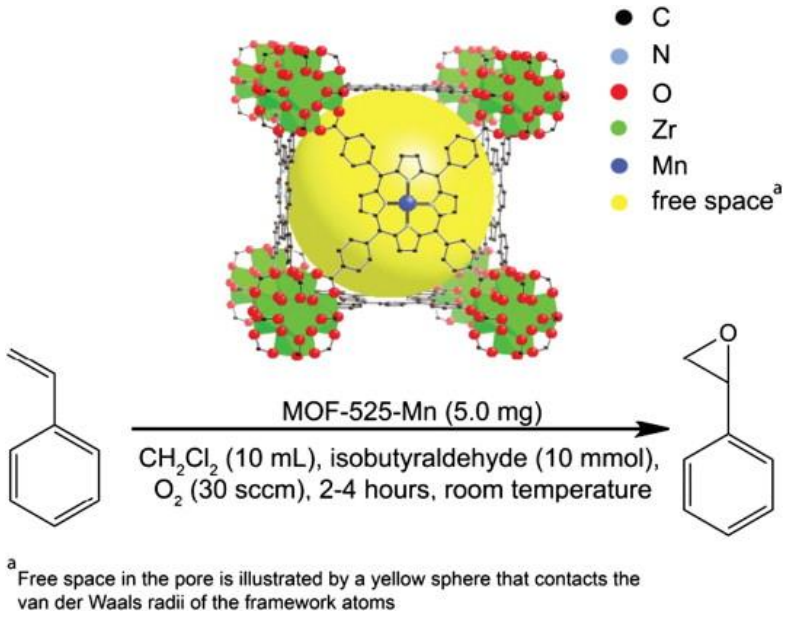

Figure 17. Epoxidation of styrene to styrene epoxide by the use of dioxygen as oxidizing agent under MOF-525(Mn) catalyst.[142] Reprint with permission from Elsevier B.V. (Copyright 2014).

Lewis-acid catalyzed reactions

PCN-224(Co) catalyst was examined in Lewis acid catalyzed CO_2 insertion into epoxides reported by Zhou and co-workers.[139] Therein, the authors described insertion of CO_2 into propylene epoxide at 20 bar CO_2 pressure and 100 °C using $^{n}Bu_4NCl$ as co-catalyst. As a result, the cyclic carbonate was obtained with a conversion ~40 % and TOFs ~120 h^{-1}. Molecular Co-porphyrin catalyst reveal comparable catalytic activity, similar to PCN-224(no metal) which was only slightly less active than PCN-224(Co). Consecutively, it is not clear what role the Co-porphyrin linkers in PCN-224(Co) plays, since it can be anticipated that the Zr-oxo-clusters significantly participate in the reaction as Lewis acidic centers. Moreover, even UiO-66 without any Co-sites and many other MOFs do catalyze the CO_2/epoxides coupling reaction under ambient conditions such as rt and atmospheric CO_2 pressure.[143]

Summarized, chemically and thermally stable Zr-porphyrin MOFs are suitable candidates for biomimetic as well as Lewis acid mediated catalysis. Hence, these MOFs had been applied in various reactions bearing reactivities which are comparable to their homogeneous counterparts.

The combined catalytic properties such as the (i) inherent Lewis acidity from the Zr_6-oxo-clusters and (ii) the biomimetic oxidation properties derived from the metalloporphyrin struts principally allow their application in tandem-like reactions, whereby two distinct catalytic sites contribute to a two-step reaction process.

2.4 Tandem catalysis

Generally, an orthogonal tandem reaction is defined by the presence of two catalytic sites or catalysts from the beginning of a reaction (1). These sites or catalysts undergo two distinct chemical transformations (2) under identical reaction conditions (3) (Scheme 5). These criteria make tandem catalysis fundamentally different compared to related terms such as cascade or domino type of reactions, whereby the two catalytic transformations are not operated synchronically but sequentially.[144]

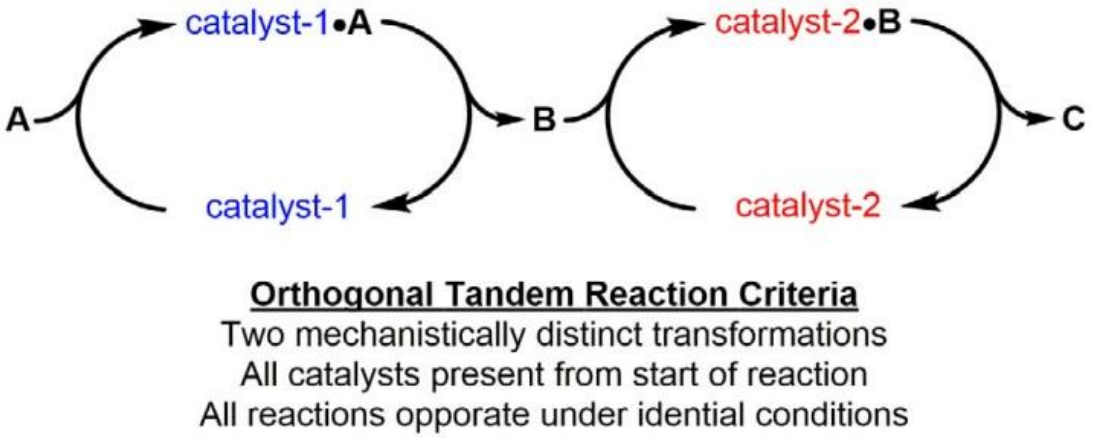

Scheme 5. General scheme of the definition of orthogonal tandem catalysis.[144] Reprinted with permission of John Wiley and Sons (Copyright 2016).

Thus, the mentioned requirements are intrinsically difficult to achieve, because often every separate reaction requires their own specific, optimized conditions (temperature, pressure, solvents, pH value etc). These reaction conditions might interfere with the conditions of another reaction which may lead to catalyst deactivation or inhibition of reaction intermediates. The great benefit of such catalytic tandem or one-pot reactions is that a reaction product B does not need to be purified or separated from the reaction mixture but undergoes the in-situ transformation to product C (see Scheme 5). This saves an additional reaction step and helps to reduce costs, making the reaction more economical. Therefore, tandem catalysis can be seen as a “high-risk, high-gain” scenario. Conceptually, MOFs exhibit an excellent platform for rational catalyst design. Their exceptional tailorbility and structural diversity enables the integration of two or more distinct catalytic sites by means of *de novo* synthesis or post-synthetical methods. Consecutively, only one catalytic system decorated with two or more catalytically active sites is obtained instead of two or more individual catalysts. Due to the rigidity of the framework, the catalytic sites are well-defined, separated (site isolation) which may prevent deactivation. Moreover, a MOF-based catalytic tandem system principally is heterogeneous which facilitates the separation of the catalyst from the reaction solution (in liquid phase) making the process more feasible and cheaper. In terms of limited resources this aspect of green chemistry becomes more and more important.

Previous work on tandem catalysis using a Hf-porpyhrin MOF, NU-1000, was reported by Hupp and co-workers.[145] Therein, the authors described the tandem epoxidation/ring-opening reaction of styrene, whereby molecular oxygen was employed as oxidizing agent. Oxidation of styrene was catalyzed by the Fe-porphyrin linkers and the ring-opening reaction of styrene epoxide occurred via reaction at the Lewis acidic Hf-nodes (Figure 18).

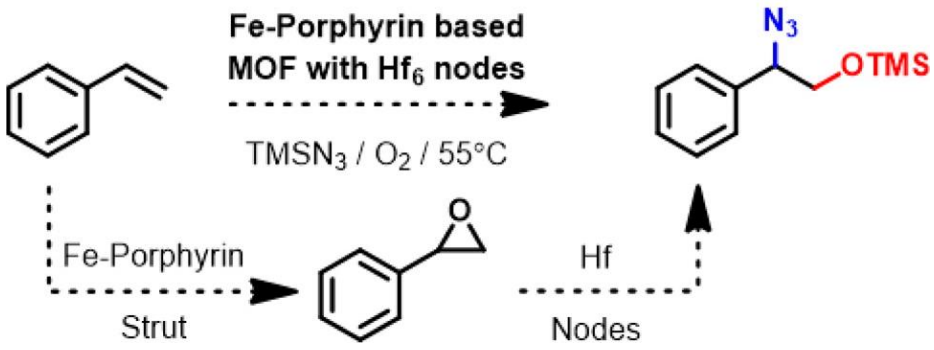

Figure 18. Proposed epoxidation/ring-opening tandem reaction of styrene. Fe-Porphyrin struts catalyze the epoxidation (1), while Lewis acidic Hf-nodes do catalyze the ring-opening of the generated styrene epoxide to give protected 1,2-hydroxylamine (2).[145] Reprinted with permission from American Chemical Society (Copyright 2015).

The end-product was obtained with a conversion of 100 % and an NMR-yield of 53 % (based on styrene). The same group also reported on the tandem olefin epoxidation/CO_2-insertion reaction using *p*-methoxystyrene as substrate and 1-(tert-butylsulfonyl)-2-iodosylbenzene as the terminal oxidant.[144] The corresponding cyclic carbonate was obtained with a yield of 60 % under quite harsh conditions, namely, 60 bar CO_2 pressure and 65 °C. The blind test gave a rather high yield of 20 %, indicating that the reaction proceeds with moderate yields even in the absence of any catalyst. These proofs of concepts demonstrate the great potential towards the development of novel tandem catalytic systems which is achieved by the implementation of two independent catalytic sites into the scaffold of the MOF. For potential commercial application, however, it is also important to utilize reagents which exhibit less hazardous risks and lower waste potential. Notably, azidotrimethylsilane ($TMSN_3$) is incompatible with moisture, oxidants, and acids. It may hydrolyze to hydrazoic acid (hydrogen azide) which is an extremely toxic and explosive material.[145] Moreover, many reports focus on the use of iodosylbenzene derivatives as mono oxygen-transfer reagents, which are highly active oxygen donors even at rt, however, they produce intrinsically organo iodine waste and might be explosive.[146, 147] So it is not surprising that their use is preferentially relevant for academic research.

3 Lewis acid catalysis

Abstract

Catalytic studies on different phases of stable Zr MOFs featuring same building units, namely, inorganic Zr-oxo-cluster nodes and organic metalloporphyrin linkers have been performed. Emphasis was given in the study of catalyst design strategies to introduce multi-functionality into porphyrin-based Zr MOFs and how these novel properties effect the performance of the catalysts. Focus was laid on the investigation of the catalytic impact upon metalation and Zr-oxo-cluster connectivity dependent catalytic activity of the different Zr MOF phases which was evaluated in the Lewis acid catalyzed carbon dioxide insertion into epoxides (1). Additionally, confinement effect dependent stereoselectivity of PCN-224(Rh) catalyst was investigated in the asymmetric cyclopropanation of styrene using ethyl diazoacetate (2). Thereby, the role of pore size and topology of achiral PCN-224(Rh) and PCN-222(Rh) catalysts were elaborated. Further, the tuning of intrinsic Lewis acidic properties of PCN-222(no metal) catalyst achieved by installation of new Mn-centers located at the porphyrin linkers were tested in the cyanosilylation reaction using benzaldehyde and trimethylsilyl cyanide (3).

3.1 Cyclic addition of CO_2 in epoxides using PCN-222/224, MOF-525 catalysts[1]

Abstract

Three Zr-oxo-cluster node and porphyrin-linker based MOFs, MOF-525, PCN-222 and PCN-224 exhibiting different linker connectivities of 12, 8 and 6 and their porphyrin-linker metalated analogues, were synthesized and tested as catalysts for CO_2 fixation by using the cycloaddition of CO_2 and propylene oxide to propylene carbonate as the test reaction. In general, the catalytic activity correlates with the connectivity of the Zr-oxo nodes. The lowest connected PCN-224 (6-fold) exhibits a superior catalytic activity in this series, while higher connected PCN-222 (8-fold) and MOF-525 (12-fold) are less active. Interestingly, the catalytic activity of the higher connected MOFs significantly depends on defects. The (ideally) 12-connected MOF-525, however exhibiting 16 % of missing linker defects, features a higher catalytic activity compared to the 8- connected PCN-222 with less defects. The overall catalytic activity is increased in dual site catalysts when the porphyrin linkers are metalated with Mn(III) and Zn(II) centers, which are acting as additional Lewis acid sites. Here, the metalated MOFs with higher connectivity exhibit the highest activity.

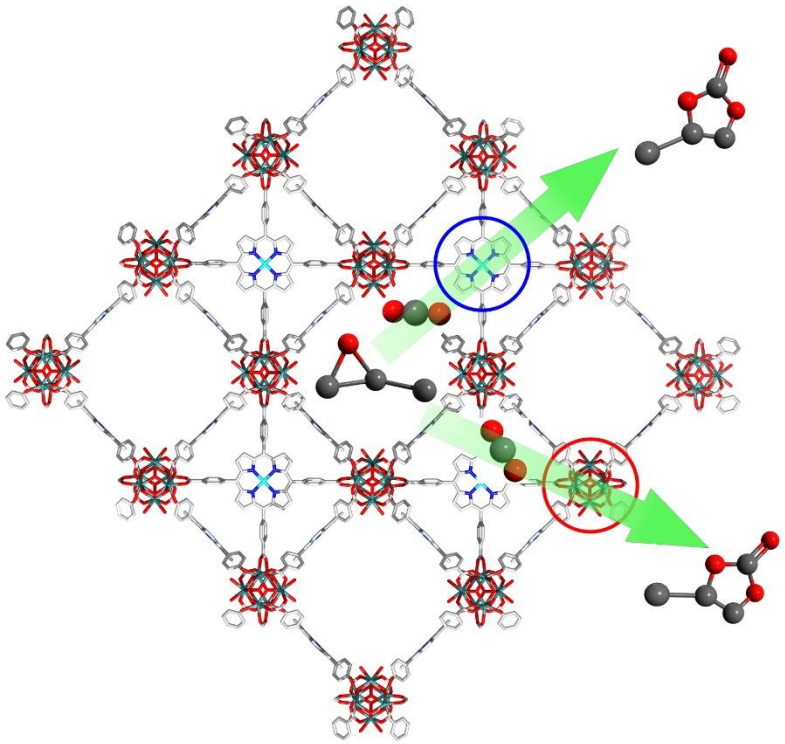

[1] This section corresponds to the published article: 'Dual Site Lewis-Acid Metal-Organic Framework Catalysts for CO_2 Fixation: Counteracting Effects of Node Connectivity, Defects and Linker Metalation'. K. Epp, A. L. Semrau, M. Cokoja, R. A. Fischer *ChemCatChem* 2018, 10, 3506–3512. Reprinted with permission from Wiley-VCH Verlag GmbH & Co. KGaA, Weinheim, 2018.

3.1.1 Introduction

Zr-MOFs represent a particularly interesting class of materials, which are increasingly being studied as model systems in catalysis.[148, 149] The inorganic node exhibits both Lewis acidic (Zr) and Brønsted acidic sites (Zr-OH) and therefore, Zr-MOFs are investigated as catalysts for various reactions requiring such catalysts.[150-152] One possibility to modify the intrinsic reactivity of the Zr_6-node of a given Zr-MOF is to create quasi-free coordination sites at the nodes by using modulators, such as monocarboxylic acids, during solvothermal synthesis.[153]

This approach primarily leads to local defect structures, called missing linker- or even missing node defects. Hence, the Zr_6-nodes are more Lewis acidic and more accessible for substrate molecules, so the catalytic activity is enhanced.[154-156] Furthermore, it is known that within the family of Zr-MOFs, different organic linkers not only lead to a variety of topologies and structures, but also the Zr_6-nodes differ in connectivity and coordination space at the proximity of the nodes. Connectivity is defined as the (ideal) number of organic linkers bridging the respective Zr_6-nodes to yield the specific framework topology. To date, the following systems are known: 12-fold (i.e. for UiO-66/-67,[96] MOF-525[137]), 10-fold (i.e. for MOF-802[157]) 8-fold (i.e. for NU-1000,[158] PCN-222[138]) and 6-fold (i.e. for MOF-808,[159] PCN-224[139]). From the conceptional point of view of this study, a lower-connected Zr_6 node (e.g. 6-fold) can be viewed as 'inherently defective' due to the lack of linkers, compared to the highest connected system with an ideal number of 12 linkers per node. Thus, lower connected Zr-MOFs are expected to be more reactive as compared to the 12-connected UiO-MOFs with a coordinatively saturated Zr_6-node. Hupp et al. reported the increase in catalytic activity with decreasing connectivity of $Zr_6(Hf_6)$-nodes using NU-1000, PCN-57, UiO-66/67 and MOF-808, which were tested in the Brønsted acid-catalyzed ring opening of styrene oxide.[160] The authors showed that 12-connected Zr_6-nodes without measurable defects expectedly exhibit a poor catalytic activity, while defects strongly contribute to the catalytic activity, due to additional Brønsted acidic –OH groups bounded to the Zr_6/Hf_6-oxo-clusters.

Beyond these effects, however, it is important to consider the role of the organic linkers of the investigated MOF types, such as differences in pore sizes and design (pore environment), as well as in hydrophilicity/hydrophobicity, which parameters might influence the penetration (diffusion), adsorption of substrates and solvents and thus may be crucial for the catalytic activity. In a comparative study, ideally, the MOFs should have the same topology and pore sizes and the only difference should be the degree in connectivity of the Zr_6-nodes and all other side variables can be excluded.

Following the above outlined concept of modulating the properties of MOFs for Lewis acid-catalyzed reactions, investigation of the combination of two reactive sites in MOFs, the Zr_6-nodes on the one hand and the introduction of additional metal centers placed at the linkers on the other hand may provide a bi-functional catalyst. The independent control of the abundance

of both sites and to distinguish between the effects of each site on the overall catalytic activity, is intrinsically difficult and may be not that straight forward but would path a way to a rational catalyst design strategy. For example, some new 8-connected Zr-based MOFs with cyclam-based linkers containing Cu or Ni centers may also feature dual reactive sites.[18] However, the synthesis of these MOFs is only possible when the cyclam moiety of the linker is metalated prior to the MOF formation, since the cyclam macrocycle itself is too flexible to provide a regular framework structure. Hence, in this case independent control of the abundance of each Lewis acid site is not possible. In this context, porphyrin-based MOFs offer the great opportunity that their non-metalated linkers can easily be synthesized.

Figure 15 displays the Zr-MOFs, which were selected for this study: MOF-525 (Zr_6L_{12}-nodes; O_h-symmetry), PCN-222 (Zr_6L_8-nodes; D_{4h}-symmetry) and PCN-224 (Zr_6L_6-nodes; D_{3d}-symmetry). All Zr-MOFs exhibit the tetratopic porphyrin linker 5,10,15,20-tetrakis(4-carboxyphenyl)porphyrin) (L = H_4TCPP-2H) and feature the nodes $Zr_6(O)_a(OH)_b$ of different connectivity.

As test reaction, the Lewis acid catalyzed coupling reaction of propylene oxide and carbon dioxide was selected, which is a relevant reaction towards the utilization of CO_2 as building block in the synthesis of further value-added products. Recently, MOFs were also applied as catalysts for this reaction.[139, 143, 161] In this context, Zr-MOFs are exceptionally suitable candidates due to their high thermal and mechanical stability and their large surface areas, which facilitate diffusion of substrates. Beyond the abovementioned chemical tunability of MOFs, another advantage of using these materials in this reaction might be due to their general ability to adsorb CO_2 and enrich its concentration at the catalytically active metal centers,[162, 163] most recently found for MOFs with porphyrin linkers.[164] However, the CO_2 adsorption is strongly temperature dependent and consequently small differences in the CO_2 absorption properties are expected to have a relatively low impact on the catalytic activity when the reaction is carried out at elevated temperatures. The effects of the degree of connectivity of the Zr_6-nodes together with the introduction of defects and combined with the presence of additional Lewis–acid metal sites on the catalytic activity have not been studied to date. In particular, it was shown that Zr-MOFs with Zn(II) and Mn(III) metalated porphyrin linkers, similar to the homogeneous congeners, yield enhanced catalytic activity for the higher connected and less defective Zr-MOFs.[16]

3.1.2 Synthesis and Characterization

The porphyrin linkers, the materials MOF-525, PCN-222 and PCN-224, as well as their metalated analogs were synthesized according to published procedures.[137, 139, 165] Briefly, Zr-salts were combined with (metallo)porphyrin linkers in a modulator (monocarboxylic acids) containing solution of DMF/DEF which were heated in an oven (65-120 ºC) for 1-3 days. The obtained porphyrin-linker metalated Zr-MOFs(M) were phase-pure and isoreticular to the parent Zr-MOFs, as shown by powder X-ray diffraction (PXRD) (Figure 19).

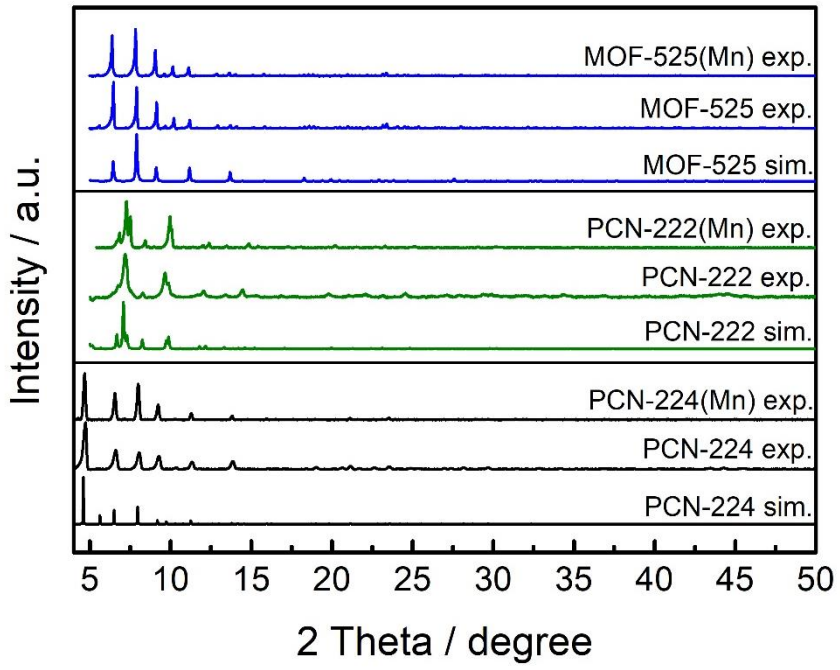

Figure 19. Experimental powder X-ray diffraction (PXRD) patterns of PCN-224, PCN-222 and MOF-525 in comparison to their simulated and metalated analogues.

Table 1. Surface areas and pore sizes.

MOF	BET-surface areas [m^2/g]	Pore-sizes [nm]
PCN-224	2286	1.1, 2.0
PCN-224(Mn)	1982	1.0, 1.9
PCN-222	1706	1.3, 3.0
PCN-222(Mn)	2037	1.3, 3.0
MOF-525	2273	1.2, 1.9
MOF-525(Mn)	2317	1.0, 1.9

The Zr-MOFs(M) feature BET surface areas which are comparable to non-metalated MOFs in the range around 1700-2300 m^2/g (see Table 1), therefore, similar diffusion rates were expect, excluding mass transport dependent effects on the observed catalytic properties of the different systems discussed below.

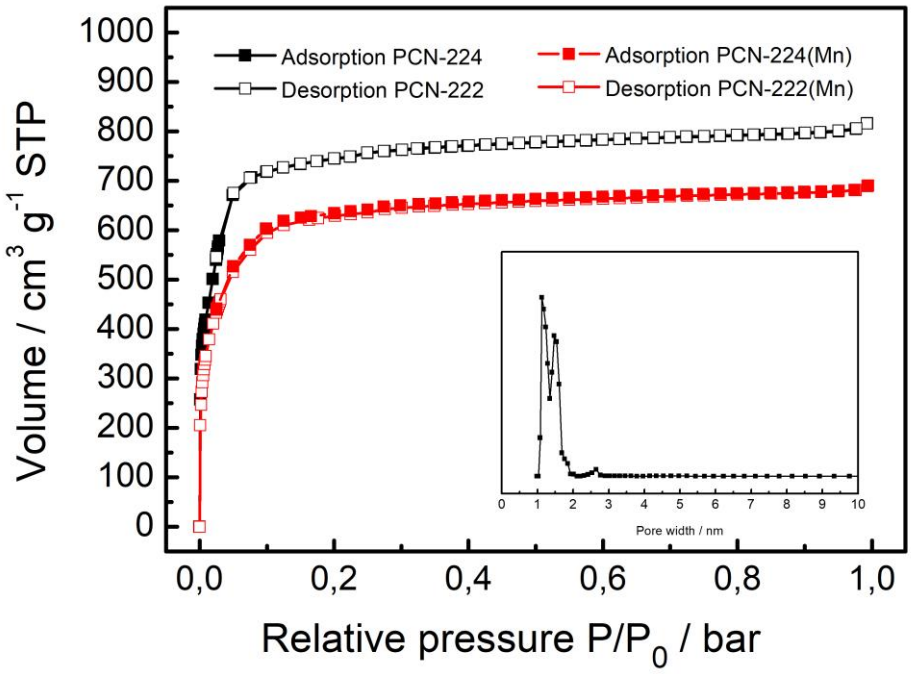

Figure 20. N_2-physisorption isotherms of PCN-224 (black) and PCN-224(Mn) (red) at 77 K. Adsorption and desorption branches are shown with closed and open symbols, respectively. The inset highlights the pore size distribution (PSD) of PCN-224, which is also representative for PCN-224(Mn).

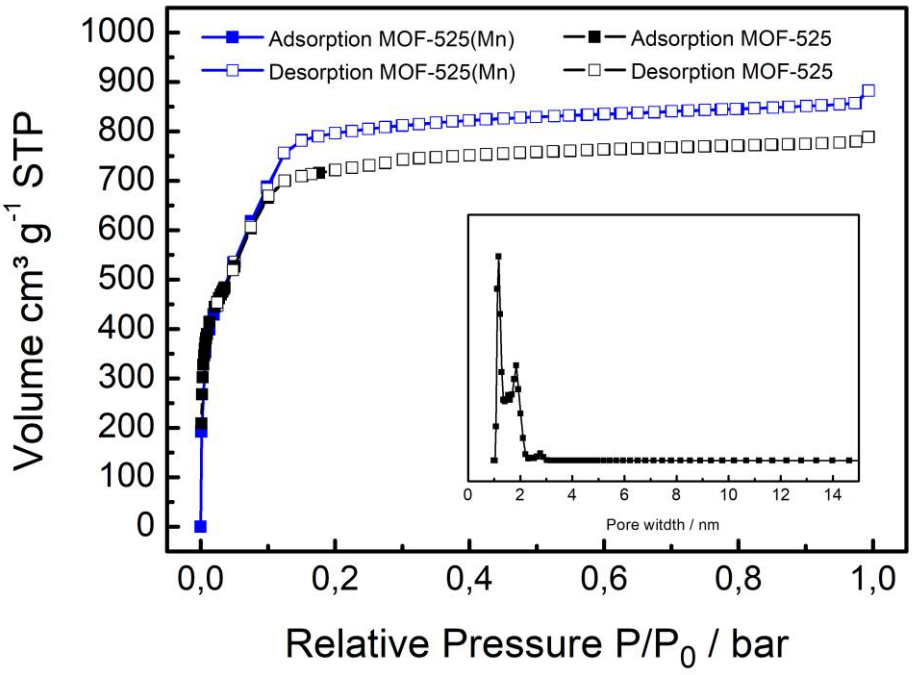

Figure 21. N_2-physisorption isotherms of MOF-525 (black) and MOF-525(Mn) (blue) at 77 K. Adsorption and desorption branches are shown with closed and open symbols, respectively. The inset highlights the pore size distribution (PSD) of MOF-525, which is also representative for MOF-525(Mn).

PCN-224 (Figure 20) and MOF-525 (Figure 21) and their metalated analogs show similar type I isotherms and two differently sized micropores with pore widths of ~1.3 and ~1.9 nm, respectively. First the small micropore is filled with N_2 (0 bar), followed by the filling of the bigger micropore (0-0.13 bar) until a saturation behavior is observed indicating complete pore filling and multi-layer N_2-adsorption. Additional pore size distribution analysis based on DFT calculations, are consistent with shape and type of the experimental isotherm (see insets). Similar to the other MOFs, PCN-222 show the initial pore filling in the low-pressure region which can be attributed to the ~1.3 nm trigonal micropores. Contrary, PCN-222 MOF show a deviation of the standard type I isotherm which is reasoned by the presence of the large hexagonal ~3 nm mesopores (Figure 22). This finding is expressed by an additional step in the isotherm at around 0.2-0.25 bar. Almost no hysteresis is observed due to the 3-dimensionality of the pore channels, which is typically found in 1-dimensional materials *e.g.* mesoporous silica.

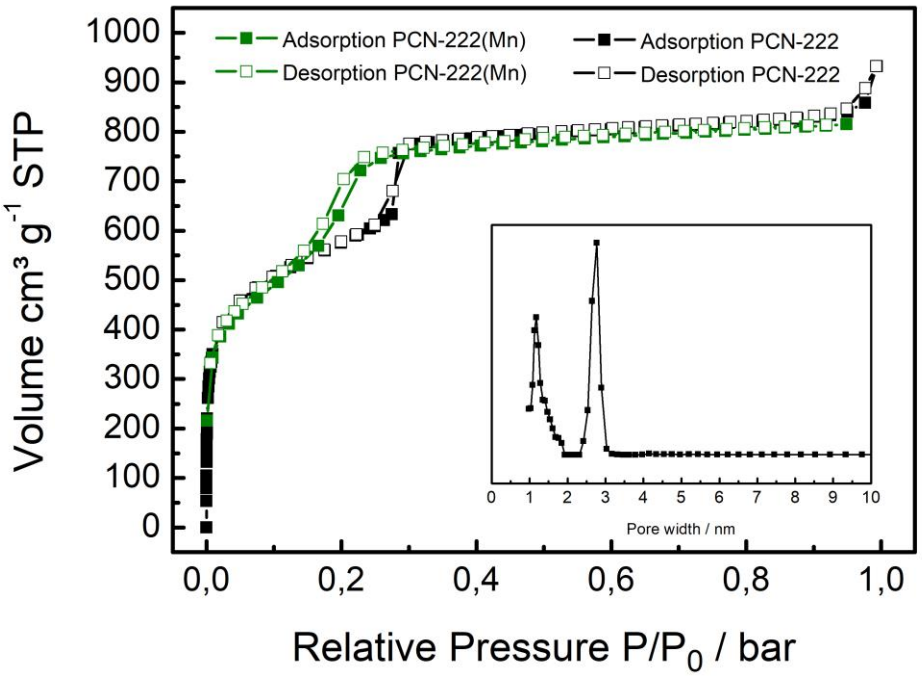

Figure 22. N_2-physisorption isotherms of PCN-222 (black) and PCN-222(Mn) (green) at 77 K. Adsorption and desorption branches are shown with closed and open symbols, respectively. The inset highlights the pore size distribution (PSD) of PCN-222, which is also representative for PCN-222(Mn).

Furthermore, infrared spectroscopy confirmed the absence of bands which are associated with free carboxylic acid groups (indicating un-reacted porphyrin linker) and show now additional vibrational bands after porphyrin metalation (Figure 23).

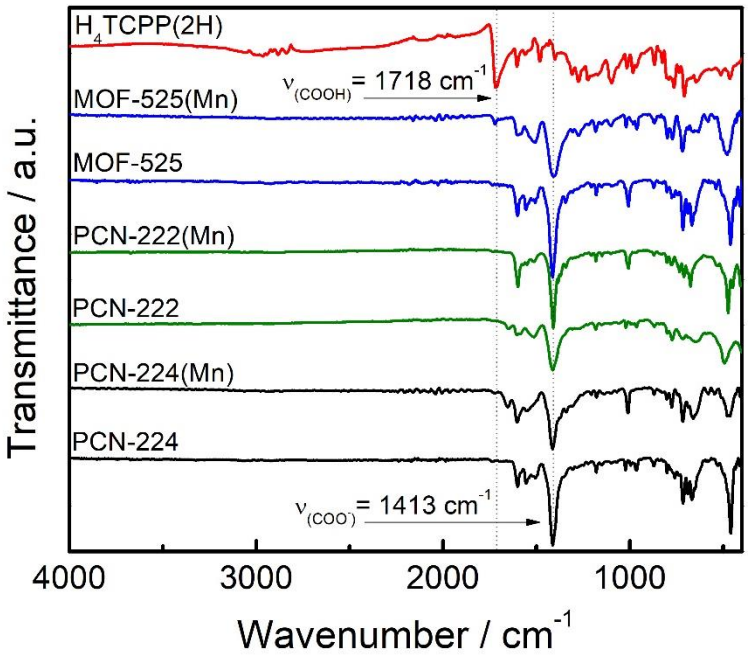

Figure 23. Infrared spectra of MOF-525, PCN-222, PCN-224 and their Mn-metalated analogs in comparison to the free porphyrin linker H_4TCPP(2H). The dotted line at 1718 cm^{-1} indicate the free -COOH vibrational band and the other at 1413 cm^{-1} can be assigned to the coordinated $-COO^-$ group (asymmetric stretching).

Free carboxylic acid bands are usually found in the region around 1600-1750 cm^{-1}. Deprotonated, negatively charged carboxylate groups are typically shifted towards lower wavenumbers ~1300-1420 cm^{-1} (asymmetric stretching vibration), which indicate their coordination to a metal and successful incorporation into the framework (Figure 23).[166]

To access the thermal stability of the MOF series, thermogravimetric analysis (TGA) was applied. Due to the similar thermal decomposition behavior and stability of MOF-525, PCN-222 and PCN-224, herein, PCN-222 and PCN-222(Mn) are shown exemplary (Figure 24).

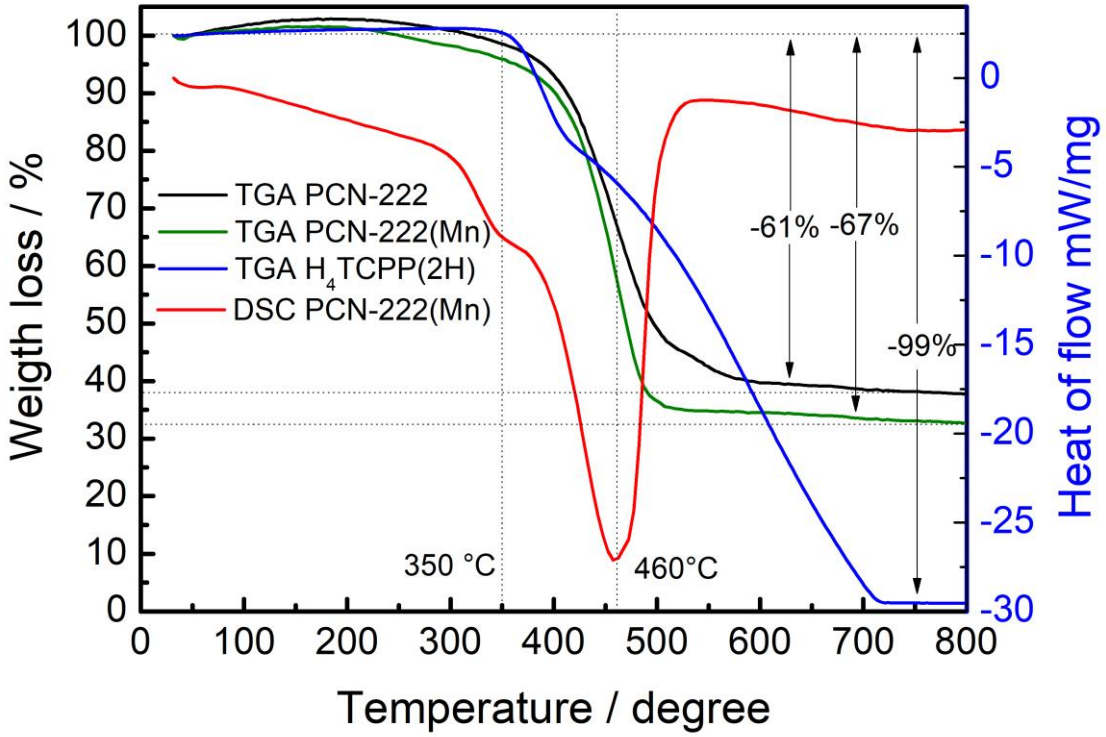

Figure 24. Thermogravimetric analysis (TGA) under synthetic air (80 % N_2, 20 % O_2) of activated PCN-222 (black), PCN-222(Mn) (green) in comparison to porphyrin linker (H_4TCCP(2H)) (blue). The red line shows the differential scanning calorimetry (DSC) curve of PCN-222(Mn). Respective mass losses and decomposition temperatures are highlighted with arrows.

Thermally pre-activated PCN-222 show a decomposition temperature onset at around 350 °C, which was attributed to the decomposition of the organic porphyrin. This was confirmed by TGA of the molecular porphyrin (Figure 24, blue) which shows a very similar decomposition onset with complete decomposition to volatile products (CO_2 etc.) at 700 °C. PCN-222(Mn) reveal comparable thermal stability as PCN-222 upon full degradation to mainly ZrO_2 at around 500-550 °C. The decomposition of the MOFs is accommodated by the typical exothermic heat release which was demonstrated by parallel differential scanning calorimetry (DSC) experiments showing a relatively sharp curve with a maximum at 460 °C. These findings highlight the good thermal stability of the investigated Zr MOFs(M) series which is typical for Zr-based MOFs and makes them attractive candidates for various applications.

3.1.3 Catalytic studies

First, non-metalated Zr-MOFs were selected as catalysts to examine the effect of the nominal connectivity of the Zr_6-nodes on the catalytic activity. The amount (mass) of Zr-MOF-catalyst used in all catalytic test reactions was normalized to the same molar amount of Zr in order to allow the comparison of the specific activities. The catalytic reactions were performed using activated Zr-MOFs (at least 24 h at ≥ 120 °C in dynamic vacuum of 10^{-3} mbar). This treatment ensures that the OH-groups attached to the Zr-nodes are mostly removed, which is confirmed by IR spectroscopy (Figure 23) and thus a significant Brønsted acidic catalyst contribution is excluded.[56] The obtained results are in line with the presented general working hypothesis that low-connected Zr-MOFs should exhibit better accessible and thus more reactive Zr(IV) centers. Indeed, PCN-224 is the most active Zr-MOF among the series (Figure 25, left), reaching quantitative yield of propylene carbonate (100 % selectivity) within 24 h at 50 °C and 1 bar CO_2 and 10 mol% NBu_4Br as co-catalyst.

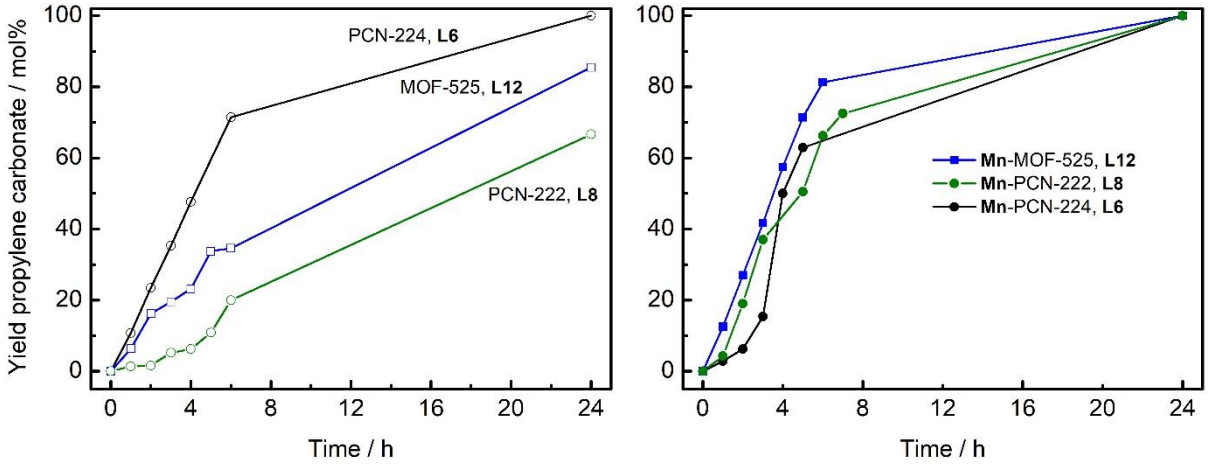

Figure 25. Time-yield plots of the reaction of CO_2 with propylene oxide to propylene carbonate using PCN-224, PCN-222 and MOF-525 as catalysts (left) in comparison to their Mn-metalated analogues (right) at 1 bar CO_2 and T = 50 °C with 10 mol% Bu_4NBr as a co-catalyst (see also Table 2). The nominal node connectivity (number of coordinated linkers) is depicted as L6, L8 and L12.

Table 2. Catalytic reaction parameters.

Catalyst	TOF [1/h]	Yield[a] [%]	co-cat[b] [mol%]	Zr [mol%]	T [°C]	p [bar]
PCN-224	124	99	10	0.1	50	1
PCN-224	210	99	10	0.1	50	4
PCN-224(Mn)	104	99	10	0.1	50	1
PCN-222	18	66	10	0.1	50	1
PCN-222(Mn)	85	99	10	0.1	50	1
PCN-222(Zn)	135	99	10	0.1	50	1
MOF-525	66	85	10	0.1	50	1
MOF-525(Mn)	100	99	10	0.1	50	1
Zr-methacrylate	210	99	10	0.1	50	1
no co-cat	0	8	0	0.1	50	1
no MOF	0	5	10	0	50	1

[a]Yield found after 24h.[b] Bu_4NBr was used as co-catalyst. No solvent was used.

Next to propylene oxide (PO) other more demanding substrates, such as cyclic, long-chained and substituted epoxides were tested and found to be more difficult to convert to the corresponding cyclic carbonates (section 5.2, Table 4).

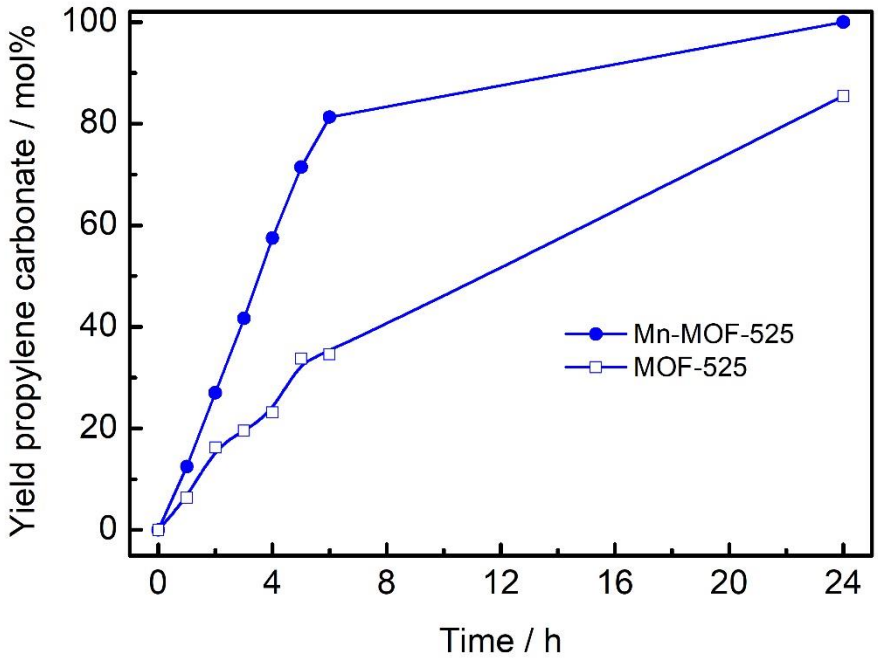

Figure 26. Yield-time plots for the reaction of CO_2 with propylene oxide using MOF-525 and Mn-MOF-525 as catalysts under 1 bar CO_2 and T = 50 °C with 10 mol% Bu_4NBr as a co-catalyst. This Figure combines the respective traces of Figure 25 (above) for better comparison.

For the reaction with PO a hot filtration test excluded leaching of reactive species into the solution, indicating the heterogeneity of the catalytic reaction with respect to Zr-MOF (Figure 69). After end of the reaction, the supernatant solution was investigated by element analysis (no Zr found) and UV-Vis spectroscopy (only an extremely weak porphyrin signal was found; Figure 54). The catalyst was still highly crystalline after the catalysis test, thus showing good structural stability under the applied reaction conditions (Figure 61). PCN-224 as the most active MOF of the non-metalated series was then tested under optimized catalytic conditions, namely, 4 bar CO_2 at 50 °C, reaching full conversion already after 8 h (Figure 67). Additionally, the blind tests, where no Zr-MOF catalyst was used and as well a blind test without any co-catalyst (Bu_4NBr) were conducted, providing evidence that almost no conversion occurs if only either one of them is used (Figure 67). The reaction was followed using ^1H NMR spectroscopy (Figure 66). Importantly, MOF-525, L12, is more active than PCN-222, L8, (Figure 25, left). In contrast, following the proposed hypothesis and matching with the results of Hupp et al.,

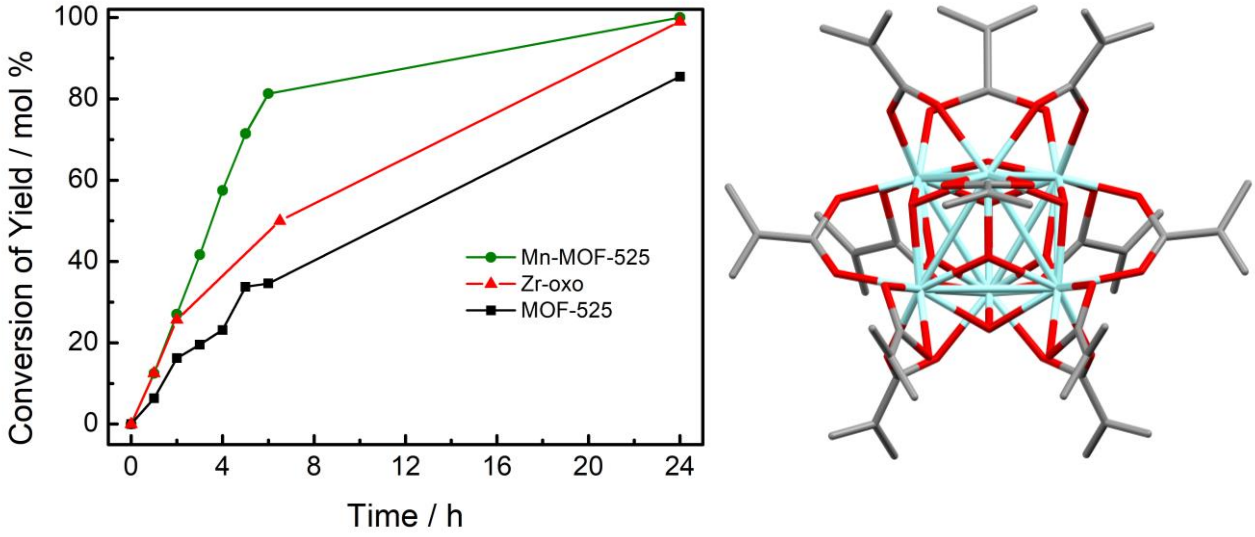

Figure 27. Left: Time-conversion plot of propylene oxide to propylene carbonate under MOF-525 (black), molecular Zr_6-oxo cluster, $Zr_6(OH)_4O_4(OMc)_{12}$ (OMc = methacrylate) (red) and MOF-525(Mn) (green) catalysts. Right: Illustration of Zr_6-oxo cluster, $Zr_6(OH)_4O_4(OMc)_{12}$. Zr: teal, O: red, C: grey, H has been omitted for clarity.

PCN-222 should be expected to be more active than MOF-525, since the Zr_6-node of PCN-222 is lower connected. To answer the unexpected high activity of the nominally 12-connected MOF-525 vs. 8-connected PCN-222 the catalytic activity of the Zr-oxo-cluster [$Zr_6(OH)_4O_4(OMc)_{12}$] (OMc = methacrylate) was also investigated which can be seen as the *molecular* analog of the node of MOF-525 (Figure 27, right).[167] The cluster was obtained by literature protocols as a white solid and characterized by ^1H NMR (Figure 50) and PXRD (Figure 51). This cluster features the same Zr_6 octahedron, which is capped by 12 methacrylate groups instead of being bound to porphyrin linkers. It was anticipated that these structural motifs are comparable in terms of coordinative saturation due to the same 12-fold connectivity of the Zr_6 cores. These molecular clusters were used in the ring-opening metathesis

polymerization,[168] however, were not investigated in terms of Lewis acidity yet. Interestingly, the catalytic activity of the molecular Zr_6-oxo cluster for the cycloaddition of CO_2 and propylene oxide is comparable to that of MOF-525 (Figure 27, left).

The slightly higher activity is expected, since the reaction is homogeneous, in contrary to the heterogeneous reaction using the MOF. This shows that even a coordinatively saturated Zr_6-core exhibits moderate Lewis acid catalyst activity. The reactivity can be explained by the highly dynamic substitution kinetics of such clusters and the dissociation/coordination process of the capping carboxylates, as reported by Schubert et al.[169]

In order to rationalize the unexpected activity of the MOF-525, the amount of missing linker defects in MOF-525 was estimated by thermogravimetric analysis (TGA) to around 16 % (calculated by Valenzano's method).[105] This is shown exemplary for MOF-525 (Figure 28).

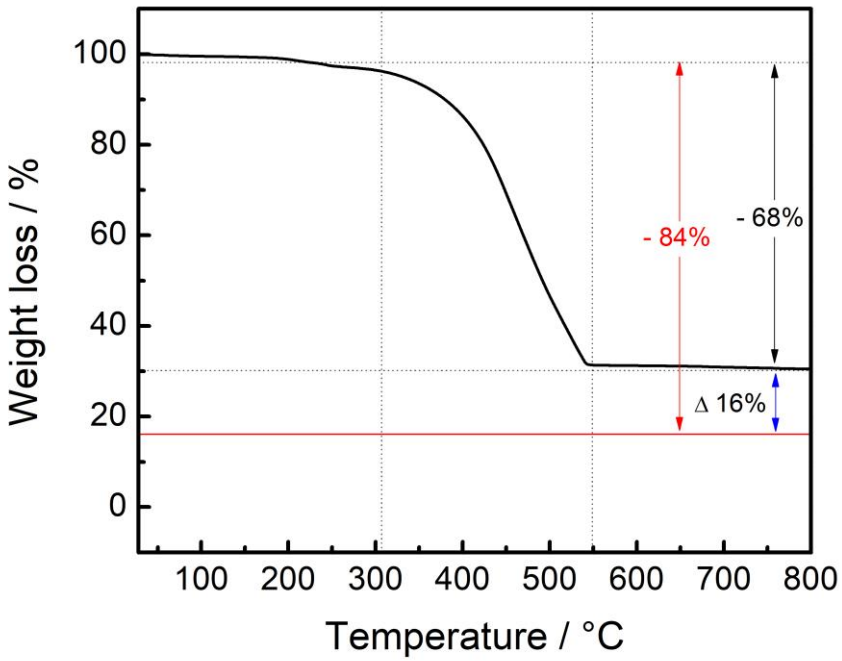

Figure 28. TGA of thermally pre-activated MOF-525 under synthetic air (80 % N_2, 20 % O_2). Illustration the expected mass loss of 'ideal' MOF-525 structure (red) in comparison to the experimentally observed mass loss, indicating the presence missing linker defects (16 %).

This data leads to an effective (average) linker/node ratio of about 10, instead of 12 as expected for the ideal structure. Similar to the isoreticular UiO-66, also MOF-525 it is very stable and tolerant to relatively high numbers of missing linker defects.[151, 153, 154] Thus, the unexpected high activity can be partly explained by these defects, however, the number of linkers (connectivity) is still higher than in PCN-222, which has only 8 linker / node and a linker deficiency of 4.5% (Figure 58). TGA of PCN-224 reveal the 'defect free' structure of the MOF with no linker deficiency (0.02%, Figure 59). These findings match quite well with the reasoning that the lower the connectivity of Zr_6-nodes the least tolerant the system becomes to

linker defects. Thereby, it seems that the 6-connected Zr_6-nodes somehow represent the lower limit, since this system seems to be almost intolerant towards missing linker defects and removal of linkers would possibly lead to destruction of the framework and/or increased instability under the conditions of the catalytic test reactions. In summary, the observed difference in specific catalytic activity of the PCN-222 system versus PCN-224 and MOF-525 is most likely originating from the differences in topology and pore geometry. These latter systems are similar due to their cubic and microporous structure, while PCN-222 is hexagonal and micro- as well as mesoporous.

Porphyrin Linker Metalation

Metalation of the MOF series leads in all cases to a higher activity (see Figure 25, right), as the newly introduced Mn(III) sites can act as additional Lewis acids, contributing to the overall activity originated from the Zr(IV) sites. Interestingly, the metalation of PCN-224 only slightly improves the catalytic activity, while the enhancement is more significant in PCN-222 (Figure 25) and in MOF-525 (Figure 26). This can be explained by the specific quantity of newly introduced Mn(III) sites. PCN-222 has 2 linkers and MOF-525 even has 6 linkers more per / Zr_6-node when compared to PCN-224, so the effect of metalation is much more pronounced the more linkers are attached to the Zr_6-node. It is important to mention that this selected porphyrin-based test series allows the differentiation of the contribution to the overall catalytic activity of the two independent Lewis-acidic sites, namely Zr and Mn, which is more difficult in other catalytic systems, i.e. in case of cyclam-based MOFs due to the lack of a non-metalated reference system. Control of Zr_6-node connectivity and subsequent metalation leads to counteracting or compensation effects: Firstly, the activity of the non-metalated MOFs is higher, the less linkers are attached to the Zr_6-nodes (more accessible Zr(IV) ions). Secondly, metalation generally enhances the catalytic activity of the MOFs; however, the effect is more pronounced in the higher connected MOFs, which have more linkers attached to the Zr_6-nodes and thus less accessible Zr(IV)-ions. This combination of effects results in an overall counterbalancing of catalytic activity among the metalated MOF series. Due to these compensating effects, the metalated MOFs are all very similar in their specific activity. The catalytic activity can further be improved, when stronger Lewis acids are installed. This was demonstrated by the Zn(II) metalated PCN-222(Zn) with an increase in catalytic activity as compared to PCN-222(Mn) (Figure 68).

3.1.4 Summary and Conclusion

Three closely related, porphyrin linker and Zr_6-oxo-cluster node based MOFs of different node connectivity, namely MOF-525, PCN-222 and PCN-224, were compared as catalysts for the cycloaddition of CO_2 and propylene oxide to propylene carbonate with tetrabutylammonium bromide as co-catalyst. The lower connected PCN-224 (6 linker/node) showed higher catalytic activity than the high-connected MOF-525 (12 linker/node). However, the trend of the

connectivity dependent catalytic activity is not fully linear, since MOF-525 outperformed PCN-222 (8 linker/node), which may be explained by high amount of missing linker defects (~16%) and the difference in topology of PCN-222 and MOF-525. The Mn-metalated Zr-MOFs showed higher catalytic activity than their non-metalated counterparts, which could be further improved by introduction of stronger Lewis acids, i.e. Zn, which was exemplary demonstrated for PCN-222. The enhancement of the catalytic activity by linker metalation was more pronounced for PCN-222(Mn) and MOF-525(Mn) which exhibit a higher linker/node molar ratio as compared to lower connected PCN-224(Mn). In such dual site Lewis acid Zr-MOF(M) catalysts, the effective node connectivity, defined by topology and by defect engineering, and the linker metalation partly compensate each other. The properties of MOF-525 were compared to the 12-connected molecular analog, the cluster $[Zr_6(OH)_4O_4(OMc)_{12}]$ (OMc = methacrylate), whereby similar catalytic activity was observed. The most active non-metalated Zr-MOF, PCN-224, was found to be stable after one catalytic cycle and the heterogeneity of the reaction was confirmed by a hot filtration test.

These results show that Z_6-oxo-cluster node and porphyrin linker-based MOFs are a tunable platform in which the Lewis-acid catalytic activity can be adjusted via (1) the choice of topology and connectivity of the Zr-nodes and (2) subsequent metalation of the porphyrin linkers, as well as by (3) the presence of missing linker defects. Metalation of porphyrin linkers can be useful to enhance the catalytic activity in high connected Zr-MOFs, where the Zr-nodes are saturated by large amounts of linker. Defects play a crucial role and the precise engineering of missing linker defects, is a tool to enhance catalytic reactivity is such systems. The presented case study dealt with dual site Lewis-acid catalyst MOFs and demonstrated the interdependence of independently adjustable structural and compositional parameters. Even beyond the case study such kind of counterbalancing effects need to be taken into account for understanding and optimizing catalyst properties of multifunctional MOFs.

3.2 Cyclopropanation under PCN-224/222(Rh) catalysts[2]

Abstract

In this work, it is shown that the stereoselectivity of a reaction can be controlled by combining substrates with directing functional groups, and metal-organic frameworks (MOFs) with an appropriate network topology inducing local cavity confinement. Porphyrin-based PCN-224(Rh), which contains no stereocenters, was applied as catalyst in the cyclopropanation reaction using ethyl diazoacetate (EDA) as carbene source. When styrene and other innocent, non-coordinating olefins are used as substrates, high activity, but no diastereoselectivity is observed. Interestingly, conversion of 4-amino- and 4-hydroxystyrene substrates occurs with high diastereomeric ratios (*dr*) of up to 23:1 (*trans:cis*). This is attributed to local pore confinement effects as a result of substrate coordination to neighboring Rh-centers, which position the olefin with respect to the active site, causing a break of local symmetry of the coordinated substrate. The effect of local pore confinement was improved by using PCN-222(Rh) as catalyst, which is a structural analog of PCN-224(Rh) with characteristic Kagomé topology featuring shorter Rh–Rh distances. A remarkable *dr* of 42:1 (*trans:cis*) was observed for 4-aminostyrene. In this case, the length of the substrate corresponds to the average distance between two neighboring Rh centers within the pores of PCN-222(Rh), which drastically boosts the diastereoselectivity. This work showcases how diastereomeric control can be achieved by favorable substrate-catalyst interactions and thoughtful adjustment of confined reaction space using porphyrin-based MOFs, in which stereocenters are inherently absent.

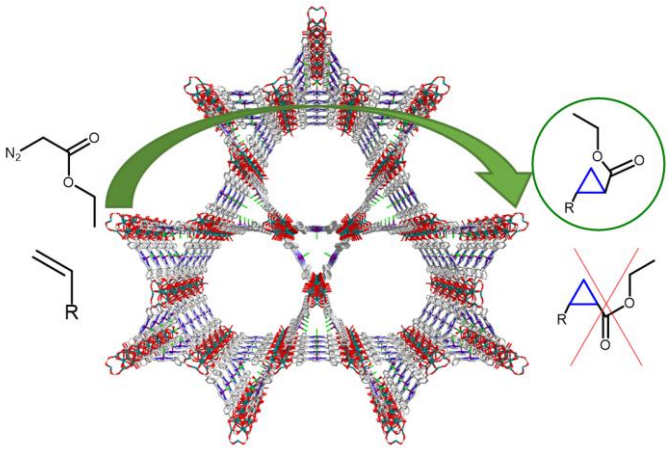

[2]This section corresponds to the submitted manuscript 'Network topology and cavity confinement-controlled diastereoselectivity in cyclopropanation reactions catalyzed by porphyrin-based MOFs' K. Epp, B. Bueken, B. J. Hofmann, M. Cokoja, D. De Vos and R.A. Fischer.

3.2.1 Introduction

Stereoselective catalysis is a key technology due to its enormous economic relevance towards the production of pharmaceuticals, agrochemicals, fungicides, pheromones, flavors and fragrances.[170] In stereoselective organometallic catalysis, one of the most exploited 'classic' design principles is 'catalyst control', i.e. the coordination of catalytically active metal centers by chiral ligands to drive stereoselectivity,[171] such as diamines or diphosphines, as for instance in the well-known BINAP,[172] or chiral multidentate carboxylates, as is the case with the Sharpless epoxidation catalyst.[173] The design of heterogeneous stereoselective catalysts is however more intricate. In heterogeneous catalysts, the stereoselectivity usually originates from a molecular catalyst immobilized on a solid support. The high tuneability of metal-organic frameworks (MOFs) as heterogeneous catalysts allows much versatility in tailoring and manipulating their structural and chemical properties. In the context of stereoselective catalysis, MOF design approaches involve either the heterogenization of stereoselective molecular catalyst to the MOF linker,[174] or using linkers,[175] which themselves act as stereoselective ligands to catalytically active metals.[176, 177]

While the classic 'catalyst-controlled' concept for both homogeneous and heterogenized molecular catalysts requires well-defined stereocenters, very few reports describe the stereoselectivity of solid catalyst@host materials, in which neither the catalyst nor the host exhibit such well-defined stereocenters. In this case, the induction of stereoselectivity is derived from pore confinement effects of the host. While this type of stereocontrol is known for soluble, defined macromolecular cage compounds and others,[178, 179] only a handful examples using solid/polymeric porous materials such as zeolites,[180, 181] mesoporous silica[182, 183] or MOFs[73, 184-186] are known. 'Confinement' or 'confinement effects' are rather broad terms and not explicitly specified in literature. Hence, it is not exactly clear how the confinement of a host defines the stereochemical outcome of a reaction, since the local substrate arrangement through its interaction with the host is a multi-component problem.[187] In many homogeneous catalysis reactions, the stereo- or regioselectivity can be influenced by interactions of 'directing' functional groups of the substrate with the catalyst, e.g. via hydrogen-, covalent- or coordinative bonds, or Coulomb or Lewis acid−base interactions, which induce a preferential conformation or orientation of the substrate at the catalyst.[188] Therefore, it is reasonable to assume that directing effects of functional groups attached to substrates may also play a crucial in role in MOF-based catalysis by coordination to suitable sites located within the pores. A thorough understanding of the origin of stereocontrol in these cases is of great interest, as the insights gained could enable further control over confinement effects in MOF-based catalysts.

Previous work by Fischer et al. dealt with metalloporphyrin (MP) MOFs as catalysts for the cycloaddition of carbon dioxide to propylene oxide to form propylene carbonate,[140] the motivation was to extended their application as heterogeneous catalysts to (dia)stereoselective

reactions. Molecular, biomimetic MPs have been widely studied in literature, because of their ability to act as ligands for various metals (M = Fe(II,III),[43, 44] Co(II),[31] Rh(III),[33, 48, 49] Ru(II),[50] Ir(III),[51] Os(III)[52] and others). Thus, it is not surprising that their chemistry and catalytic properties are rich.[29, 47] To be used in stereoselective catalysis, MPs are often functionalized with bulky[33, 35] and/or chiral groups[189-191] on the *meso*-positions at the porphyrin backbone in order to induce stereochemical or even chiral information and most importantly, to engineer a pocket-like environment around the catalytically active MP center. On the one hand catalytic activities may increase to TOFs > 100.000 h^{-1} as demonstrated by Gallo *et al*. using 'totem'-shaped Fe(III)-porphyrins in the cyclopropanation of styrene,[35] while on the other hand synthetic yields of these sophisticated MPs are extremely low (often <1%) and purification is necessary to isolate the compounds. Moreover, deactivation via dimerization may hinder their application in catalysis. Motivated by the remarkable catalytic properties of molecular MPs and the challenges in their synthesis, stability and recyclability, it is interesting to investigate how their heterogeneous counterparts, namely, MP-MOFs (metal = Cu, Co, Fe, Rh), would perform as catalysts. Heterogenization is achieved when MPs are built into the structure of the framework as organic linkers, as in the Zr-MOFs MOF-525[137], PCN-222[138] and PCN-224.[139] Consequently, MP-MOFs can be seen as rigid, self-supported heterogeneous catalysts with well-defined, spatially distributed MP-sites, which are catalytically active and not susceptible to μ-oxo dimerization. Thus, is this work it was investigated for the first time how different MP-MOFs phases, PCN-224(Rh) and PCN-222(Rh), constructed from the same building blocks, i.e. Zr_6 inorganic nodes and MP linkers, but with different topologies influence the stereoselectivity of a catalytic reaction. The utilization of unaltered building units, especially the MP linkers as the catalytically active sites, allows direct comparability of the obtained catalytic results. Hence, the difference in stereoselectivity can be attributed to the different confinement effects of altered pore sizes and geometries.

Cyclopropane motifs are not only found in natural products; they are also important synthetic targets in pharmaceuticals like antibiotics, in perfume compounds and in biomimetic insect repellents.[39, 42] The specific reactivity of the strained three-membered ring system and its ability to induce conformational constraints on otherwise flexible acyclic chains is a key feature of this motif.[40-42] The transition-metal catalyzed cyclopropanation of double bonds using diazo compounds as a carbene source is well studied and has been recognized as a useful design route for substituted cyclopropanes. Since there is a vast number of reports using Rh(II,III) catalysts in the CP reaction,[33, 48, 49, 192, 193] it was decided to start with the Rh(III)-metalated porphyrin, namely [5,10,15,20-tetrakis(4-methoxycarbonylphenyl)porphyrinato]-Rh(III) chloride ([Rh(TCPPCO_2Me)Cl]) as a homogeneous reference system in the cyclopropanation of styrene and ethyl diazoacetate (EDA) to the corresponding cyclopropanation products (*trans* and *cis*). Consecutively, these results with those obtained on stable heterogeneous MP-based PCN-224(Rh) and PCN-222(Rh) catalysts were compared with regard to activity and *dr*.

3.2.2 Synthesis and Characterization

PCN-224(Rh) was obtained by solvothermal synthesis. A metalated Rh-porphyrin linker[194] was synthesized by saponification of the Rh(TCPPCO$_2$Me)Cl ester. Metalation was confirmed via UV-Vis spectroscopy (Figure 53). The obtained linker [5,10,15,20-tetrakis(4-carboxyphenyl)porphyrinato]Rh(III) chloride, $ZrCl_4$ and benzoic acid as modulator were mixed in DMF and heated for one day at 120 °C.[139] PCN-224(Fe) was synthesized by post-synthetic metalation of PCN-224 using $FeCl_2$. Accordingly, PCN-222(Rh) was synthesized under similar conditions.[139] MP-MOFs were obtained as phase pure microcrystalline powders, which was confirmed by powder X-ray diffraction (PXRD) (see Figure 60 for PXRD of PCN-222(Rh)). Comparison to patterns of parent non-metalated MOFs and to the simulated powder pattern reveals that all MP-MOFs are isostructural to each other.

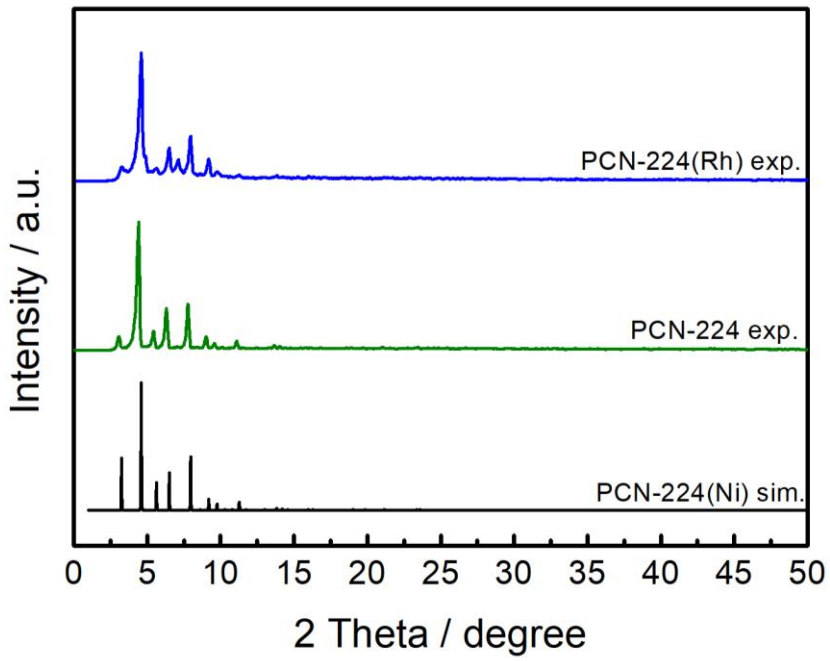

Figure 29. Experimental (exp.) powder X-ray diffraction pattern of PCN-224(Rh) compared to non-metalated exp. PCN-224 and the simulated (sim.) pattern of PCN-224(Ni) calculated from a model obtained from single crystal data.

A type I isotherm and a Brunauer-Emmett-Teller (BET) surface area (S_a) of 1400 m^2/g were found for PCN-224(Rh) (Figure 30). This value is lower than, but still in the same order of magnitude as for non-metalated PCN-224 (S_a = 2147 m^2/g) which might indicate slightly incomplete activation prior to the measurement or possibly by the presence of additional Rh-ions, which would increase the molar weight but hardly affect the pore volume. The synthesized micro- and mesoporous PCN-222(Rh) sample exhibited a surface area of 1912 m^2/g (literature S_a of non-metalated PCN-222 = 2223 m^2/g),[138] showing an expected additional step in the isotherm which could be attributed to the large hexagonally shaped 3D mesoporous channels (Figure 31).

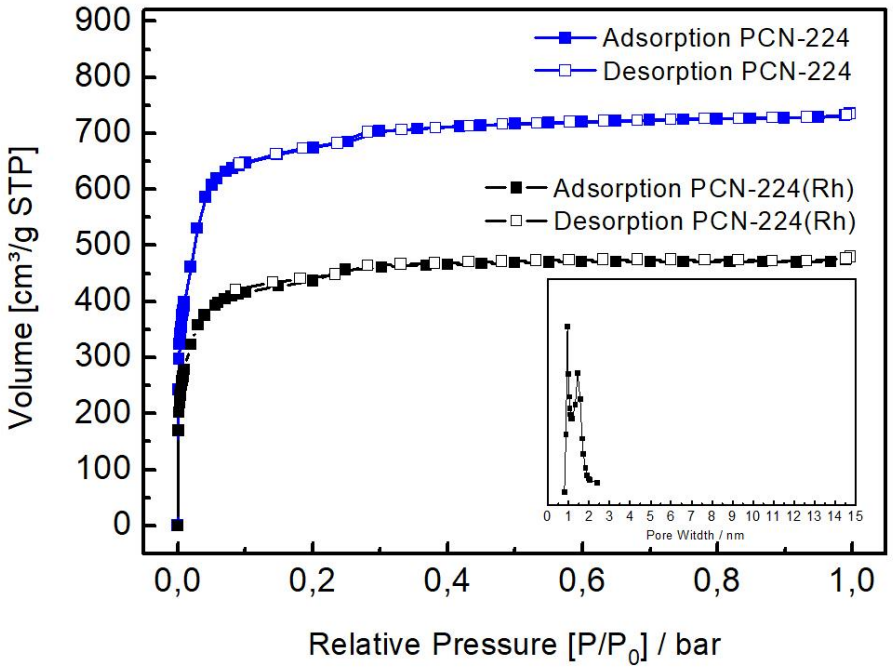

Figure 30. N_2-physisorption measurements of PCN-224 and PCN-224(Rh) measured at 77 K. Adsorption and desorption branches are shown with closed and open symbols, respectively. The inset highlights the pore size distribution (PSD) of PCN-224(Rh), which is also representative for PCN-224.

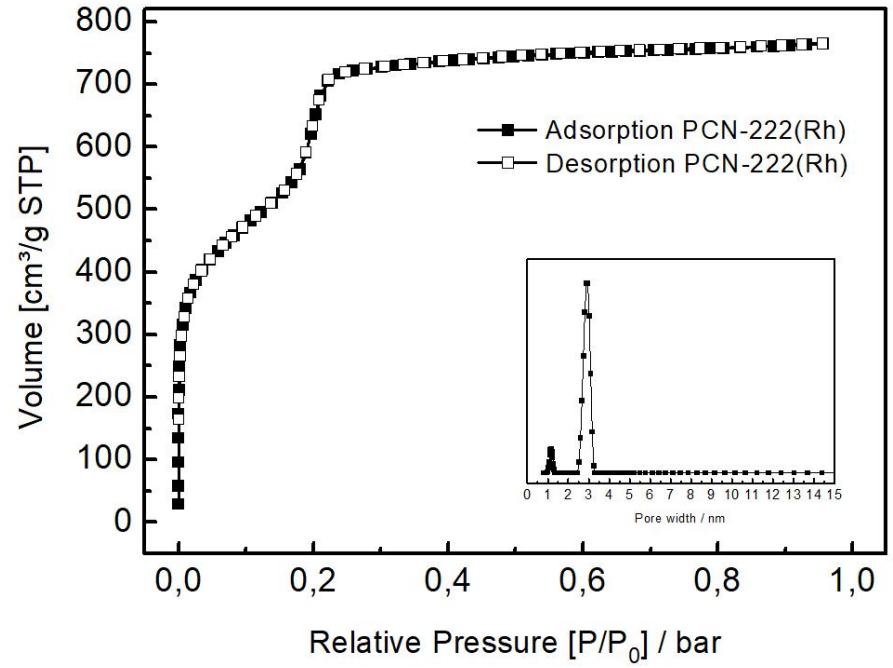

Figure 31. N_2-physisorption measurements of PCN-224(Rh) measured at 77 K. Adsorption and desorption branches are shown with closed and open symbols, respectively. The inset highlights the pore size distribution (PSD) of PCN-222(Rh).

3.2.3 Catalytic studies

As a test reaction, the cyclopropanation (CP) of olefins (Scheme 6) using ethyl diazoacetate (EDA) as carbene source was selected.

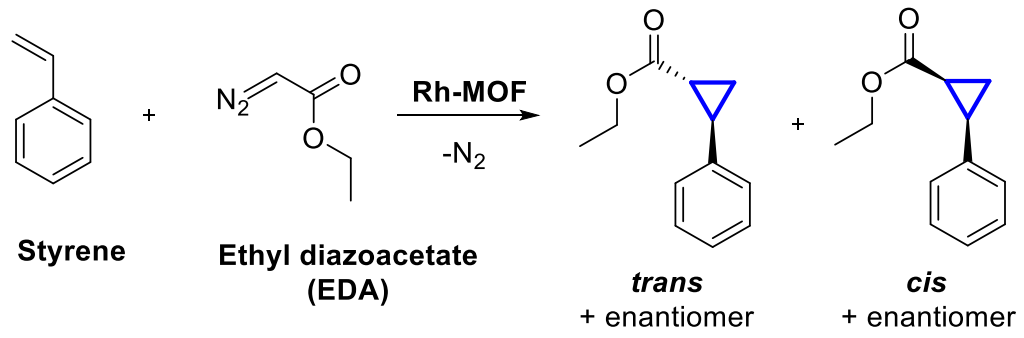

Scheme 6. Cyclopropanation of styrene using ethyl diazoacetate (EDA) to the corresponding diastereomeric cyclopropanation products (*trans*, *cis* and their corresponding enantiomers (not shown)) under Rh-MOF catalyst.

Firstly, Rh(TCPPCO$_2$Me)Cl as a homogeneous reference system was investigated. In the catalytic reaction 135µL EDA (1.1 mmol) was diluted in 2 mL CH_2Cl_2 and added manually via a syringe to a solution of 75 µL styrene (0.8 mmol) in 3 mL CH_2Cl_2 within 20 min. Further manual introduction of EDA did not lead to full conversion. The activity at room temperature (rt) under stirring in CH_2Cl_2 is moderate (yield = 20% after 22 h; see Table 3). Expectedly, there is no diastereoselectivity (1:1), since this porphyrin ligand is nearly planar and lacks directing bulky groups attached at the *meso*-position of the porphyrin backbone.

Secondly, the heterogeneous counterpart PCN-224(Rh) was used as catalyst under the same reaction conditions as above and found a similar yield (29% after 22 h). The selectivity towards the cyclopropanation products was decreased due to the uncontrolled dimerization of EDA (found by GC-MS and ^{1}H and ^{13}C NMR analysis), as the dimerized EDA is no longer available for the carbene transfer to the olefin. Therefore, the reaction was executed using a motorized syringe pump and with an excess of olefin: Hereby, 135 µL (1.1 mmol) EDA diluted in 3 mL CH_2Cl_2 was added at a rate of 0.5 mL/h to a suspension of catalyst in 2 mL olefin solution. As a result, a conversion of 71% styrene and a *dr* of 1:1 (*trans*:*cis*) was observed with a drastically reduced formation of the coupling side product, revealing the crucial dependence of controlled introduction of EDA on the yield of the reaction.

Furthermore, the scope of the reaction was determined, as summarized in Table 1. Products of the substituted 4-methyl-, 4-methoxy-, 4-nitro-, 4-chlorostyrenes were obtained in moderate to good yields up to 68% at rt after 6 h under stirring under air applying excess substrate. Cyclic and terminal olefins exhibited yields of 49% (cyclooctene) and 22% (1-octene). In addition, 3,4-dihydro-*2H*-pyran, a sugar-based glycal, which can be obtained from biological feedstock which makes it relevant in terms of sustainability, showed a moderate yield of 20%.

Table 3. Catalytic results for the cyclopropanation of olefins and ethyl diazoacetate (EDA) using MP-MOFs as catalyst.

Entry	Olefin	Catalyst[1]	Yield[3] [%]	*dr*[4] [*trans:cis*]	t [h]
1	Styrene	PCN-224(Rh)	71	1:1	6
2	Styrene[2]	PCN-224(Rh)	29	1:1	6
3	Styrene	PCN-224(Fe)	23	1:1	6
4	Styrene	Rh-TCCPOMe	20	1:1	6
5	4-Methylstyrene	PCN-224(Rh)	58	1:1	6
6	4-Methoxystyrene	PCN-224(Rh)	52	1:1	6
7	4-Nitrostyrene	PCN-224(Rh)	68	1:1	6
8	4-Chlorostyrene	PCN-224(Rh)	52	1:1	6
9	4-Aminostyrene	PCN-224(Rh)	35	23:1	6
10	4-Aminostyrene	PCN-222(Rh)	29	42:1	6
11	4-Hydroxystyrene	PCN-224(Rh)	4	21:1	6
12	*N*,*N*-Dimethyl-4-aminostyrene	PCN-224(Rh)	31	1.5:1	6
13	*N*,*N*-Dimethyl-4-aminostyrene	PCN-222(Rh)	16	1:1	6
14	1-Octene	PCN-224(Rh)	22	1:1	6
15	Cyclooctene	PCN-224(Rh)	49	1:1	6
16	3,4-Dihy*dr*o-*2H*-pyran	PCN-224(Rh)	20(35)	1:1	6(24)

All reactions were carried out at room temperature and stirring (rpm = 500) operated under air. Yields are obtained applying an excess of substrate: 135 µL (1.1 mmol) EDA diluted in 3 mL CH_2Cl_2 was added via a motorized syringe pump (rate = 0.5 mL/h) to a suspension of catalyst in 2 mL substrate. [1]Catalyst loading: 0.0033 mmol, 0.4 mol% Rh and 0.4 mol% Fe, respectively. [2]Manual addition of 135 µL EDA (1.1 mmol) in 2 mL CH_2Cl_2 to a solution of 75 µL styrene in 2 mL CH_2Cl_2 within 20 min. [3]GC-Yield. [4]Diastereomeric ratio (*trans*:*cis)* of the product.

Interestingly, a high *dr* of 23:1 (*trans:cis*) was observed with 4-aminostyrene as substrate. Presumably, the amino functionality acts as an anchoring ligand to the Rh-porphyrin linkers and/or via hydrogen bonding to the Zr-oxo-clusters. Infrared studies (Figure 56 and Figure 57) indicate possible interactions of 4-aminostyrene with the MOF host, wherein the amino-stretching vibration is affected (most likely via coordination) when 4-aminostyrene is exposed to the MOF. This kind of coordination mode is likely to align the substrate in a certain position, and sterically orienting the olefin moiety to the Rh-carbene in a favored fashion. In this sense, the reaction can be considered catalyst-controlled, because of the well-defined and rigid Rh(Zr)-Rh distances favoring certain olefin orientations. On the other hand, the reaction can be viewed as substrate-controlled, whereby the coordination ability of functional groups on the substrates drives the stereoselectivity. In this example, the linkers and/or nodes carrying functional groups may act as binding sites facilitating substrate-catalyst interactions for possible enrichment fixation, and activation of substrates, providing special transfer pathways for stereoselective chemical transformation.[195] Hence, coordination of the substrate caused by the pore confinement results in its symmetry breaking, with the carbene transfer proceeding no longer statistically but favorably towards one diastereomer over the other. The high

diastereoselectivity thus follows from stabilization of an alternative transition state, compared to molecular Rh-porphyrins in solution, which naturally lack of any pore confinement effect or substrate-controlled preferential steric orientation in the transition state of the carbene transfer. The abovementioned stabilization is also known from cage-catalyzed reactions leading to unusual reactivity/selectivity compared to their bulk counterparts.[179, 196, 197]

Further, 4-hydroxystyrene was tested and a similarly high *dr* of 21:1 (*trans*:*cis*) was observed, which supports the idea of the directing group effect of the substrate. However, the yield of the corresponding cyclopropane was low due to side reactions with propylene glycol, which is present in the solution of 4-hydroxystyrene (10 wt%), acting as a stabilizer. As a control experiment to test that the diastereoselectivity is controlled by coordinating groups attached to the styrene, *N*,*N*-dimethyl-4-aminostyrene and 4-methoxystyrene substrates were investigated. In both substrates, the coordination ability is reduced by sterical hindrance the absence of H-bonding interactions. In neither case diastereoselective transformations were observed, while the product yield for *N*,*N*-dimethyl-4-aminostyrene was consistent with that of 4-aminostyrene (4-methoxystyrene does not contain a stabilizer, hence a direct comparison of yields cannot be made). In contrast to other substrate-directed reactions which often proceed via an intramolecular pathway, the ascribed reaction is intermolecular, since coordination and catalytic reactions do proceed at two distinct centers. When the coordination of the amino group to a Rh-porphyrin is considered, the Rh-porphyrin has two important different functions: (1) Coordination acceptor and pre-alignment of non-innocent substrate and (2) catalytically active center. This interplay of two neighboring Rh-centers critically influences the diastereoselectivity of the reaction.

3.2.3.1 Topology-dependent diastereoselectivity

To investigate how the distance between two neighboring Rh-porphyrins affects the diastereoselectivity of the reaction, PCN-222(Rh) was studied, which consists out of the same building units as PCN-224(Rh) but differs in pore geometry and topology. In contrast to a Rh‑Rh distance of 13.6 Å found in PCN-224(Rh), PCN-222(Rh) provides smaller Rh‑Rh distances of 9.7 Å within its smaller trigonal micropores (Figure 31). 4-Aminostryrene has a dimension of 8.1 Å and when a bond length of around 2 Å for Rh-carbene is considered,[198] a cumulative length of ~10 Å is obtained. Hence, the summed distance of substrate and carbene matches quite well with the Rh–Rh distance of 9.7 Å in PCN-222(Rh). Indeed, reaction of EDA and 4-aminostyrene proceeds with a moderate yield of 29%, but with an exceptional *dr* of 42:1 (*trans*:*cis*). The small trigonal pore is built from three distinct Rh-centers with identical Rh–Rh distances.

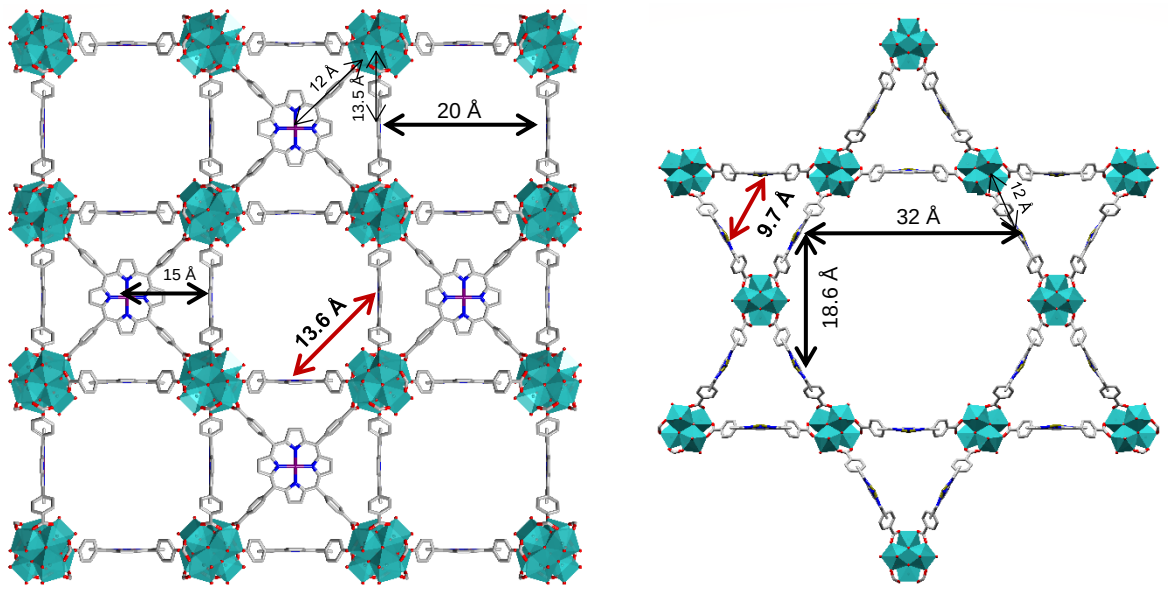

Figure 32. Schematic representation of PCN-224(Rh) (left) exhibiting squared micropores and PCN-222(Rh) revealing its small trigonal micropores and large hexagonal mesopores (right). Black and bold arrows indicate Rh-Rh distances, while black arrows represent Zr–Rh distances, respectively. Red arrows highlight the most feasible (shortest possible) Rh–Rh distances, which would favor the assisted binding of a coordinating substrate molecule.

Thus, this specific micro environment confines the reaction space and makes it more likely that these two species will react in very selective manner, leading to strongly enhanced diastereoselectivity (see Figure 33). This qualitative graphic illustration highlights the possible orientations of 4-aminostyrene inside a trigonal cavity of PCN-222(Rh)).

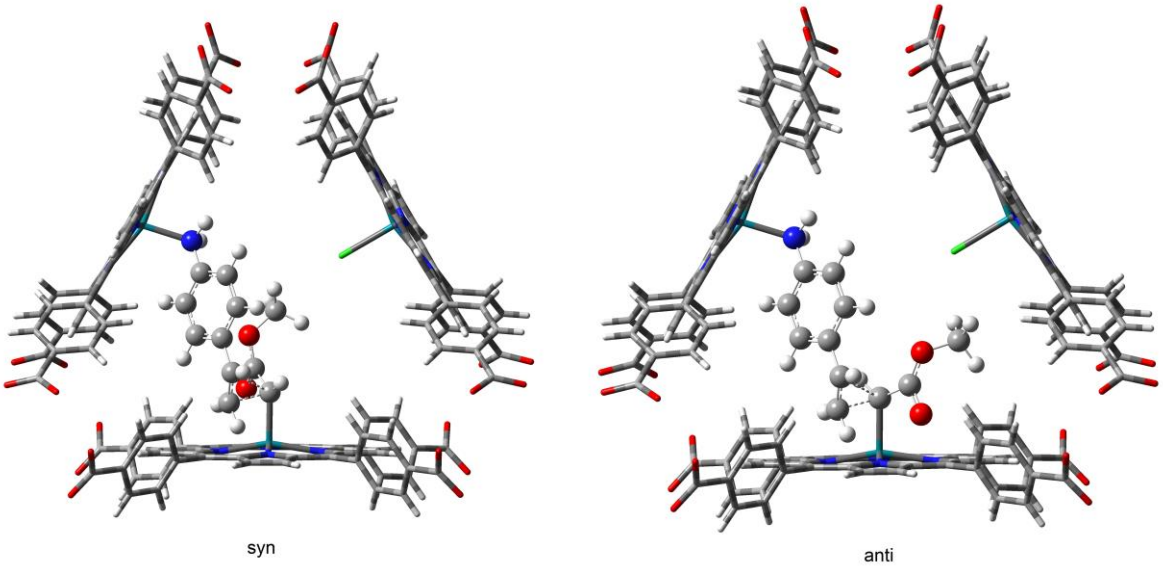

Figure 33. Graphical illustration of both transition states[a)] for the cyclopropanation of 4-aminostyrene (PCN-222(Rh)) yielding either the *syn*- (left) or the *anti*-product (right). Aminostyrene and the simplified carbene moiety (methyldiazo ester) are tentatively oriented in order to demonstrate the steric hindrance of the TS yielding the *syn*-product. [a)]PCN-222(Rh) structure is derived from the CIF file whereat the Zr-oxo clusters are omitted for clarity. The organic compounds are optimized by DFT (B97D3/def2SVP, ECPstutt for Rh). Visualized by GaussView 6.0.

The transition state (TS) of the *syn*-product is disfavored due to the sterical hindrance of 4-aminostyrene and the Rh-carbene moiety, whereas the TS of the *anti*-product reveal significantly less sterical hindrance, thus, is more favored. These findings support the drastic excess formation of the *trans*(anti)-products compared to *cis*(syn)-product. However, computational calculations on DFT level are required (energies of both TS) to exactly prove these qualitative observations.

Since the Zr–Rh distances in both MOFs are identical and the major differences in the Kagomé structure of PCN-222(Rh) are the shorter Rh–Rh distances, it is anticipated that the role of H-bonding interactions of amino or hydroxy groups with the Zr-oxo clusters are not that dominant. However, the contribution of H-bonding interactions cannot be exluded. In a conceptually similar study Zhang et al. applied Zn-BCTA MOF (BTCA = bis[4-(5-carboxy-2-thienyl)phenyl](4-carboxyphenyl)amine) as a photocatalyst in the sulfonylation–cyclization of activated alkenes.[199] Interpenetration of the MOF allowed closer substrate-redox center contacts, resulting in superior efficiency and more importantly, in higher diastereoselectivities compared to its homogeneous counterpart.[199] These results are in line with the obtained diastereoselectivities in this work, which also critically depend on confinement effects and suitable substrate-catalyst distances.

3.2.4 Summary and Conclusion

An example of a catalytic process was introduced wherein the diastereoselectivity crucially depends on specific local confinement effects, which can be adjusted by the careful choice of an appropriate MOF system. For the first time, heterogeneous porphyrin-based metal-organic frameworks PCN-222(Rh) and PCN-224(Rh) catalysts were applied in the diastereoselective cyclopropanation of styrene and styrene derivatives with ethyl diazoacetate. Styrene and substituted styrenes were converted with high catalytic activity. Interestingly, styrenes carrying coordinating amino and hydroxy groups show a high diastereomeric ratio (*dr*) of up to 23:1 (*trans*:*cis*) under PCN-224(Rh) catalyst, which was attributed to their coordination to Rh centers caused by pore confinement effects derived from favorable substrate-catalyst interactions. The diastereoselectivity is further improved to a *dr* of 42:1 (*trans*:*cis*) by selecting PCN-222(Rh) catalyst, a structural analog of PCN-224 with Kagomé topology, featuring closer Rh–Rh distances. These results demonstrate that the diastereoselectivity of the cyclopropanation reaction can be controlled by (1) the choice of functional groups attached to substrates and (2) by structural and topological differences of the two MOFs used in this study, i.e. the distances between two rhodium centers. The insights obtained in this work may be interesting for the development of novel MOFs catalysts, since the results showcase possible structure-property relationships and more importantly, stress the impact of confined space as a critical reaction parameter to obtain stereoselective reaction products.

3.3 Cyanosilylation of benzaldehyde

The Zr_6-oxo-clusters of PCN-222 provide accessible Lewis acidic Zr(IV) centers which can be used as catalytic sites. Cyanosilylation, which is catalyzed by Lewis acids, is an efficient process to access cyanohydrin compounds, which are desired intermediates and can easily be transformed to industrially relevant products.[200, 201] Historically, the cyanosilylation was catalyzed using simple metal salts like ZnI_2 as shown by Evans and co-workers,[202] however, solid Lewis acids such as Zr-MOFs can be re-used by simple filtration. Moreover, porphyrin MOFs allow the introduction of novel Lewis acidic sites via metalation of the tetrapyrrole core as already demonstrated for the CO_2/propylene oxide coupling in chapter 3.1. Herein, PCN-222(no metal) as well as PCN-222(Mn) were investigated in the cyanosilylation of benzaldehyde which is a test reaction for the Lewis acidity (Scheme 7).

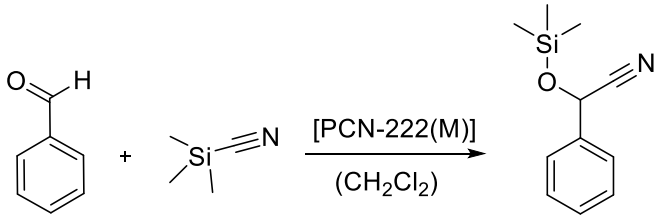

Scheme 7. Cyanosilylation reaction of benzaldehyde using trimethylsilyl cyanide (TMSCN) under PCN-222(M) catalysts.

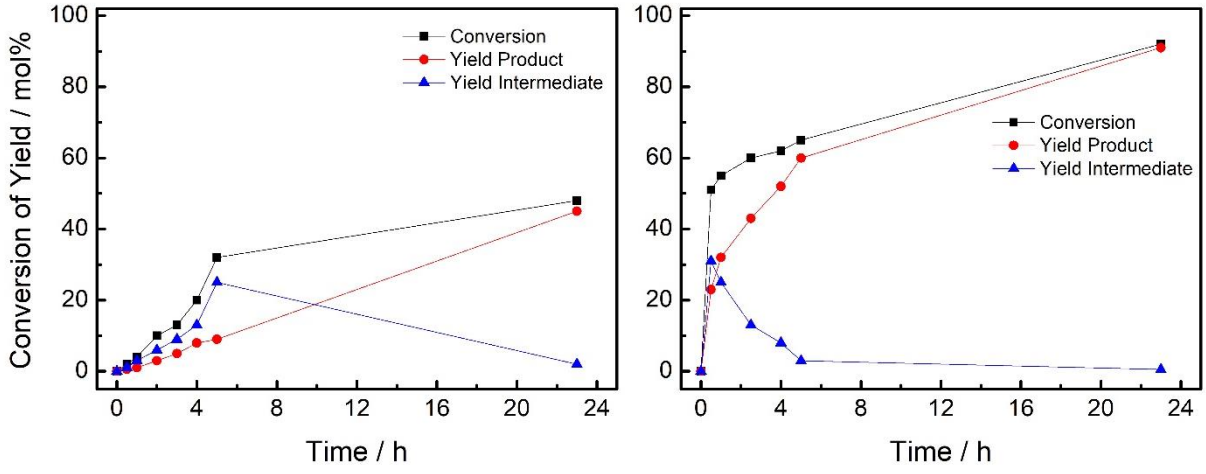

Figure 34. Cyanosilylation of benzaldehyde using TMSCN under PCN-222(no metal) (left) and PCN-222(Mn) (right) catalysts.

The catalysts PCN-222(no metal) and PCN-222(Mn) were activated at 120 °C under dynamic vacuum in order to remove residual (weakly) coordinated guests at the Zr-sites, such as water or hydroxyl groups, acetone and DMF which, ideally, makes the Zr-sites more accessible for incoming substrate molecules. The pre-activated catalysts were introduced with benzaldehyde and trimethylsilyl cyanide (TMSCN) in CH_2Cl_2 under Ar atmosphere at 40 °C in small Schlenk

tubes for 22 h under stirring. PCN-222(no metal) converts benzaldehyde to the desired 2-phenyl-2-((trimethylsilyl)oxy)acetonitrile with a yield of ~40 % after 23 h and full selectivity towards the cyanohydrin derivative. Notably, an induction period of about 5 h is observed at the beginning of the reaction, which can be attributed to the reversible formation of a benzoin-condensation product. In accordance to our expectation, PCN-222(Mn) catalyst showed a doubled yield of ~90 % after 23 h when compared to non-metalated PCN-222. Introduction of additional Mn-centers located at the porphyrin struts of the framework, significantly contribute to the overall Lewis acidic properties of PCN-222 leading to an improved catalytic activity.

4 Biomimetic oxidation catalysis

Abstract

In this chapter PCN-222(Fe, Mn) MOFs were used as biomimetic oxidation catalysts using unfunctionalized hydrocarbons as substrates and (alkyl)peroxides as oxygen transfer agents. The selectivity of the radical process is substrate dependent. Conversion of cyclohexene shows greatly improved selectivity compared to styrene, due to the allylic stabilization. The reaction was optimized by the use of "green" dioxygen as oxidant which exhibits good oxygen efficiency (50 %) and a better environmental impact producing only water as by-product. Under dynamic conditions PCN-222(Mn) catalyst outperforms its homogeneous Mn-porphyrin counterpart in the epoxidation of cyclic olefins. Switching to static set-up using Fisher-porter bottles facilitates the reactions process and gives comparable catalytic reactivity, even using air as oxidant under mild conditions (rt).

4.1 Introduction

As already outlined above, metalloporphyrin derived enzymes, such as the well-known Fe-based cytochrome P450 (CYP) enzyme,[203] are important structural units in many biological systems. The active sites in such monooxygenases are able to oxidize a variety of substrates efficiently and under mild conditions.[204] Accordingly, the first MPs were used in 1979 by Groves et al. who investigated their oxidation properties using iodosylbenzene in order to oxidize unreactive C-H and C-C bonds.[21] This demonstrated that, bio-inspired, artificial MPs may mimic the catalytic activity of natural enzymes and display an alternative route to fabricate powerful and selective catalytic systems.[18] In 2012 Zhou et al. successfully tested PCN-222(Fe) in the oxidation of pyrogallol, 3,3,5,5-tetramethylbenzidine, and o-phenylenediamine, which are considered as model substrates to characterize the catalytic performance of heme-like enzyme mimics. These substrates are useful indicators for the principle biomimetic catalytic activity, however, their industrial relevance is limited. Another major drawback is that often alkyl peroxides or iodosylbenzene derivatives are applied as oxygen transfer reagents which exhibit hazardous potentials as well as low oxygen efficiency. Recently, more economical and “green” oxidants such as dioxygen are used which is favorable to reduce the environmental fingerprint of the reaction and improving the O-efficiency, respectively.

4.1.1 Synthesis of PCN-222(M), M = Fe, Mn

PCN-222(Fe) was synthesized in accordance to Zhou and co-workers.[165] Briefly, $ZrCl_4$ (70 mg), $H_4TCPP(FeCl)$ (50 mg) and benzoic acid (2700 mg) were dissolved in 8 mL of DEF in a 20 mL scintillation vial and placed in an oven at 120 °C for 48 h. As-synthesized PCN-222(Fe) in DMF was activated with 1.5 mL 8 M HCl at 120 °C for 12 h, washed with DMF and acetone and soaked in fresh acetone for 24 h. Similar to already characterized PCN-222(Mn) in chapter 3.1.2, PCN-222(Fe) is isostructural to PCN-222(no metal) and was obtained as phase pure microcrystalline brown powder and was analyzed by PXRD (Figure 35).

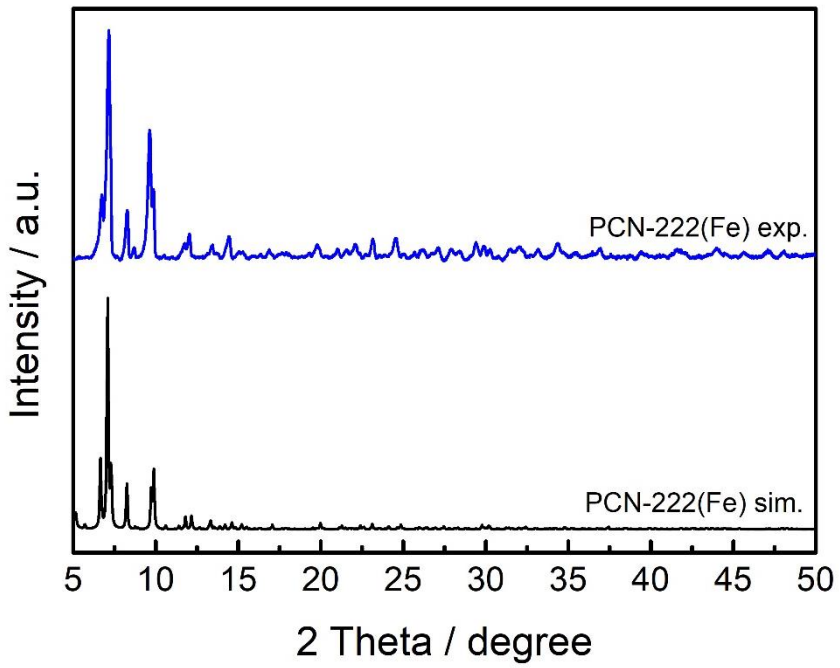

Figure 35. Experimental and simulated PXRD pattern of PCN-222(Fe).

Analogously, highly porous PCN-222(Fe) contains large hexagonal mesoporous ~3 nm 3D channels and trigonal shaped micropores with a pore width of 1.3 nm as shown by N_2-physiosorption measurements and pore size distribution analysis calculated by density functional theory (DFT). Overall a BET surface area of 2270 m^2/g was observed (Figure 36).

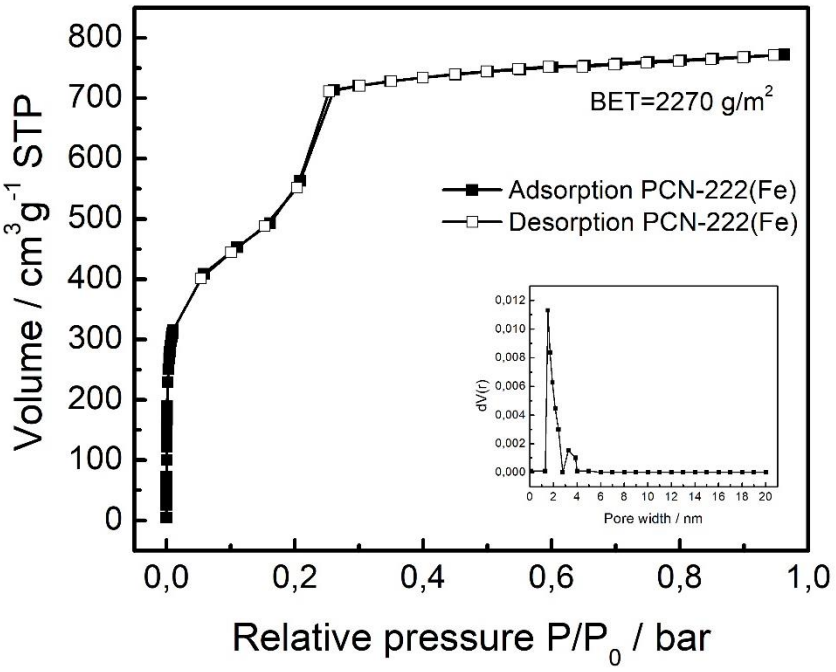

Figure 36. N_2-physisorption measurements of PCN-222(Fe) at 77 K. The inset shows the pore size distribution (PSD) calculated by density functional theory (DFT).

The full metalation of PCN-222(Fe) was qualitatively indicated by the brown color compared to the violet color of non-metalated PCN-222(no metal) sample and proven by UV-Vis measurements of dissolved MOF samples (Figure 52). To ensure that all porphyrin linker do coordinate to the respective Zr-oxo-cluster, PCN-222(Fe) was analyzed by infrared spectroscopy and compared to free H_4TCCP(FeCl) porphyrin linker (Figure 55).

4.1.2 Catalytic studies

4.1.2.1 Oxidation using peroxides

Thus, we were interested if PCN-222(Fe) could be applied in catalytic reactions using commercially more important substrates like unfunctionalized olefins, which is in contrast to the used model substrates used in literature.[165] Highly porous PCN-222(Fe) is chemically and thermally stable, moreover, it contains large mesoporous ~3 nm 3D channels which facilitate mass transfer and reduce possible diffusion limitations. Therefore, PCN-222(Fe) is a promising potential candidate to participate in heterogeneous oxidation reactions. In a first attempt, PCN-222(Fe) catalyst was tested in the epoxidation reaction. Therein, cyclooctene was selected as a substrate using hydrogen peroxide as oxidant at room temperature (rt) (Scheme 8), however, only poor activity was observed (5 % conversion).

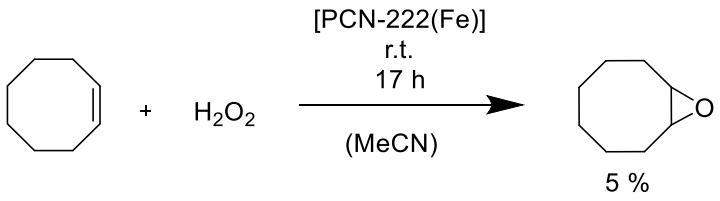

Scheme 8. Epoxidation of cyclooctene using H_2O_2 (3 eq.) under PCN-222(Fe) catalyst.

Due to the insufficient catalytic activity of PCN-222(Fe) at rt and motivated by the vast literature reports utilizing manganese porphyrins as oxidation catalyst in *e.g.* olefin epoxidation, hydroxylation of alkanes (aliphatic and cyclic) or alcohol oxidation,[205] PCN-222(Mn) was selected as novel catalyst and its catalytic activity was intensively studied.

Styrene oxidation

As another relevant substrate styrene was selected and *tert*-butyl hydroperoxide (TBHP) in decane[1] was used as oxidizing agent (Scheme 9).

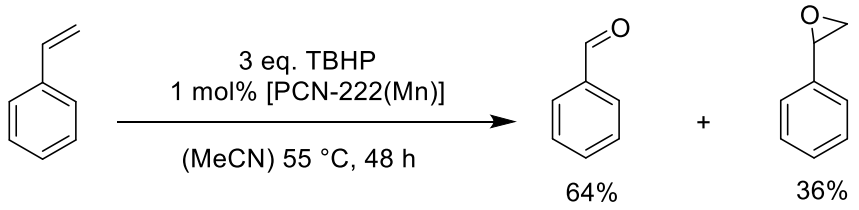

Scheme 9. Catalytic oxidation of styrene over PCN-222(Mn) catalyst in acetonitrile.

A conversion of ~55 % was achieved after 30 h with a selectivity of 64 % towards benzaldehyde and 36 % for styrene epoxide, respectively (Figure 37). Additional introduction of TBHP after 30 h lead to full conversion, however, a decreased selectivity of the reaction was observed. It can be assumed that the reaction follows a radical mechanism.[206] It is expected that the *tert*-butylperoxyl radical is formed by reducing the manganese center and releasing the respective proton. The radical attaches to the styrene double bond at the primary carbon atom generating the more stable benzylic radical species (to form the other aliphatic radical attaching to the secondary carbon atom). Subsequently, it is either possible that a ring closing reaction occurs leading to styrene oxide (1) or that another *tert*-butylperoxyl radical reacts with the benzylic radical. In this case, C-C bond cleavage occurs resulting in the formation of benzaldehyde and formaldehyde (2). In both cases, *tert*-butanol is formed as byproduct. Most likely, the low selectivity is intrinsic due to the radical-based mechanism of the reaction and possibly by the low stability of radical intermediates.

[1] Using TBHP in H_2O lead to the ring-opening reaction of styrene epoxide to the undesired 1-phenylethane-1,2-diol.

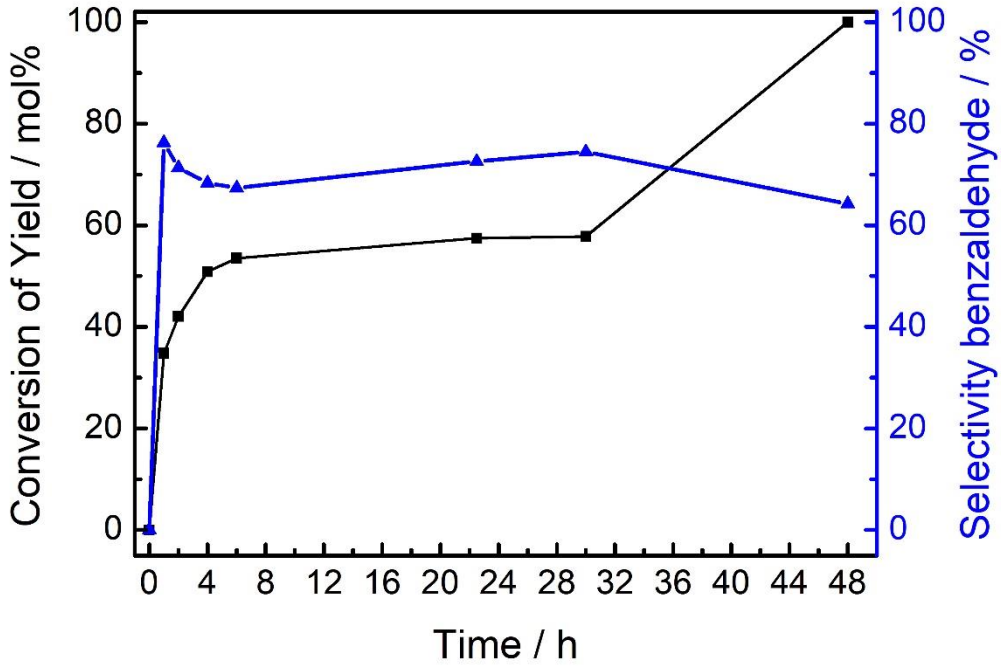

Figure 37. Time-conversion plots of the epoxidation of styrene to styrene epoxide (ketone) using TBHP under PCN-222(Mn) catalyst.

Therefore, the substrate scope was expanded by the use of cyclic olefins with internal double bonds.

Cyclohexene oxidation

Cyclohexene was selected as a substrate to examine the oxidation properties of PCN-222(Mn) catalyst towards the allylic position in a cyclic olefin which might exhibit different stabilization mechanism of the radical intermediates, thus improving the selectivity of the reaction (Scheme 10).

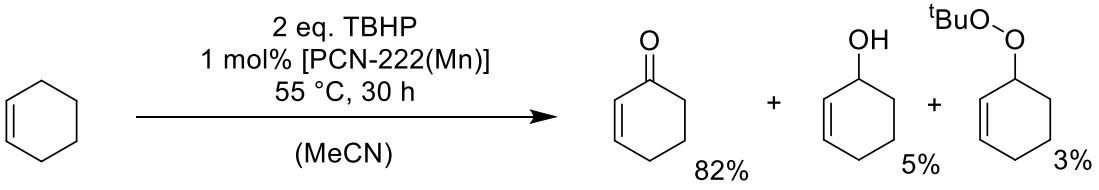

Scheme 10. Catalytic oxidation of cyclohexene using TBHP over PCN-222(Mn) catalyst.

Indeed, cyclohexene-1-one was obtained with a yield of 82 % and a significantly improved selectivity of 92 % at 90 % conversion (Figure 38). Blank tests using no catalyst showed a yield

of 11% for the ketone and a reversed selectivity for the respective alcohol which was obtained as the major product with a yield of 35%.

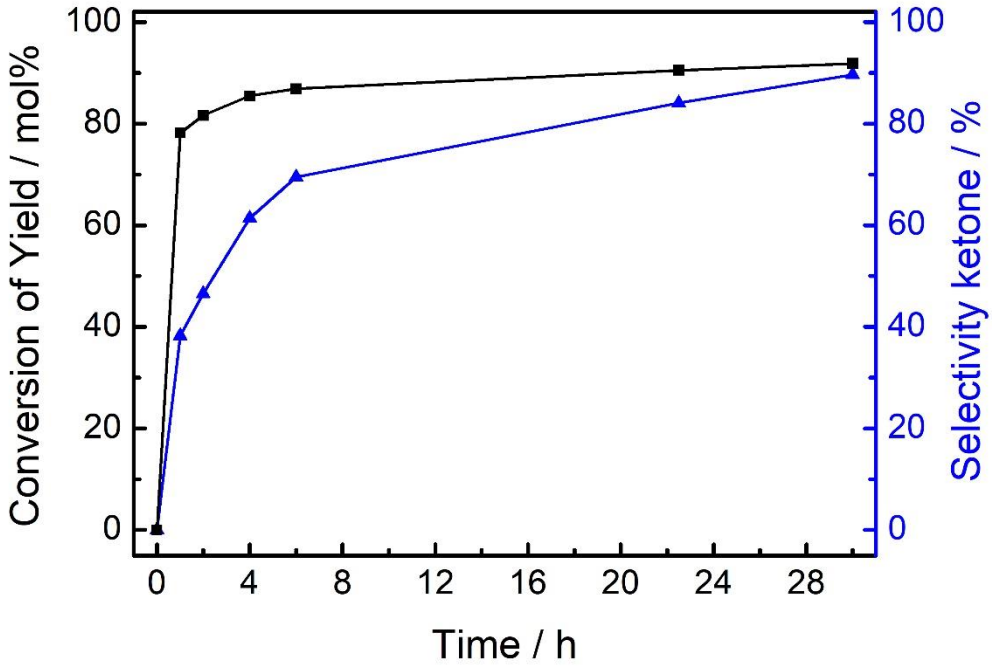

Figure 38: Time-conversion plots of the oxidation of cyclohexene to cyclohexene-1-one (ketone) using TBHP under PCN-222(Mn) catalyst.

Mechanistically wise, it is likely that an allylic hydrogen is removed by the *tert*-butylperoxyl radical, a theory that is supported by the high stability of allylic radicals (Scheme 11). Recombination with another *tert*-butylperoxyl radical leads to *tert*-butylperoxyl adduct which is also found as a by-product. Homolytic cleavage and subsequent hydrogen radical abstraction for example would lead to the observed ketone. A driving force of this proposed reaction the energetically favorable formation of the resulting enone moiety.

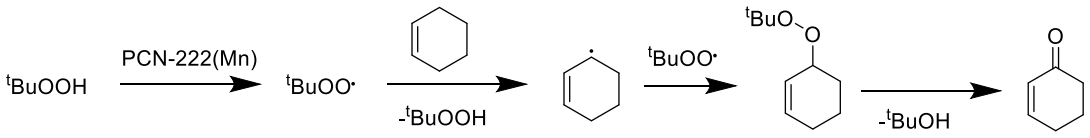

Scheme 11: Possible mechanism for the cyclohexene oxidation with TBHP over PCN-222(Mn) catalyst.

4.1.2.2 Oxidation using molecular O_2

Generally, various oxidizing agents such as $NaClO_4$, NaOCl, $KHSO_5$, 2,6-Dichloropyridine *N*-oxide, *tert*-butyl hydroperoxide and iodosylbenzene are being used in literature.[9] Most of them are less feasible with respect to environmental aspects like the formation of undesired by-products, toxicity and their hazardous potentials. Hence, the use of H_2O_2 can be seen as an improvement, since only water is produced as a by-product. Moreover, industrial application often requires the use of gases in order to operate gas-solid phase-type reactions. In this context, molecular oxygen displays an alternative and is recognized as a more 'green' oxidizing agent, due to its natural abundance and less pronounced safety concerns compared to often unstable and explosive peroxides. Recently, also MOFs had been applied as oxidation catalysts employing O_2 as oxidant. Bouchard et al. used MOF-525(Mn) as catalyst in the epoxidation of styrene and found a remarkable conversion of 99 % and a selectivity of 82 % towards styrene epoxide at rt.[142]

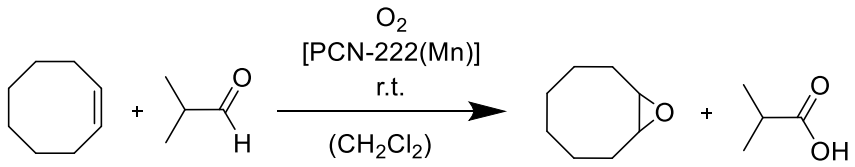

Scheme 12. Epoxidation of cyclooctene using molecular oxygen under PCN-222(Mn) catalyst and isobutyraldehyde.

In their set-up dioxygen is bubbled through a mixture of olefin in CH_2Cl_2 using isobutyraldehyde as a sacrificial agent being oxidized to the corresponding carboxylic acid (Scheme 12). Motivated by these remarkable results further investigations employing O_2 as oxidant were initiated.

4.1.2.2.1 Dynamic conditions (open set-up, bubbling O_2)

Repetition of these experiments using PCN-222(Mn) as catalyst lead to similar results. In the catalytic reaction 5 mg PCN-222(Mn) (0.26 mol % Mn), 15 mL CH_2Cl_2, 0.91 mL isobutylaldehyde (10 mmol) and 0.26 ml cyclooctene (2 mmol) were introduced in a Schlenk tube which was sealed with a septum carrying a needle to ensure pressure release. Through a fixed metal needle which was immersed into the reaction solution, a constant flow of O_2 (30 sccm) was adjusted. Under dynamic conditions (constant bubbling of O_2) PCN-222(Mn) exhibits the highest activity (TOF = 100 h^{-1}), converting cyclooctene to the corresponding cyclooctene epoxide with full selectivity in 1 h at rt (Figure 39).

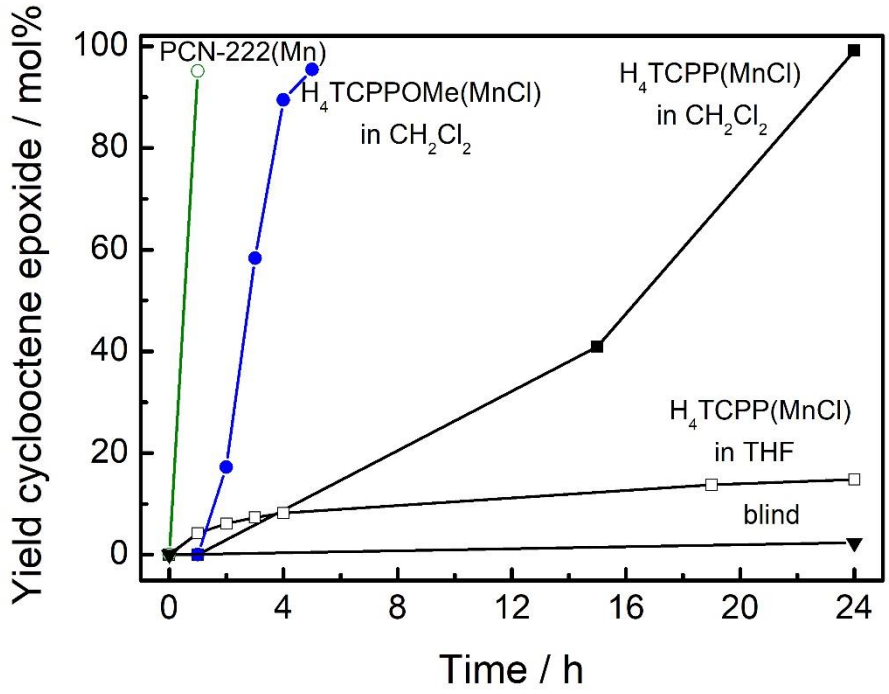

Figure 39. Epoxidation of cyclooctene using O_2 under dynamic conditions (bubbling) under PCN-222(Mn) catalyst in comparison to molecular Mn-porphyrins in CH_2Cl_2 and THF as solvents.

Homogeneous H_4TCPPOMe(MnCl) was more active (TOF = 11 h^{-1}) than its sopanificated analog H_4TCPP(MnCl) which is reasoned by the better solubility in non-polar CH_2Cl_2. Interestingly, heterogeneous PCN-222(Mn) catalyst outperformed the homogeneous Mn-porphyrin ester. This might be explained by the absence of dimerization and self-oxidation which is prevented when the catalytically active Mn-porphyrins are installed into the rigid scaffold of the MOF. The blind test using no catalyst showed almost no reaction. Despite the positive results, the dynamic conditions are not ideal and require improvement due to the constant removal of solvent which is caused by the opened set-up with permanent bubbling of O_2.

4.1.2.2.2 Static conditions (closed set-up, 1 bar O_2 / air)

Thus, static conditions using a closed set-up operated in Fisher porter bottles (pressurizable borosilcate glass vessels) which were charged with 1 bar O_2 in the beginning of the reaction were tested (Figure 40).

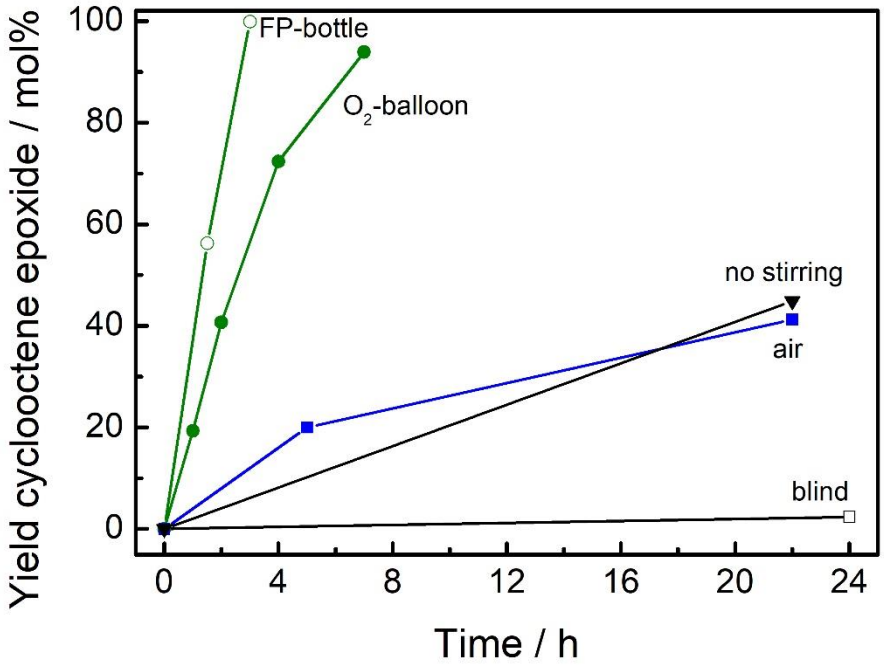

Figure 40. Epoxidation of cyclooctene using O_2 and air under static conditions (1 bar O_2 and air) under PCN-222(Mn) catalysts utilizing different closed reaction set-ups: A Fisher porter bottle (FP bottle) and a O_2-balloon. In the FB bottle set-up, the reaction was operated under stirring and no stirring, as well as using air as an oxidant.

As a result, the catalytic activity was lower (TOF = 37 h^{-1}) due to overall less available O_2, however, the experimental set-up was much more facilitated under these static conditions. Even a simple balloon filled with O_2 lead to similar results compared to the Fisher porter bottle set-up. Remarkably, the reaction could be operated using compressed air instead of O_2, however, the catalytic activity decreased under these conditions. The reaction was repeated without stirring, showing moderate dependence to mass transport and decreased yields of 40 % after 22 h. Additionally, the blind test revealed no conversion.

5 Tandem catalysis

5.1 Tandem oxidation of benzaldehyde / cyanosilylation using PCN-222(Mn)

The general idea was to combine the catalytic oxidation properties of metalloporphyrin struts with the Lewis-acidic properties of the Zr_6-oxo-nodes of PCN-222(M) materials in order to attain a heterogeneous MOF-based catalytic tandem catalyst. As described in chapter 4.1.2 and 3.3, PCN-222(Mn) catalyzes the independent reactions, namely, the oxidation of olefins as demonstrated for styrene, cyclohexene-1-one and cyclooctene (1), as well as the Lewis acidic cyanosilylation of benzaldehyde (2). In order to establish a tandem process, the two distinct catalytic processes need be integrated in a one-pot reaction.

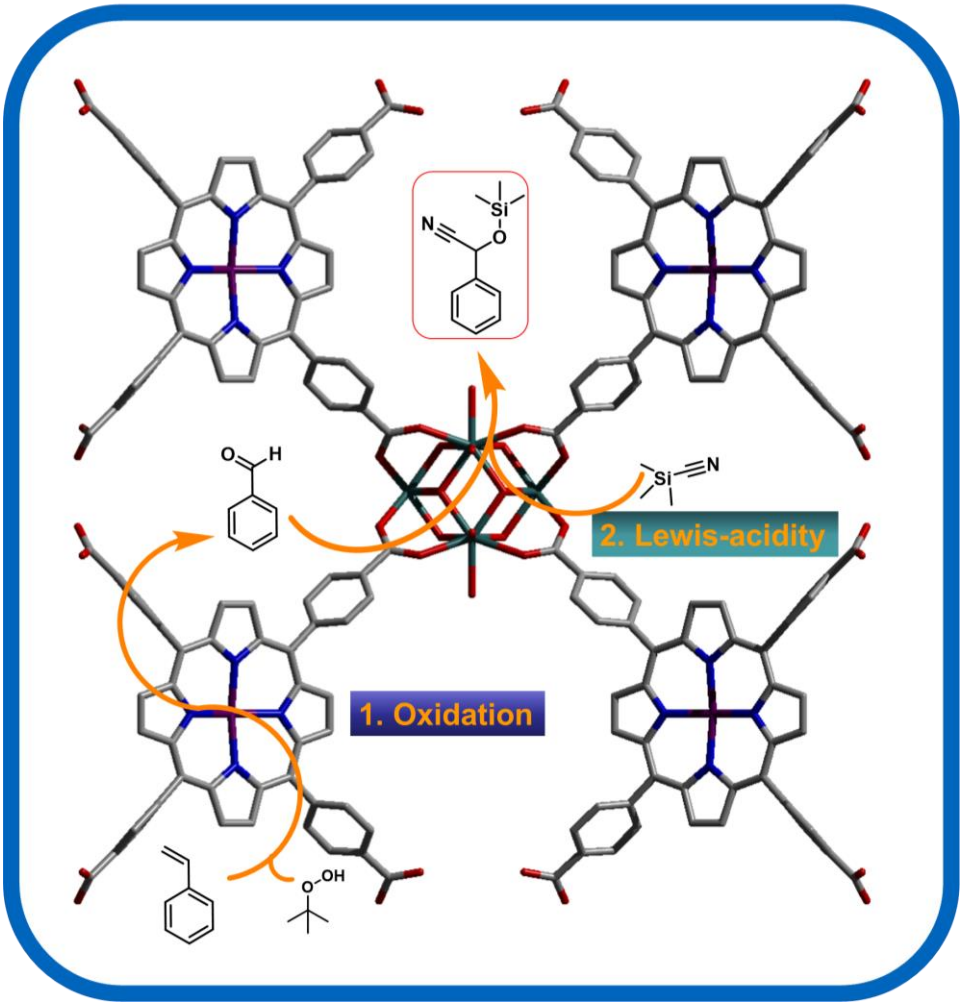

Scheme 13. Illustration of the reaction pathway of styrene in the oxidation/Lewis acid mediated tandem reaction under multi-functional PCN-222(Mn).

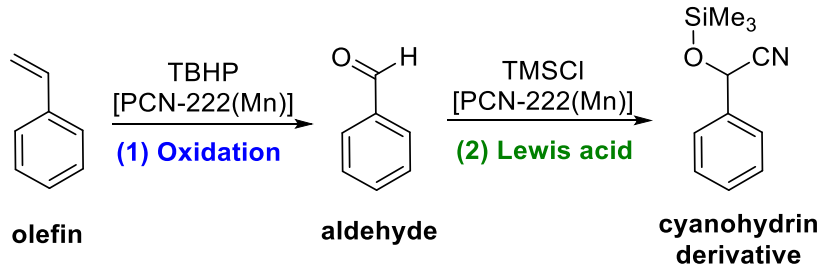

Scheme 14. Idealized tandem oxidation of styrene using *tert*-butyl hydroperoxide (TBHP) (1) and cyanosilylation of in-situ generated benzaldehyde with trimethylsilyl cyanide (TMSCN) (2) to the corresponding cyanohydrin end-product.

In the one-pot tandem reaction styrene, TBHP, trimethylsilyl cyanide (TMSCN) and catalytic amounts of PCN-222(Mn) were introduced in CH_2Cl_2 at 55 °C under stirring in a closed Schlenk tube. Product analysis revealed the oxidation products of styrene, but no formation of the cyanohydrin derivative was observed. Interestingly, GC-MS analysis showed adducts of TBHP / TMS and *tert*-butanol / TMS (Scheme 15), which indicates the quenching of the oxophilic siliylation agent TMSCN by TBHP or *tert*-BuOH under formation of HCN.

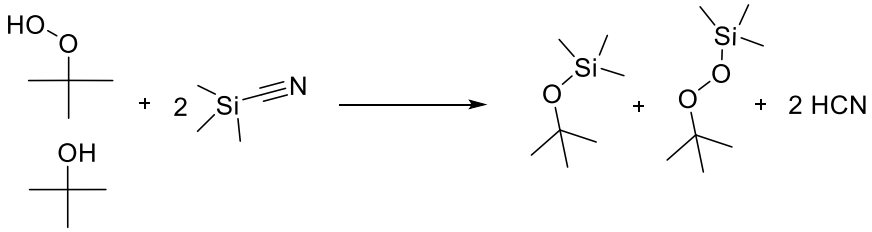

Scheme 15. Illustration of the supposed quenching reaction of TMSCN by TBHP and *tert*-BuOH in the tandem oxidation/cyanosilylation of styrene/benzaldehyde.

Consecutively, no TMSCN is available for the second reaction with benzaldehyde. This shows the drastic impact of incompatible reagents on the outcome of a tandem reaction and the intrinsic challenge to perform tandem-like reactions. Thus, all reagents must be carefully selected in order to minimize side reactions.

5.2 Tandem olefin epoxidation/ CO_2-insertion

As discussed in chapter 4 dioxygen is a cheap and abundant oxidant with relatively low hazardous potential.[207] It's utilization as oxidizing agent instead of *e.g.* iodosylbenzenes or peroxides has a huge advantage in the context of the combability of reactants. Compared to relatively unstable and highly reactive peroxides, O_2 is a rather mild oxidant with moderate reactivity. This property is favorable in terms of reaction control and possible interferences with other reactants and reactions intermediates as well as toxicity.

According to the studies in chapter 4.1.2, PCN-222(Mn) was successfully applied as heterogeneous epoxidation catalyst converting cyclooctene to cyclooctene epoxide using

molecular oxygen as green oxidizing agent. Additionally, the Lewis acidic catalytic properties of PCN-222(Mn) and other porphyrin MOFs were intensively studied in chapter 3.1 demonstration their potential in the CO_2-insertion in epoxides to yield cyclic carbonates. In terms of an optimized reaction-controlled process, it is appealing and more economical to combine those independent reactions in a tandem one-pot reaction. This would directly lead to the desired, value-added cyclic carbonate products when starting with an unfunctionalized olefin using PCN-222(Mn) as multifunctional catalyst (Scheme 16).

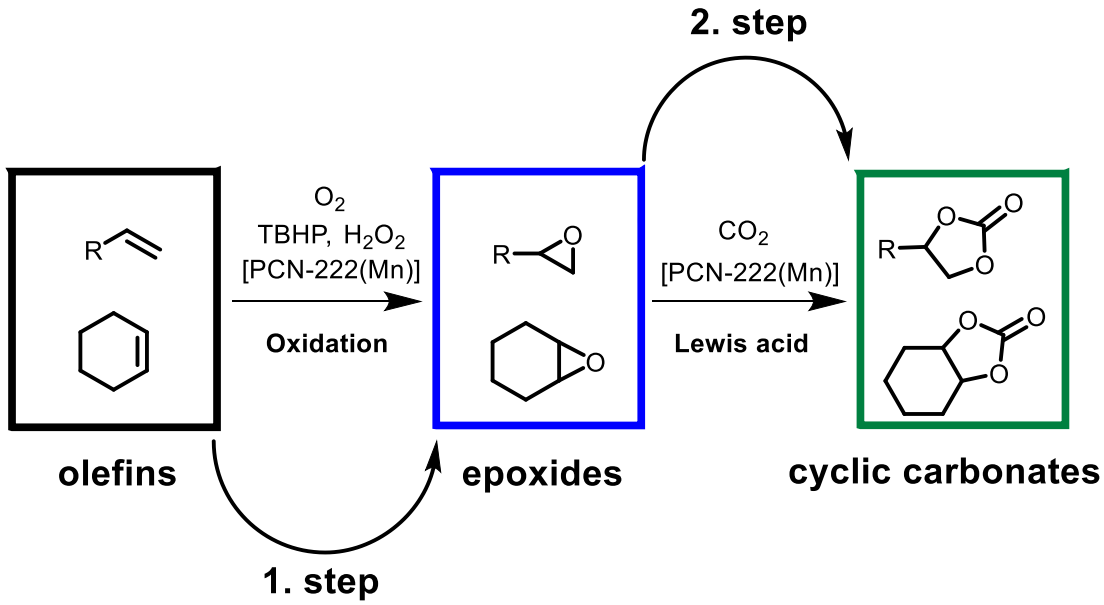

Scheme 16. Illustration of a PCN-222(Mn) catalyzed epoxidation/CO_2-insertion tandem process: Cyclic or linear olefins are oxidized to epoxides (first step) and further converted to the corresponding cyclic carbonates under Lewis acidic activation in the second step.

Notably, the reaction requires the right choice of substrate which is suitable for both reaction steps. On the one hand, cyclic (strained) olefins such cyclooctene oxide are comparably easy to epoxidize which is the reason for its popularity among academic research. On the other hand, the insertion of CO_2 into cyclooctene oxide is not that straight forward, mainly due to steric effects (attack of the nucleophile for the ring-opening reaction). For terminal olefins, the situation is opposed: Epoxidation often is more difficult, and the CO_2-insertion is rather facile. Thus, cyclohexene (or cyclopentane) might be the right compromise between the mentioned extreme cases, since the oxidation still proceeds in good yields and it has less steric hindrance compared to cyclooctene which might facilitate the CO_2 insertion.

Table 4. CO_2 insertion into various epoxides.

Catalyst	Substrate	Yield[a] [%]	co-cat[a] [mol%]	Zr [mol%]	T [°C]	p [bar]	t [h]
PCN-222(Mn)	1-octene oxide	24	0.02	0.1	rt	1	96
PCN-222(Mn)	cyclooctene oxide	2	0.02	0.1	60	1	48
PCN-222(Mn)	cyclohexene oxide	40	0.02	0.1	50	2	48
PCN-222(Mn)	cyclohexene oxide	17	0.02	0.1	rt	4	43
PCN-222(Mn)	styrene oxide	5	0.02	0.1	rt	4	15
PCN-222(Mn)	propylene oxide	99	0.02	0.1	50	1	22
PCN-222(Mn)	propylene oxide	65	0.02	0.1	rt	1	22
PCN-222(Mn)	epichlorohydrin (rac)	23	0.02	0.1	rt	1	22

[a]Bu_4NBr. No solvent was used.

Table 5. Epoxidation of various olefins.[a]

Catalyst	Substrate	Yield[a] [%]	Mn [mol%]	T [°C]	p [bar]	t [h]
PCN-222(Mn)	cyclooctene	99	1	rt	1	1
PCN-222(Mn)	cyclohexene	90	1	rt	2	16
PCN-222(Mn)	Styrene[a]	99	1	rt	4	4
PCN-224	epichlorohydrin (rac)	12	1	rt	1	24

[a]Isobutyraldehyde (10 mmol) was used as a sacrificial agent. [a]Full decomposition of MOF-catalyst to a homogeneous solution was observed.

In the epoxidation/CO_2-insertion tandem process 0.91 mL isobutyraldehyde (10 mmol), 0.2 mL cyclohexene (2 mmol), 0.365 g tetra-n-butylammonium bromide (TBAB) (1.1 mmol) were mixed in 2 mL dichloromethane in a closed Fisher porter bottle set-up and charged with 1 bar oxygen and 3 bar carbon dioxide at 50 °C under stirring using 25 mg PCN-222(Mn) as catalyst. A Conversion of 61 % was found (based on cyclohexene as initial educt) after two days of reaction time. Cyclohexene carbonate as the desired product after the two distinct reactions steps was obtained with a poor yield <5 % (Figure 41). Cyclohexene oxide was identified as the main product (yield = 43 %) next to other undesired oxidation by-products (yield = 11 %). This indicates that the oxidation of cyclohexene to cyclohexene oxide (first step) proceeds with reasonable yields, however, only a small fraction of in-situ generated cyclohexene oxide reacts further to the desired cyclic carbonate (second step). This could be reasoned by the potential blocking of the catalytically active Zr-/Mn-sites either by polar compounds such as the sacrificial aldehyde, cyclohexene oxide or carbonate (highly polar). Another explanation could be the low CO_2 pressure of only 3 bar, since for this type of reaction it is known that the catalytic transformation to the carbonate directly correlates with increasing CO_2 pressure which was also

demonstrated by Hupp et al. who applied 60 bar (!) CO_2 pressure as described above. Another problem might be the slight acidic conditions, which are caused by the oxidation of the isobutyraldehyde to the corresponding acid: The proton can be transferred to the cyclohexene oxide resulting in the undesired ring-opening reaction and other possible side reactions. This, however, is an intrinsic problem since the isobutyraldehyde is crucial for the transfer of the second O-atom of O_2.

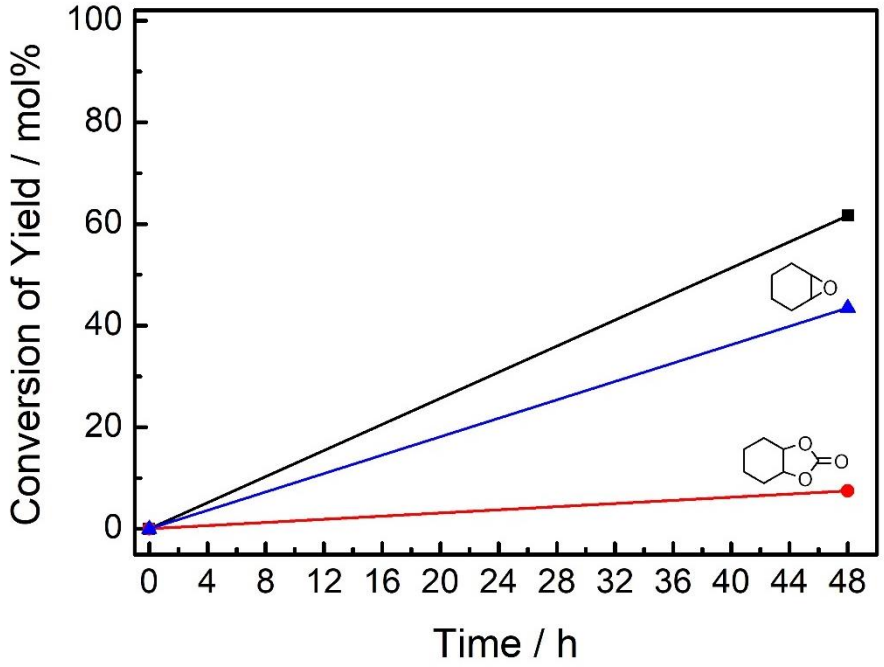

Figure 41. One-pot tandem reaction starting from cyclohexene to give cyclohexene oxide and cyclohexene carbonate.

Summarized, the chosen tandem reaction pathway principally is promising since the conversion of the first step produces high amount of cyclohexene oxide, however, the yield for the end-product is low which might be due to blocking of active sites or too low CO_2 pressure. Therefore, the reaction requires further optimization, namely, the increase of CO_2 pressure to further facilitate the transformation to the cyclic carbonate

6 Summary and Outlook

Functional coordination network compounds, especially the class of metal-organic frameworks (MOFs) are known for their multi-faceted properties such as high surface area, permanent porosity and more importantly, exceptional tailorability. Due to their thermal and chemical stability metalloporphyrin (MP) based Zr-MOFs are suitable candidates for the design of novel multi-functional heterogeneous catalysts which, ideally, can perform multi-step catalytic processes.

In this work well-selected MP (M = Fe, Mn, Zn, Rh) Zr-MOFs bearing altered degrees of connectivity, topology and pore environment were synthesized and their catalytic properties were elaborated towards Lewis-acidity and biomimetic oxidation catalysis conducted in liquid-phase type of reactions. Additionally, multi-functional Zr-MOFs(MP) with two catalytic sites with altered catalytic reactivity were studied in one-pot tandem reactions.

Initially, the study was focused on biomimetic oxidation reactions, whereby PCN-222(Fe) was employed as catalyst under ambient reaction conditions. The obtained catalytic activity in the (ep)oxidation of cyclooctene was low using H_2O_2 as oxidant. Hence, PCN-222(Mn) with Mn(III) sites was tested in the oxidation of styrene using *tert*-butyl hydroperoxide (TBHP) in decane as oxidizing agent. Under these conditions the reactivity was improved and a conversion of ~55 % was achieved after 30 h with good selectivity of 64 % towards benzaldehyde. Additional introduction of TBHP after 30 h lead to full conversion, accompanied by a slight decrease in selectivity towards the formation of styrene epoxide. A strong dependency of oxidizing agent towards the selectivity was observed, since TBHP in water mainly gave 1,2-dihydroxybenzene. Nevertheless, the selectivity could not be optimized due to the radical-based reaction mechanism. Therefore, cyclohexene as cyclic olefin with the potential feature of the stabilization of radical intermediates in allylic positions was selected. Indeed, cyclohexene-1-one was obtained with a yield of 82 % and a significantly improved selectivity of 92 % at 90 % conversion, indication that the selection of appropriate substrates is crucial for the product selectivity. In terms of sustainability and economy molecular oxygen was employed as an alternative oxidizing agent in the epoxidation of cyclooctene. Under dynamic conditions (constant bubbling of O_2 trough the reaction solution) PCN-222(Mn) catalyst exhibited the highest activity (TOF = 100 h^{-1}), with full conversion and selectivity in 1 hour at rt, outperforming its homogeneous Mn-porphyrin counterpart. Thus, static conditions using a closed set-up operated in Fisher porter bottles which were charged with 1 bar O_2 in the beginning of the reaction, revealed slightly lower catalytic activity (TOF = 37 h^{-1}) due to overall less available O_2, however, the experimental set-up was much more facilitated under these static conditions. Remarkably, the reaction could be operated using compressed air instead of O_2.

In contrast to the oxene transfer, as demonstrated by the abovementioned biomimetic olefin epoxidation and alkane and aromatic hydroxylation reactions, reactions involving the transfer of carbenes are not known in biologic systems.[38] Therefore, the utilization of artificial MPs for establishing new C-C bonds via carbene transfer, is a milestone on how mankind can learn from nature and transfer this knowledge to new reactions. In this study the focus was to use Zr-MOFs(MP) as solid catalysts, which was exemplary shown in the stereoselective reaction of cyclopropanes. In this study, PCN-224(Rh), was applied in the asymmetric cyclopropanation of styrene with ethyl diazoacetate. A high diastereomeric ratio (*dr*) of up to 16:1 (*trans*:*cis*) was achieved due to the confinement by smaller pore sizes, which is absent in the PCN-222(Rh) catalyst which contains larger mesopores. The investigated substrate scope included substituted styrenes and linear and cyclic olefins, which showed lower reactivity and *dr*, however, the yields could be successfully improved when the reaction was conducted under excess olefin conditions. PCN-224(Fe) as catalyst revealed lower activity but a *dr* very close to the Rh-system, demonstrating Fe as a cheaper alternative. This work presented an example for asymmetric heterogeneous MOF-based catalysis, where the transfer of stereochemical information is induced by the specific pore confinement of the host matrix and doesn't rely on i.e. asymmetric (chiral) groups or template molecules to produce asymmetric compounds.

Based on the results obtained by the Lewis-acid mediated carbene transfer, emphasis was given to the investigation on how the inherent Lewis-acidity in MP-MOFs is related to connectivity of inorganic SBU and organic MP linker, and how the Lewis-acidic catalytic properties can be optimized upon porphyrin metalation. Hence, the catalytic properties of Lewis-acidic MOF-525, PCN-222 and PCN-224, were explored in the cycloaddition of CO_2 and propylene oxide to propylene carbonate with tetrabutylammonium bromide as co-catalyst. The lower connected PCN-224 (6 linker/node) showed higher catalytic activity than the high-connected MOF-525 (12 linker/node). However, the trend of the connectivity dependent catalytic activity is not fully linear, since MOF-525 outperformed PCN-222 (8 linker/node), which may be explained by high amount of missing linker defects (~16%) and the difference in topology of PCN-222 and MOF-525. Installation of new Mn-sites upon metalation of the Zr-MOFs resulted in higher catalytic activity than their non-metalated counterparts, which could be further improved by introduction of stronger Lewis acids, i.e. Zn, which was exemplary demonstrated for PCN-222. The enhancement of the catalytic activity by linker metalation was more pronounced for PCN-222(Mn) and MOF-525(Mn) which exhibit higher linker/node densities as compared to lower connected PCN-224(Mn). In such complex dual-site Lewis acid Zr-MOF(MP) catalysts, the effective node connectivity, defined by topology and by defect engineering, and the linker metalation partly compensate each other. Additionally, the properties of MOF-525 were compared to the 12-connected molecular analog, the cluster $[Zr_6(OH)_4O_4(OMc)_{12}]$ (OMc = methacrylate), whereby similar catalytic activity was observed. The obtained results show that Z_6-oxo-cluster node and porphyrin linker-based MOFs are a tunable platform in which the Lewis-acid catalytic activity can be adjusted via (1) the choice of topology and connectivity of

the Zr-nodes and (2) subsequent metalation of the porphyrin linkers, as well as by (3) the presence of missing linker defects. Metalation of porphyrin linkers can be useful to enhance the catalytic activity in high connected Zr-MOFs, where the Zr-nodes are saturated by large amounts of linker. Defects play a crucial role and the precise engineering of missing linker defects, is a tool to enhance catalytic reactivity is such systems. Similar observations were made in the cyanosilylation of benzaldehyde. In accordance to our expectation, PCN-222(Mn) catalyst showed a doubled yield of ~90 % after 23 h when compared to non-metalated PCN-222. Introduction of additional Mn-centers located at the porphyrin struts of the framework, significantly contribute to the overall Lewis acidic properties of PCN-222 leading to an improved catalytic activity.

In the last chapter of this work, the aim was to combine the intrinsic Lewis-acidic properties with the biomimetic oxidation activity found in MP-MOFs to perform multi-step tandem reactions. PCN-222(Mn) was selected as catalyst, since it catalyzes the independent reactions, namely, the oxidation of olefins as demonstrated for styrene, cyclohexene-1-one and cyclooctene (1), as well as the Lewis acidic cyanosilylation of benzaldehyde (2). In the first attempt, trimethylsilyl cyanide (TMSCN) was combined with styrene and tertbutyl hydroperoxide TBHP in a one-pot tandem reaction, using PCN-222(Mn) as catalyst. Product analysis revealed the oxidation products of styrene, but no formation of the desired cyanohydrin derivative was observed. Interestingly, GC-MS analysis showed adducts of TBHP / TMS and *tert*-butanol / TMS which indicates the quenching of the oxophilic siliylation agent TMSCN by TBHP or *tert*-BuOH under formation of HCN, showing how critical the combability of reaction participants is. In the next trial, PCN-222(Mn) was used to catalyze the epoxidation/CO_2-insertion tandem process, which involves the epoxidation of cyclic or linear olefins (first step) and their further transformation to the corresponding cyclic carbonates under Lewis acidic activation in the second step. The one-pot reaction gave a conversion of 61 % (based on cyclohexene as initial educt) and cyclohexene oxide was identified as the main product (yield = 43 %) next to other undesired oxidation by-products (yield = 11%). Cyclohexene carbonate as the desired product after the two distinct reactions steps was obtained with a poor yield <5 %. This indicates that the oxidation of cyclohexene to cyclohexene oxide (first step) proceeds with reasonable yields, however, only a small fraction of generated cyclohexene oxide reacts further to the desired cyclic carbonate (second step). This could be reasoned by the potential blocking of the catalytically active Zr-/Mn-sites or due to not fully optimized reaction conditions (low CO_2-preussure).

7 Experimental Section

7.1 Materials and methods

All starting materials were used as received from commercial sources (Sigma Aldrich, Alfa Aesar, TCI, abcr etc.) without undergoing any further purification. Common organic solvents, like *n*-hexane, *n*-pentane, toluene, tetrahydrofurane, diethyl ether were dried using an MBraun solvent purification system (SPS) in which solvents were passed through consecutive filter columns containing suitable adsorbents by application of argon pressure gradients. Used adsorbent materials included a copper catalyst and molecular sieve for *n*-hexane or *n*-pentane, and activated alumina for toluene, tetrahydrofurane and diethyl ether. Benzene and mesitylene were dried using standard purification procedures, i.e. by passing the solvent over a column of activated alumina under an inert atmosphere. Thus, treated solvents exhibited a purity above 99 % and water contents below 5 ppm, as verified by Karl-Fischer titration. Reactions involving air-sensitive compounds were generally performed under an argon atmosphere (99.998%, *Westfalen AG*, Münster) using flame dried glassware (in vacuum), standard Schlenk equipment and techniques.

Analytics

Nuclear Magnetic Resonance Spectroscopy (NMR)

^{1}H and ^{13}C NMR spectra were recorded on a *Bruker* Ultrashield spectro-meter (400 MHz) and on a Bruker AMX-300 spectrometer (300) MHz and 75 MHz, respectively. Usually, 16 and 1024 scans were measured for ^{1}H and ^{13}C NMR, respectively. at 298 K using standard deuterated solvents and evaluated with *MestReNova* software. Chemical shifts (δ) are reported in ppm (parts per million). Spectra are referenced relative to the residual solvent signals. The observed coupling constants are obtained as an average of forward and backward coupling in Hertz. Following abbreviations are used for the assignment of the observed signal multiplicities: s = singulet, d = dublet and m = multiplet.

Elemental Analysis

Elemental analysis and AAS measurements were performed at the Microanalytical Laboratory of the Technical University of Munich, Germany on a HEKAtech Euro EA CHNSO-Analyzer and a Varian AA280FS fast sequential AAS spectrometer. Prior to the measurement, the MOF samples (2 – 5 mg) were thermally activated at 100 - 130 °C in dynamic vacuum.

Powder X-Ray Diffraction (PXRD)

Powder X-ray diffraction measurements were performed on a *PANalytical* Empyrean diffractometer equipped with a *PANalytical* PIXcel 1D detector in *Bragg-Brentano* geometry. X-ray Cu Kα radiation (λ_1 = 1.5406 Å, λ_2 = 1.5444 Å, I_2/I_1 = 0.5) was used for the measurements. Kβ radiation was removed with a Ni-filter. Voltage and intensity were 45 kV and 40 mA, respectively. The measurement range was from 4.0° up to 70.0° (2θ), with a step size of 0.040° (2θ) and an acquisition time of 35 seconds per step. The measurement was performed at 298 K, and the sample was rotated on a reflection-transmission spinner during the measurement at 0.5 rps. High-throughput powder X-ray diffraction patterns were recorded on a STOE COMBI P diffractometer (monochromated Cu Kα-1 radiation, λ = 1.540 60 Å) equipped with an IP-PSD detector in transmission geometry.

Gas Chromatography - Mass Spectrometry

Gas chromatograms were recorded on an *Agilent* 7890B Gas Chromatograph equipped with an *Agilent* HP-5 column with 30 m length, 0.32 mm inner diameter and 0.25 µm film thickness of the stationary phase. Helium was used as mobile phase and the injected volume was 1 µL. Gas chromatograms with coupled mass spectrometry were recorded on an *Agilent* 7890B Gas Chromatograph equipped with an *Agilent* HP-5ms UI column with 30 m length, 0.32 mm inner diameter and 0.25 µm film thickness of the stationary phase. Helium was used as mobile phase and the injected volume was 1 µL. This was coupled with an *Agilent* 5977AGC/MSD device.

Fourier Transform Infrared Spectroscopy (FTIR Spectroscopy)

FTIR measurements were performed on a Bruker Alpha-P FT-IR spectrometer in ATR geometry equipped with a diamond ATR (spectral region = 4000 – 375 cm^{-1}) unit under inert gas atmosphere inside a glovebox. All spectra were processed with the OPUS 6.5 software provided by Bruker. Bands are consecutively reported as position (wave number ν in cm^{-1}) and relative band intensity (vs = very strong, s = strong, m = medium, w = weak).

Thermogravimetric analysis (TGA)

Thermogravimetric studies were conducted using a *Mettler Toledo* TGA/STA 409 PC apparatus and a *Netzsch* QMS 403 Aeolos device for additional mass spectrometry analysis with a continuous heating ramp of 10 °K/min applied under oxidizing conditions in a synthetic air (N_2/O_2 = 80/20) flow or under inert conditions using Ar. Around 5 mg of sample were used.

N_2-Physisorption (Brunauer–Emmett–Teller, BET)

N_2 adsorption-desorption isotherms were measured using a *Quantachrome* NOVA 4000e multi-station device and on a Micromeritics 3Flex surface analyzer using N_2 (N_2 = 99.999%) at 77 K. Before starting the measurement, the samples (~100 mg) were thermally activated in dynamic

vacuum for 12-24 h at 100 - 130 °C. The specific surface area of the materials was calculated using the multipoint BET method (Brunauer−Emmett−Teller) applied to the isotherm adsorption branch, while taking into account the Rouquerol consistency criteria. Pore size distributions were analyzed using DFT calculation with the according software.

UV-Vis

UV-Vis spectroscopy was performed on an Agilent Cary 60 UV-VIS instrument in the range 300 - 800 nm.

Computational optimizations

All calculations have been performed with Gaussian-16.B.01[1] using the B97 functional[2]with the Grimme's D3BJ dispersion[3] and the split valence basis set def2-SVP[4]. Rh atoms have been treated with the Stuttgart/Dresden 1997 relativistic effective core potential (ECP). Optimizations were obtained without using constraint coordinates.

[1] M. J. Frisch, G. W. Trucks, H. B. Schlegel, G. E. Scuseria, M. A. Robb, J. R. Cheeseman, G. Scalmani, V. Barone, G. A. Petersson, H. Nakatsuji, X. Li, M. Caricato, A. V. Marenich, J. Bloino, B. G. Janesko, R. Gomperts, B. Mennucci, H. P. Hratchian, J. V. Ortiz, A. F. Izmaylov, J. L. Sonnenberg, Williams, F. Ding, F. Lipparini, F. Egidi, J. Goings, B. Peng, A. Petrone, T. Henderson, D. Ranasinghe, V. G. Zakrzewski, J. Gao, N. Rega, G. Zheng, W. Liang, M. Hada, M. Ehara, K. Toyota, R. Fukuda, J. Hasegawa, M. Ishida, T. Nakajima, Y. Honda, O. Kitao, H. Nakai, T. Vreven, K. Throssell, J. A. Montgomery Jr., J. E. Peralta, F. Ogliaro, M. J. Bearpark, J. J. Heyd, E. N. Brothers, K. N. Kudin, V. N. Staroverov, T. A. Keith, R. Kobayashi, J. Normand, K. Raghavachari, A. P. Rendell, J. C. Burant, S. S. Iyengar, J. Tomasi, M. Cossi, J. M. Millam, M. Klene, C. Adamo, R. Cammi, J. W. Ochterski, R. L. Martin, K. Morokuma, O. Farkas, J. B. Foresman, D. J. Fox, Wallingford, CT, **2016**.

[2] S. Grimme, *J. Comput. Chem.* **2006**, *27*, 1787-1799.

[3] S. Grimme, S. Ehrlich, L. Goerigk, *J. Comput. Chem.* **2011**, *32*, 1456-1465.

[4] F. Weigend, R. Ahlrichs, *PCCP* **2005**, *7*, 3297-3305.

7.2 Catalytic tests

General procedures for liquid-phase typed of reactions:

CO_2-insertion in propylene epoxide

Catalytic reactions were carried out in pressurizeable Fisher-Porter bottles charged with specific amount of thermally activated MOF catalyst (0.1 mol% Zr) (activated under dynamic vacuum at T = 120 °C for 12 h) (28.8 µmol Zr), 0.805 g Bu_4NBr (2.5 mmol), 2.1 mL (30 mmol) propylene oxide and 1 bar CO_2 at 50 °C. Before introduction of propylene oxide, the bottle was evacuated and flushed with argon. Aliquots were taken every hour, whereupon the suspension was filtered by a syringe filter and analyzed by ^{1}H NMR.

Cyanosilylation of benzaldehyde

The thermally pre-activated MOF-catalyst (activated under dynamic vacuum at T = 120 °C for 12 h) was placed in a Schlenk tube in which 62 µL (0.5 mmol, 2 eq.) trimethylsilyl cyanide (TMSCN), 25.4 µL (0.25 mmol, 1 eq.) benzaldehyde and 1 mL acetonitrile were added under constant flow of argon. The Schlenk tube was closed and the reaction mixture was stirred at rt or 40 °C, respectively. After the reaction, the mixture was analyzed using GC.

Oxidation reactions

1. Oxidation of cyclooctene using H_2O_2

5 mg of thermally activated PCN-222(Fe) catalyst (2 mol% Fe) was placed in a Schlenk tube and 12.9 µL cyclooctene (0.1 mmol), 16 µL hydrogen peroxide (0.3 mmol, 50% w.t. in water) and 1 mL acetonitrile was added under constant argon flow. The Schlenk tube was closed and the reaction mixture was stirred at rt and analyzed by GC using p-xylol and acetophenone as internal standards.

2. Oxidation of cyclooctene using O_2 under 'dynamic conditions'

In the catalytic reaction 5 mg PCN-222(Mn) (0.26 mol% Mn) catalyst, 15 mL CH_2Cl_2, 0.91 mL isobutylaldehyde (10 mmol) and 0.26 ml cyclooctene (2 mmol) were introduced in a Schlenk tube which was sealed with a septum carrying a needle to ensure pressure release. Through a fixed metal needle which was immersed into the reaction solution, a constant flow of O_2 (99.99999%, Westfalen AG) (30 sccm) was adjusted. The reaction mixture was stirred under rt and aliquots were analyzed using ^{1}H NMR.

3. Oxidation of cyclooctene using O_2 under 'static conditions'

In the catalytic reaction 15 mg of PCN-222(Mn) (~1 mol% Mn) catalyst, 7 mL CH_2Cl_2, 0.45 mL isobutylaldehyde (5 mmol) and 0.13 ml cyclooctene (1 mmol) were introduced in a Fisher-porter bottle which was charged with 1 bar O_2 (99.99999%, Westfalen AG) or air. The reaction mixture was stirred under rt or elevated temperatures and aliquots were analyzed by ^{1}H NMR.

4. Oxidation of styrene/cyclohexene

In a small Schlenk flask under inert conditions 2 mg of thermally activated PCN-222(Mn) catalyst were mixed with 1 mL of acetonitrile, 33 µL of styrene (30.03 mg, 0.29 mmol, 1 eq.) or 30 µL of cyclohexene (24.30 mg, 0.30 mmol, 1 eq.), respectively. As oxidant, 100 µL of tert-butyl hydroperoxide (in decane, 2 eq.) was added and the reaction mixture was stirred at 55 °C. During the reaction, aliquots were taken after the reaction mixture was allowed to cool down to rt and analyzed by gas chromatography.

Tandem reactions

1. Tandem oxidation of benzaldehyde / cyanosilylation

The thermally pre-activated MOF-catalyst (activated under dynamic vacuum at T = 120 °C for 12 h) was placed in a Schlenk tube in which 62 µL (0.5 mmol, 2 eq.) trimethylsilyl cyanide (TMSCN), 33 µL (0.29 mmol, 1 eq.) styrene, 1 mL acetonitrile and 26 µL H_2O_2 (50% w.t. in water) were added under constant flow of argon. The mixture was stirred at 55 °C. After the reaction, the mixture was allowed to cool down to rt and the aliquots were analyzed by GC. Alternatively, the reaction was done in a cascade-typed fashion. Herein, usually 2 mg PCN-222(Mn) catalyst were combined with 33 µL (0.29 mmol) styrene, 82 µL (2 eq.) tert-butylhydroperoxide (TBHP) in 1 mL acetonitrile and stirred for 24 h. After that 62 µL TMSCN were added and the reaction was stirred.

2. Tandem olefin epoxidation/ CO_2-insertion reaction

25 mg pre-activated PCN-222(Mn) were transferred into a Fisher-porter bottle and mixed with 2 mL CH_2Cl_2, 0.91 mL isobutylaldehyde (10 mmol), 0.16 g Bu_4NBr (0.5 mmol), and specific amounts of olefin substrate (2 mmol) and charged with different ratios of both CO_2 / O_2, (usually 3 bar CO_2 / 1 bar O_2) and stirred under elevated temperatures. After the reaction, the mixture was allowed to cool down to rt and the aliquots were analyzed by ^{1}H NMR.

Cyclopropanation of styrene using ethyl diazoacetate (EDA)

All catalytic reactions were conducted in 10 ml glass-vials at room temperature under stirring in air. Ethyl diazoacetate (EDA) was manually introduced into the olefin solution within max. 20 min using a syringe. Controlled addition of EDA was operated as followed: 135 µL

(1.1 mmol) EDA diluted in 3 mL CH_2Cl_2 was added via a syringe pump (rate = 0.5 mL/h) to a suspension of 5 mg PCN-224(Rh) (0.0033 mmol, 0.4 mol% Rh) catalyst in 3 mL CH_2Cl_2 using mesitylene as an internal standard. Aliquots were taken from the dispersed reaction solution and filtered through a syringe filter to separate the MOF from the reaction solution. The clear solution was analyzed and quantified via GC and product identification was achieved using GC-MS and ^{1}H and ^{13}C NMR.

Catalytic parameters such as conversions, selectivities, yield and turnovers were calculated using following equations:

Conversion $$X = \frac{\sum n(products)}{\sum n(products)+n(educt)}$$

Selectivity $$S = \frac{n(main\ product)}{\sum n(side\ products)+n(main\ product)}$$

Yield $$Y = X * S$$

Turnover Frequency $$TOF = \frac{X*n(educt)}{n(catalyst)*time}$$

7.3 Synthesis of porphyrinic organic linkers (H_4TCPP(2H)/ H_4TCPP(MCl))

The synthesis of the metalated organic linker (M-TCPP, where M = Mn) was generally performed in three-steps, as can be seen in Figure 42. Mechanistically, the esterified porphyrin system (TPPCOOMe) is formed by multiple condensation reactions between pyrrole and methyl *p*-formylbenzoate. The subsequent metalation was then carried out by addition of a suitable metal salt (*e.g.* $MnCl_2 \cdot 4H_2O$ for Mn-TCPP). In a final reaction step, the ester groups were saponified. The desired product was subsequently afforded by an aqueous/acidic work up. The non-metalated species (H_2TCPP/TPPCOOH, free-base) was obtained by direct saponification of the first reaction product (TPPCOOMe).

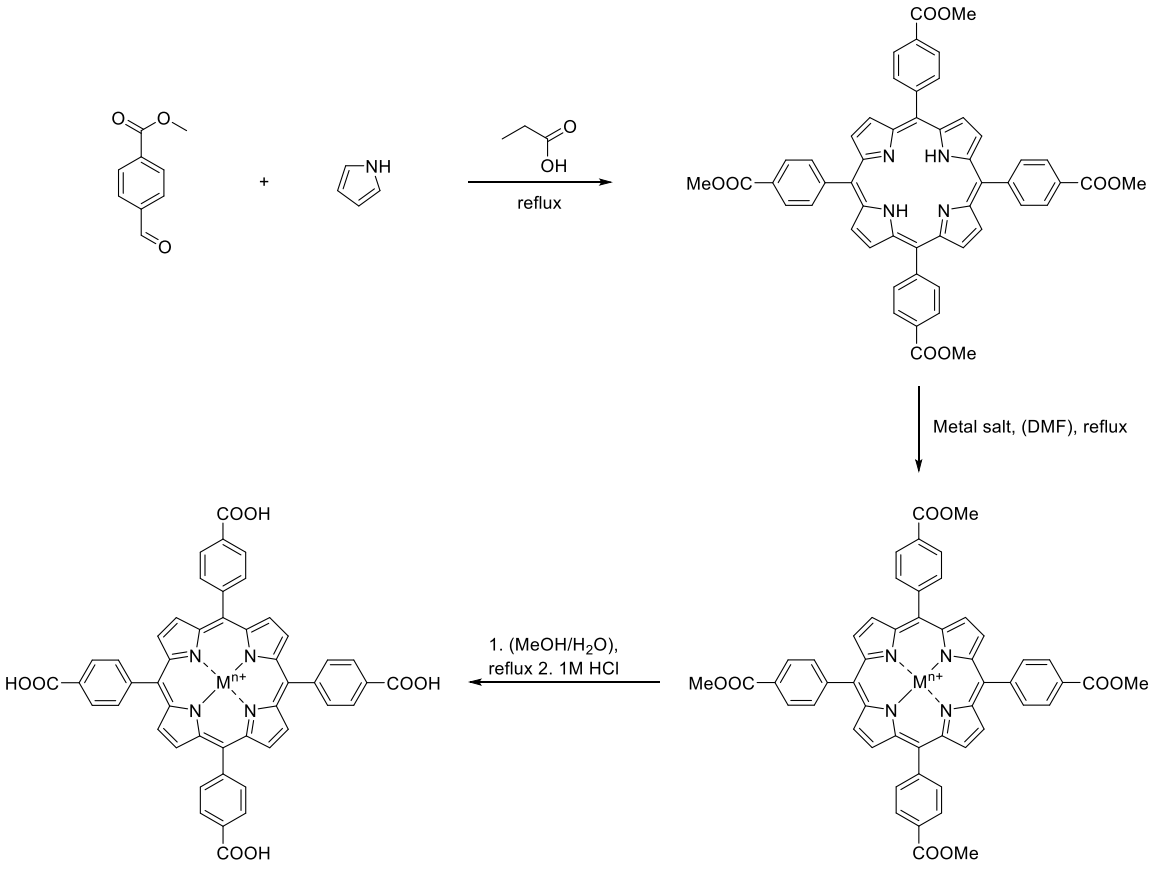

Figure 42. General overview for the three-step synthesis of the H_4TCPP(MCl) organic linker

5,10,15,20-Tetrakis(4-methoxycarbonylphenyl)porphyrin [TPPCOOMe]

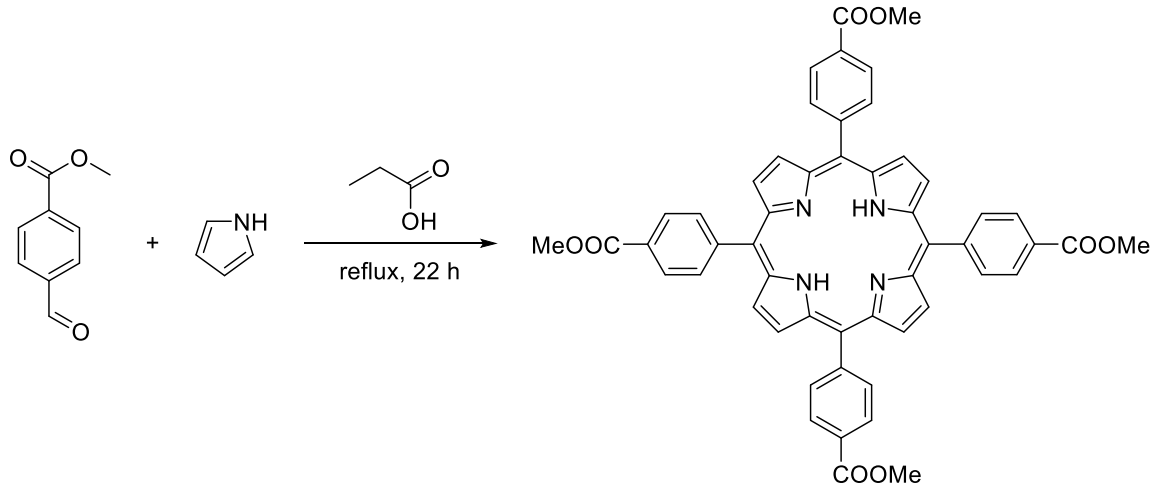

Figure 43. Synthesis of TPPCOOMe.

3.09 mL (3.00 g, 44.7 mmol, 1.0 eq.) pyrrole and 6.93 g (42.2 mmol, 1.0 eq.) methyl *p*-formylbenzoate were added to refluxed propionic acid (100 mL). The solution was then refluxed for 22 h under continuous stirring. After the reaction mixture was cooled to room temperature, the obtained purple crystals were collected by suction-filtration (1.65 g, 1.95 mmol, 20 % yield).[208] **^{1}H-NMR** (DMSO, 400 MHz): δ [ppm] = 8.86 (s, 8H, β-pyrrole), 8.42 (d, ^3J = 8.2 Hz, 8H, phenyl), 8.38 (d, ^3J = 8.2 Hz, 8H, phenyl), 4.05 (s, 12H, COO*Me*), -2.95 (s, 2H, N*H*). UV-VIS: (DMSO, λ_{max}, (logε)) 421 (sorret-band), 515, 550, 588, 645 (Q-bands) nm.

5,10,15,20-Tetrakis(4-carboxyphenyl)porphyrin [TCPPOH, H$_4$TCPP(2H)]

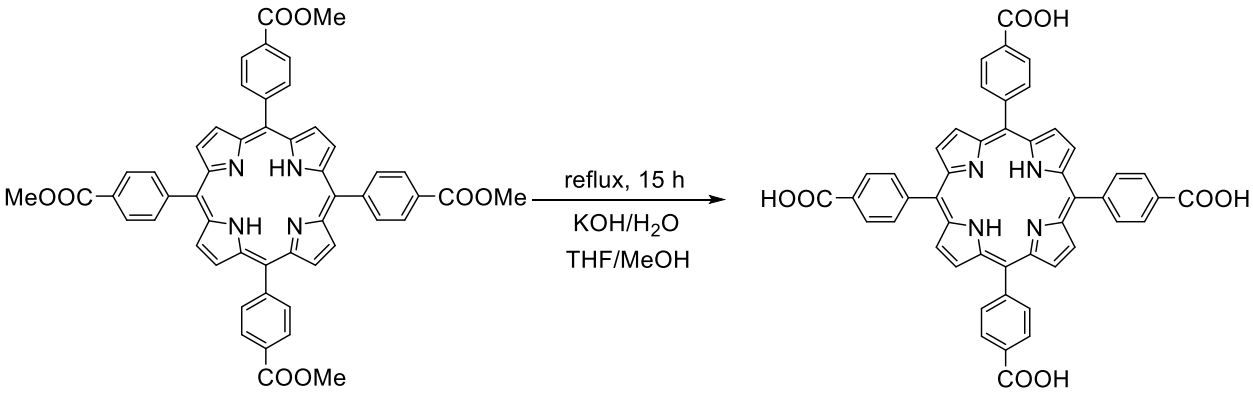

Figure 44. Saponification of porphyrin ester.

In a 250 mL flask, 1 g (1.18 mmol, 1 eq.) of TPPCOOMe (compound #1) was dissolved in a mixture of THF/MeOH 1:1 (70 mL). Subsequently, 3.5 g (62.38 mmol, 52.9 eq.) of KOH were dissolved in 30 mL H_2O and added to the first solution. The mixture was refluxed for 15 hours. THF and MeOH were evaporated, the ocurring solid in water was redissolved with additional amount of water (150 mL) under heating at 90 °C for 15 min. The resulting mixture was

acidified with 1M HCl and the precipitate was filtrated, washed with H_2O (3 x 50 mL) and dried under dynamic vacuum overnight. The product was obtained as purple crystals (0.8635 g, 1.09 mmol, 92.6% yield). **FTIR**: ῦ = 3063 (m), 2977 (br), 2881 (w), 2838 (w), 2086 (br), 1990 (m), 1928 (m), 1717 (vs), 1602 (s), 1559 (s), 1400 (vs), 1309 (m), 1237 (w), 1223 (w), 1174 (br), 1097 (s), 1015 (s), 984 (m), 962 (m), 867 (w), 827 (s), 797 (m), 783 (s), 764 (s), 708 (s), 643 (s), 563 (s), 464 (s) cm^{-1}. **^{1}H-NMR** (DMSO, 400 MHz): δ [ppm] = 8.86 (s, 8H, β-pyrrole), 8.42 (d, ^3J = 8.2 Hz, 8H, phenyl), 8.38 (d, ^3J = 8.2 Hz, 8H, phenyl), 13.28 (s, 4H, COO*H*), -2.95 (s, 2H, N*H*). UV-VIS: (DMSO, λ_{max}, (logε)) 421 (sorret-band), 515, 550, 588, 645 (Q-bands) nm.

5,10,15,20-Tetrakis(4-methoxycarbonylphenyl)porphyrin-M (M = Fe(III), Mn(III)) [Mn, Fe(III)Cl(TPPCOOMe)]

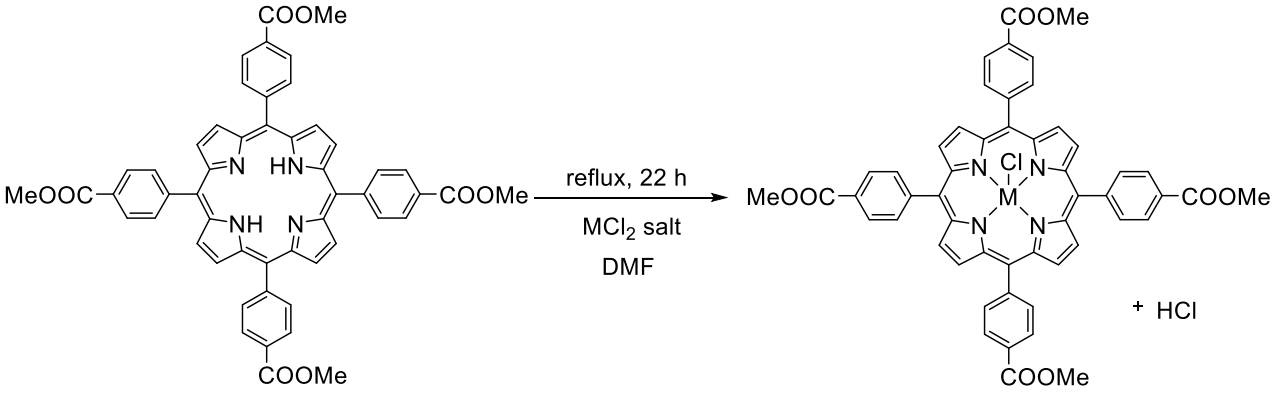

Figure 45. Metalation of porphyrin ester using Fe- and $MnCl_2 \cdot 4H_2O$ salts.

A solution of 0.88 g (1.04 mmol, 1 eq.) TPPCOOMe and 2.5 g (12 mmol, 12 eq.) $FeCl_2 \cdot 4H_2O$ 2.5 g (12 mmol, 12 eq.) or $MnCl_2 \cdot 4H_2O$ in 100 mL DMF was refluxed for 22 h. After the mixture was cooled down to room temperature, 150 mL of H_2O was added. The resulting precipitate was filtered and washed with 2 x 50 mL H_2O. The solid was then dis-solved in $CHCl_3$ and washed three times with water. The organic phase was dried over anhydrous magnesium sulfate and evaporated to afford a shiny dark green crystalline solid. A yield of 93.7% (0.91 g, 0.97 mmol) was determined for ester compound.[208]
^{1}H-NMR (DMSO, 400 MHz): δ [ppm] = 8.86 (s, 8H, β-pyrrole),
8.42 (d, ^3J = 8.2 Hz, 8H, phenyl), 8.38 (d, ^3J = 8.2 Hz, 8H, phenyl), 4.05 (s, 12H, COO*Me*).
Paramagnetic Mn(III) sample show very broad chemical shifts, thus, the signals are not integrateable.

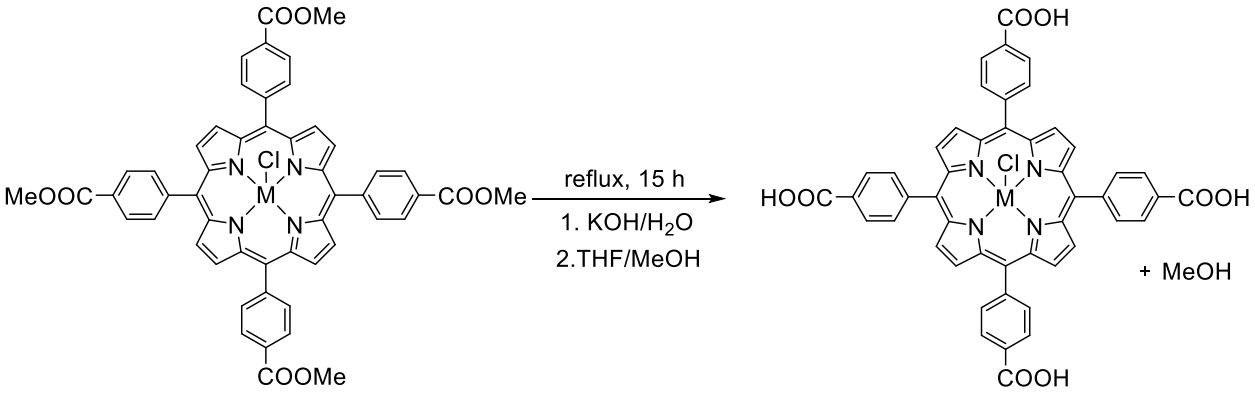

Figure 46. Sopanification of Mn/Fe-metalated porphyrins.

Similar as their non-metalated analog, the metalated porphyrins were saponificated. In a 250 mL flask, 1 g (1.18 mmol, 1 eq.) of Mn(III)Cl(TPPCOOMe) or Fe(III)Cl(TPPCOOMe) were dissolved in a mixture of THF/MeOH 1:1 (70 mL). Subsequently, 3.5 g (62.38 mmol, 52.9

eq.) of KOH were dissolved in 30 mL H_2O and added to the first solution. The mixture was refluxed for 15 hours. THF and MeOH were evaporated, the occurring solid in water was redissolved with additional amount of water (150 mL) under heating at 90 °C for 15 min. The resulting mixture was acidified with 1M HCl and the precipitate was filtrated, washed with H_2O (3 x 50 mL) and dried under dynamic vacuum overnight.
^{1}H-NMR (DMSO, 400 MHz): δ [ppm] = 8.86 (s, 8H, β-pyrrole),
8.42 (d, ^3J = 8.2 Hz, 8H, phenyl), 8.38 (d, ^3J = 8.2 Hz, 8H, phenyl), 13.28 (s, 4H, COO*H*).
However, due to the paramagnetism of Mn(III) the chemical shift are very broad and not integrateable. UV-VIS: (Fe(III)Cl(TPPCOOMe, DMSO, λ_{max}, (logε)) 406 nm (sorret-band), 575, 625 nm (Q-bands). (Mn(III)Cl(TPPCOOMe, DMSO, λ_{max}, (logε)) 411 nm (sorret-band), 528, 566 nm (Q-bands).

[5,10,15,20-Tetrakis(4-methoxycarbonylphenyl)porphyrinato]-Rh(III) chloride ([Rh(TCPPCO$_2$Me)Cl])

Rh-porphyrin ester Rh(TCPPCO$_2$Me)Cl was prepared with slight changes to J. Liu et al.[194] TCPPCO$_2$Me (168.2 mg, 0.2 mmol) and $RhCl_3$ (104.2 mg, 0.8 mmol) were refluxed in benzonitrile (5 mL) under stirring at 220°C for 2h. Residual benzonitrile was removed under reduced pressure and dried at 80 °C overnight. The dried product was purified with column chromatography on silica using a mixture of DCM and EtOAc as elutent.
^{1}H-NMR (DMSO, 400 MHz): δ [ppm] = 8.86 (s, 8H, β-pyrrole),
8.42 (d, ^3J = 8.2 Hz, 8H, phenyl), 8.38 (d, ^3J = 8.2 Hz, 8H, phenyl), 4.05 (s, 12H, COO*Me*).

[5,10,15,20-tetrakis(4-carboxyphenyl)porphyrin]-Rh(III) chloride ([Rh(TCPPCO$_2$)Cl])

The resulting Rh(TCPPCO$_2$Me)Cl was hydrolyzed (120 mg) by refluxing a mixture of THF (6 mL) and MeOH (6 mL), to which a solution of KOH (100 mg) in H_2O (6 mL) was added for 5h. After the reaction mixture was cooled down to room temperature, the organic solvents were removed by rotatory evaporation. Additional water was added to the residual product mixture and acidified with 1M HCl until no further precipitation of Rh(TCPPCO$_2$H)Cl was observed. The red product was washed with water (3x 50 mL) and dried in vacuum overnight.
^{1}H-NMR (DMSO, 400 MHz): δ [ppm] = 8.87 (s, 8H, β-pyrrole),
8.44 (d, ^3J = 8.2 Hz, 8H, phenyl), 8.35 (d, ^3J = 8.2 Hz, 8H, phenyl), 12.4 (s, 12H, COO*H*).
UV-VIS: (DMSO, λ_{max}, (logε)) 418 nm (sorret-band), 535, 570 nm (Q-bands).

5,15-bis(4-methoxycarbonylphenyl)porphyrin [DL–COOMe]

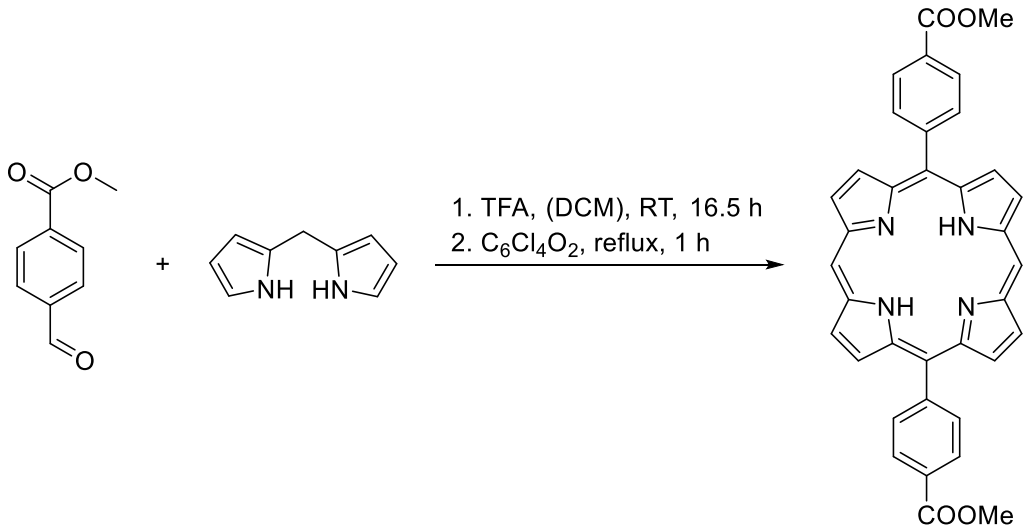

Figure 47. Synthesis of DL-COOMe.[209]

0.50 g (3.43 mmol, 1.0 eq.) dipyrromethene and 0.56 g (3.44 mmol, 1.0 eq.) methyl *p*-formylbenzoate were dissolved in 60 mL DCM and stirred at room temperature. 3-4 drops of trifluoroacetic acid (TFA) were given to the reaction mixture. After 16.5 h, 3.39 g (13.8 mmol, 4.0 eq.) chloranil was added to the purple solution, which was subsequently refluxed one hour. The mixture was then cooled to room temperature. In order to remove excess chloranil as well as side-products, column chromatography was performed (50 mm x 300 mm, silica gel, chloroform). The product was obtained as a purple crystalline solid after drying *in vacuo* (yield: 0.25 g, 12.6%).[209]

^{1}H-NMR (DMSO, 400 MHz): δ [ppm] = 10.71 (s, 2H, C*H*), 9.71 (d, ^3J = 4.7 Hz, 4H, phenyl), 9.06 (d, ^3J = 4.7 Hz, 4H, phenyl), 8.44-8.49 (m, 8H, β-pyrrole), 4.08 (s, 6H, COO*Me*), -3.28 (s, 2H, N*H*).

5,15-bis(4-carboxyphenyl)porphyrin [DL–COOH]

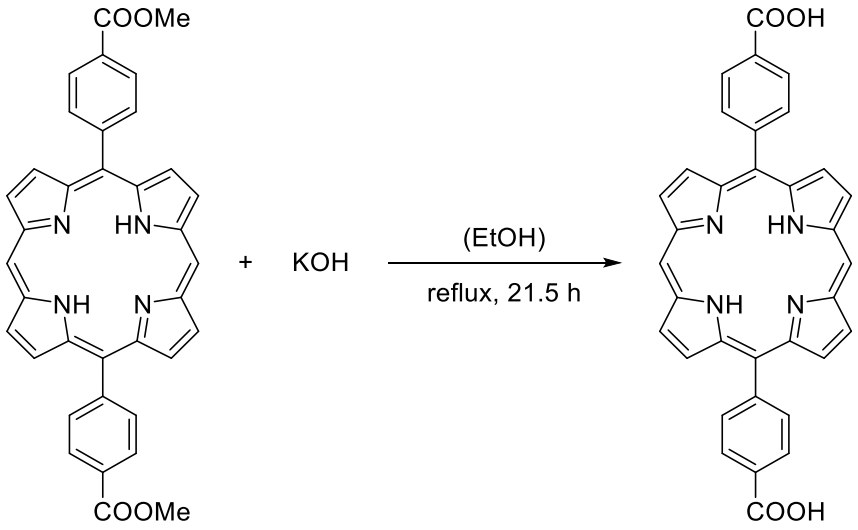

Figure 48. Synthesis of DL-COOH.[209]

0.25 g (0.43 mmol, 1.0 eq.) of DL-COOMe was dissolved in 50 mL EtOH and added to a solution of 1.42 g (25.3 mmol, 58.6 eq.) potassium hydroxide in 25 mL H_2O. The mixture was refluxed for 21.5 h. After cooling down to room temperature, additional EtOH was added and the mixture was heated until the solid was fully dissolved. The solution was then acidified with approximately 100 mL 1M HCl until no further precipitate was detected. A green solid was collected by filtration, washed with water and dried in vacuum. Ligand was obtained as a red-brick crystalline solid with a yield of 82.7% (0.20 g, 0.36 mmol).[208]
^{1}H-NMR (DMSO, 400 MHz): δ [ppm] = 10.71 (s, 2H, C*H*), 9.71 (d, ^3J = 4.7 Hz, 4H, phenyl), 9.06 (d, ^3J = 4.7 Hz, 4H, phenyl), 8.44-8.49 (m, 8H, β-pyrrole), -3.28 (s, 2H, N*H*). UV-VIS: (DMSO, λ_{max}, (logε)) 405 nm (sorret-band), 503, 537, 573, 628 nm (Q-bands).

7.4 Synthesis MOFs

PCN-222(no metal)

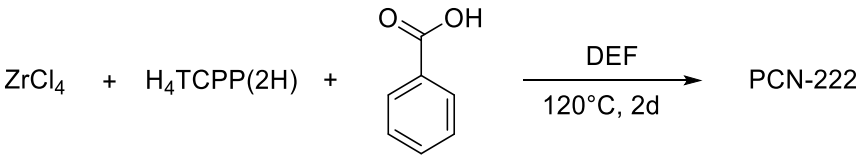

Figure 49. Solvo-thermal synthesis of PCN-222(no metal).

All PCN-222 materials were synthesized in accordance to Zhou et al.[138] In a scintillation vial of 20 mL volume, 75 mg of $ZrCl_4$ (0.32 mmol, 5 eq.) and 2.7 g of benzoic acid (22 mmol, 340 eq.) were dissolved in 8 mL of diethyl formamide (DEF) by ultrasonication (10 min). Subsequently, 50 mg of H_2TCPP (0.0625 mmol, 1 eq.) were added and dissolved by ultrasonication as well. The mixture was heated at 120 °C for 48 h. The crystals were filtrated; the product was obtained as dark violet crystals (0.12 g). These were then immersed in 80 mL of DMF to which 3.6 mL of 8 M HCl were added and heated at 120 °C for 15 h. After careful removing of the solvent from the precipitate with a pipette, the solid was resuspended in 70 mL of DMF/acetone. The solvent was removed again and the solid was resuspended in 50 mL fresh acetone. After the mixture was soaked for 23 h, the solid was separated by centrifugation and dried under vacuum (~10^{-3} mbar) for 12 h. The product was obtained as dark violet crystals (0.06 g, 0.055 mmol, 82.1%). A crucible with 0.05 g of the product was placed into a Schlenk-tube, the tube was evacuated and heated in a tube furnace to 90 °C for 1.5 h. Following, the temperature was set to 150 °C for 19.5 h. After transfer into a glovebox 63.5 mg of activated sample was obtained. **FTIR**: $\tilde{\upsilon}$ = 2921 (m), 2850 (m), 1711 (w), 1647 (w), 1598 (s), 1509 (s), 1410 (vs), 1278 (m), 1180 (w), 1097 (w), 1018 (w), 964 (m), 870 (w), 797 (m), 777 (m), 718(s), 649 (s), 487 (s), 394 (s) cm^{-1}. **EA**: Anal. calcd. (%): C, 48.18; H, 2.86; N, 4.68. Found (%): C, 46.38; H, 2.86; N, 5.40. Surface area (BET): 1882 m^2/g.

PCN-222(Mn)

In a scintillation vial of 20 mL volume, in total 75 mg of $ZrCl_4$ (0.32 mmol, 5 eq.) and 2.7 g of benzoic acid (22 mmol, 340 eq.) were dissolved in 8 mL of diethyl formamide (DEF) by ultrasonication (10 min). Subsequently, 50 mg of $H_4TCPP(MnCl)$ (0.06 mmol, 1 eq.) were added and dissolved by ultrasonication as well. The mixture was heated at 120 °C for 48 h. The dark green crystals were obtained by filtration (0.12 g). These were then immersed in 80 mL of DMF to which 3.6 mL of 8 M HCl were added and heated at 120 °C for 15 h. The solid was filtered and resuspended in 70 mL of DMF and washed with 2x 30 mL fresh DMF, followed by 3x washing (30 mL) with acetone. The solvent was removed by centrifugation and the solid

was resuspended in 50 mL fresh acetone. After the mixture was soaked for 23 h, the solid was separated by centrifugation and dried under vacuum (~10^{-3} mbar) for 12 h. The product was obtained as dark green crystals (0.07 g, 0.06 mmol, yield 95%). A crucible with 0.06 g of the product was placed into a Schlenk-tube which heated under dynamic vacuum in a tube furnace to 90 °C for 2 h. Following, the temperature was set to 150 °C for 18 h. After transfer into a glovebox 78.6 mg of activated sample was obtained. **FTIR**: ν [cm^{-1}] = 1600 (vs), 1551 (s), 1512 (s), 1421 (vs), 1344 (s), 1280 (m), 1208 (w), 1184 (m), 1151 (w), 1103 (w), 1006 (s) 875 (m), 869 (w), 804 (s), 775 (s), 707 (s), 673 (s), 471 (vs), 403 (s). **EA**: Anal. calcd. (%): C, 44.87; H, 2.51; N, 4.36; Mn, 4.28. Found (%): C, 44.89; H, 2.51; N, 4.89; Mn, 3.90. Surface area (BET): 2205 m^2/g.

Synthesis of PCN-222(Rh)

In a scintillation vial of 20 mL volume $ZrCl_4$ (70 mg), H_4TCPP(RhCl) (50 mg) and benzoic acid (2.7 g) were ultrasonically dissolved in 8 mL DMF. The mixture was placed in an oven at 120 °C for 2 d. The crystals were filtered and immersed in 80 mL of DMF to which 3.6 mL of 8 M HCl were added and heated at 120 °C for 15 h. The solid was filtered and resuspended in 70 mL of DMF and washed with 2x 30 mL fresh DMF, followed by 3x washing (30 mL) with acetone. The solvent was removed by centrifugation and the solid was resuspended in 50 mL fresh acetone. After the mixture was soaked for 23 h, the solid was separated by centrifugation and dried under vacuum (~10^{-3} mbar) for 12 h. Anal. Calcd (%) for PCN-222(Rh): C, 44.94; H, 2.36; N, 4.28%; Found: C, 46.90; H, 2.66; N, 4.41%. Surface area (BET): 1912 m^2/g.

Synthesis of PCN-222(Fe)

In a scintillation vial of 20 mL volume $ZrCl_4$ (70 mg), H_4TCPP(FeCl) (50 mg) and benzoic acid (2.7 g) were ultrasonically dissolved in 8 mL DMF. The mixture was placed in an oven at 120 °C for 2 d. The crystals were filtered and immersed in 80 mL of DMF to which 3.6 mL of 8 M HCl were added and heated at 120 °C for 15 h. The solid was filtered and resuspended in 70 mL of DMF and washed with 2x 30 mL fresh DMF, followed by 3x washing (30 mL) with acetone. The solvent was removed by centrifugation and the solid was resuspended in 50 mL fresh acetone. After the mixture was soaked for 23 h, the solid was separated by centrifugation and dried under vacuum (~10^{-3} mbar) for 12 h. Anal. Calcd (%) for PCN-222(Rh): C, 44.91; H, 2.36; N, 4.36; Found: C, 45.61; H, 3.27; N, 4.55%. Surface area (BET): 2270 m^2/g.

Synthesis of PCN-224(no metal)

All PCN-224 materials were synthesized in accordance to Zhou et al.[139] In a scintillation vial of 20 mL volume $ZrCl_4$ (30 mg), H_4TCPP(2H) (10 mg) and benzoic acid (400 mg) were ultrasonically dissolved in DMF (2 mL). The mixture was heated in an oven at 120 °C for 24 h. After cooling down to room temperature, purple crystals were collected by filtration, washed with DMF (3x 20 mL) and acetone (3x 20 mL) and soaked in fresh acetone for 24 h. The powder

was separated by centrifugation and activated at 120 °C for 24 h in dynamic vacuum. Anal. Calcd (%) for PCN-224: C, 42.01; H, 2.45; N, 4.08%. Found: C, 44.51; H, 2.74; N, 3.77%. **FTIR**: ν [cm^{-1}] = 1604 (s), 1552 (s), 1499 (s), 1413 (vs), 1307 (m), 1184 (m), 1155 (m), 1102 (m), 1025 (s), 987 (s), 963 (s), 867 (m), 805 (m), 762 (w), 714 (s), 666 (s), 465 (vs). Surface area (BET): 2286 m^2/g.

Synthesis of PCN-224(Rh)

In a scintillation vial of 20 mL volume $ZrCl_4$ (30 mg), $H_4TCPP(RhCl)$ (10 mg) and benzoic acid (400 mg) were ultrasonically dissolved in DMF (2 mL). The mixture was heated in an oven at 120 °C for 24 h. After cooling down to room temperature, orange-red crystals were collected by filtration and washed with DMF (3x 20 mL) and acetone (3x 20 mL). The crystals were kept in fresh acetone for 24 h. The crystals were separated by centrifugation and activated at 120 °C for 24 h in dynamic vacuum. Anal. Calcd (%) for PCN-224(Rh): C, 39.49; H, 2.16; N, 3.84%; Found: C, 40.20; H, 3.01; N, 3.92%. Surface area (BET): 1493 m^2/g.

Synthesis of PCN-224(Fe)

PCN-224(Fe) was obtained by post-metalation of PCN-224(no metal). 180 mg PCN-224(no metal) was dispersed in a 20 mL scintillation vial containing 8 mL DMF and 217 mg $FeCl_2 \cdot 4\ H_2O$ and heated in an oven at 120 °C for 12 h. The brown powder was collected by filtration, washed with DMF (3x 20 mL) and acetone (3x 20 mL) and soaked in fresh acetone for 24 h. The powder was separated by centrifugation and activated at 120 °C for 24 h in dynamic vacuum. Anal. Calcd (%) for PCN-224(Fe): C, 39.49; H, 2.16; N, 3.84%; Found: C, 41.10; H, 2.95; N, 3.72%. Surface area (BET): 1922 m^2/g.

Synthesis of PCN-224(Mn)

PCN-224(Mn) was obtained by post-metalation of PCN-224(no metal). 80 mg of PCN-224 was dispersed in a 20 mL scintillation vial containing 8 mL DMF and 50 mg $MnCl_2 \cdot 4\ H_2O$ and heated in an oven at 100 °C overnight. The green powder was collected by filtration, washed with DMF (3x 20 mL) and acetone (3x 20 mL) and was kept in fresh acetone for additional 24 h. The powder was separated by centrifugation and activated at 120 °C for 24 h in dynamic vacuum. Anal. Calcd (%) for PCN-224(Mn): C, 39.49; H, 2.16; N, 3.84%; Mn, 3.76% Found: C, 40.20; H, 3.01; N, 3.92%; Mn, 3.22%. **FTIR**: ν [cm^{-1}] = 1658 (s), 1598 (s), 1548 (s), 1411 (vs), 1342 (s), 1204 (m), 1169 (m), 1141 (w), 1139 (w), 1095 (w), 1011 (vs), 868 (s), 775 (m), 720 (m), 657 (m), 582 (w), 542 (s), 468 (vs). Surface area (BET): 1982 m^2/g.

Synthesis of MOF-525(no metal)

In a 20 mL scintillation vial $ZrOCl_2$ (12.5 mg), $H_4TCPP(2H)$ (2.5 mg), and acetic acid (2.5 mL) were ultrasonically dissolved in DMF (10 mL). The mixture was heated in an oven at 65 °C for 3 d. After cooling down to room temperature, violet powder was collected by filtration, washed

with DMF (3x 20 mL) and acetone (3x 20 mL) and was soaked in fresh acetone for 24 h. The powder was separated by centrifugation and activated at 120 °C for 24 h in dynamic vacuum. **FTIR**: ν [cm^{-1}] = 1609 (s), 1556 (s), 1505 (s), 1412 (vs), 1347 (m), 1178 (m), 1086 (s), 1008 (s), 868 (s), 801 (m), 771 (m), 717 (m), 663 (w), 463 (vs). Anal. Calcd (%) for MOF-525: C, 56.79; H, 2.91; N, 5.52%. Found: C, 58.21; H, 3.44; N, 5.95%. Surface area (BET): 2273 m^2/g.

Synthesis of MOF-525(Mn)

In a 20 mL scintillation vial $ZrOCl_2$ (12.5 mg), $H_4TCPP(MnCl)$ (2.5 mg), and acetic acid (2.5 mL) were ultrasonically dissolved in DMF (10 mL). The mixture was heated at 65 °C oven for 3 d. After cooling down to room temperature, green powder was collected by filtration, washed with DMF (3x 20 mL) and acetone (3x 20 mL) and was soaked in fresh acetone for 24 h. The powder was separated by centrifugation and activated at 120 °C for 24 h in dynamic vacuum. Anal. Calcd (%) for MOF-525(Mn): C, 52.24; H, 2.50; N, 5.08%. Found: C, 52.49; H, 3.61; N, 4.55%. Alternatively, a scaled-up (16x) synthesis route was applied. Herein, 200 mg $ZrOCl_2$ (12.5 mg), $H_4TCPP(MnCl)$ (40 mg), and acetic acid (20 mL) were ultrasonically dissolved in DMF (40 mL) within a Schott-glass (100 mL) instead of a scintillation vial, which led to more MOF-525(Mn) product. **FTIR**: ν [cm^{-1}] = 1713 (s), 1608 (s), 1507 (s), 1406 (vs), 1274 (m), 1178 (m), 1097 (s), 1022 (m), 961 (w), 865 (s), 799 (s), 774 (s), 715 (s), 635 (m), 580 (s), 480 (vs). Surface area (BET): 2317 m^2/g.

Synthesis Zr_6-oxo methacrylate cluster

The **$[Zr_6(OH)_4O_4(OMc)_{12}]$** (OMc = methacrylate) cluster was synthesized according to Kickelbick and Schubert.[29] In a large Schlenk tube $Zr(O^nPr)_4$ (3.1 mmol, 70 % solution in *n*-propanol) was mixed under inert atmosphere with methacrylic acid (11.8 mmol, 5.3 eq.). After shaking the reaction vessel for 5 min, the mixture was stored at rt for 13 days. The obtained colorless crystals were dried *in vacuo* for 12 h to yield 860 mg (0.51 mmol, 98 %) of the desired product. **^{1}H-NMR** (400 MHz, $CDCl_3$): δ=6.08 (d, J = 51.5 Hz, 1H), 5.40 (d, J = 76.1 Hz, 1H), 1.83 (d, J = 23.0 Hz, 3H). Anal. Calcd (%) $Zr_6O_4(OH)_4(OMc)_{12}$: C, 33.9%, H, 3.8%. Found: C, 35.37 %, H, 4.02 %. IR ῡ = 3230 (wb), 2975 (w), 2924 (w), 1694 (m), 1635 (m), 1570 (w), 1541 (s), 1458 (s), 1411 (vs), 1368 (m), 1244 (m), 1180 (w), 1007 (m), 933 (m), 825 (s), 797 (m), 660 (vs), 609 (m), 497 (s), 460 (s), 420 (vs) cm^{-1}.

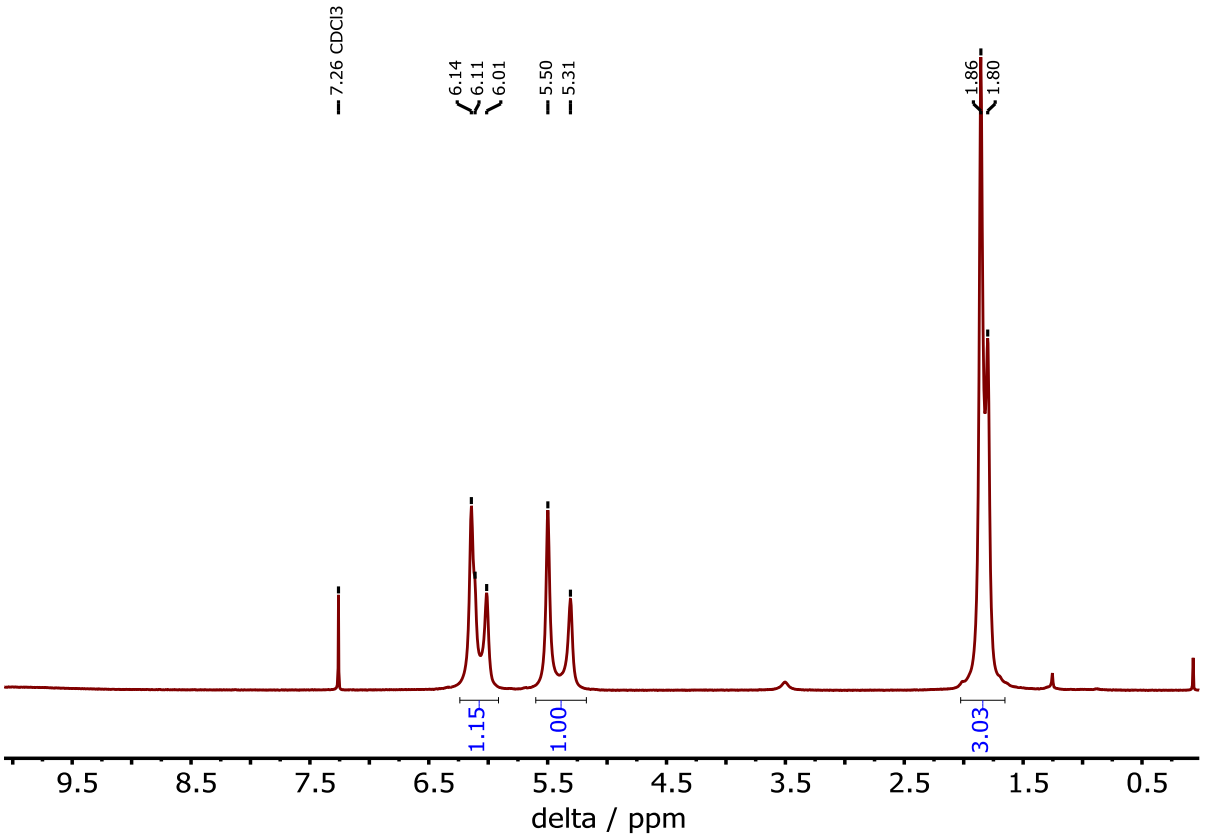

Figure 50: ^{1}H NMR spectrum of the methacrylate SBU ($Zr_6O_4(OH)_4(OMc)_{12}$) in $CDCl_3$.

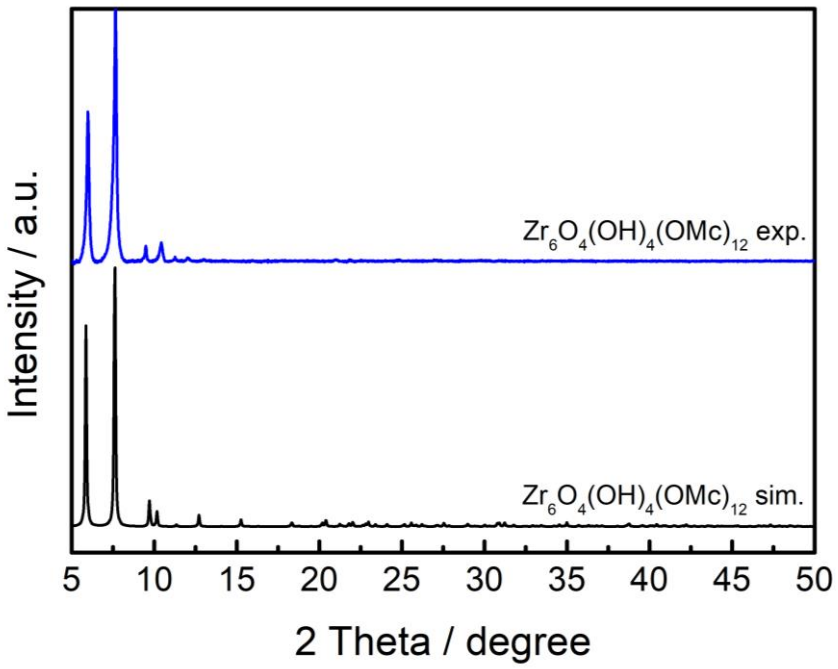

Figure 51. Experimental PXRD pattern of the molecular methacrylate cluster ($Zr_6O_4(OH)_4(OMc)_{12}$) (blue) compared to the simulated diffraction pattern calculated from the single crystal structure.

7.5 Additional data

7.5.1 UV-Vis

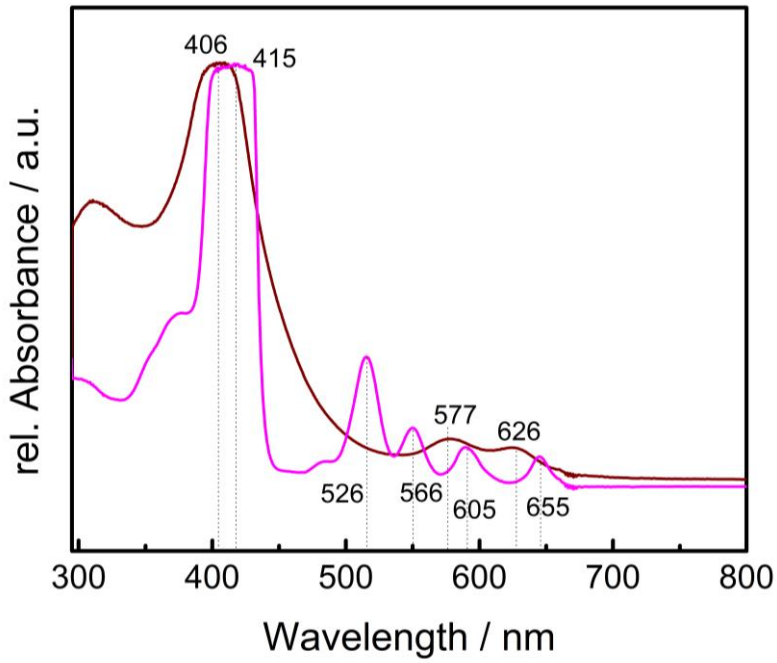

Figure 52. UV-Vis spectrum of dissolved PCN-222(Fe) (brown) in comparison to non-metalated H_4TCCP(2H) porphyrin linker.

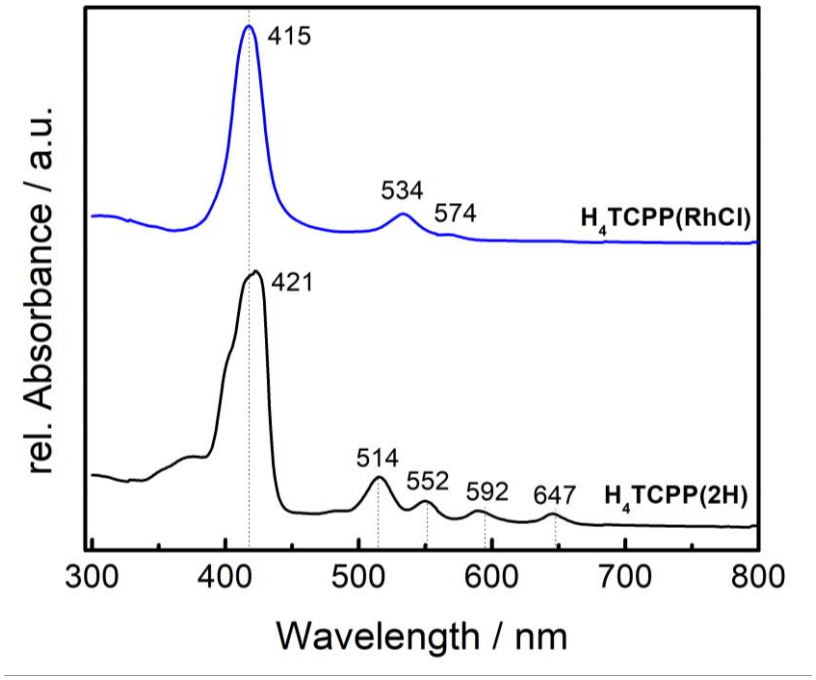

Figure 53. UV-Vis spectrum of H_4TCPP(RhCl) in comparison to non-metalated H_4TCPP(2H) porphyrin linker.

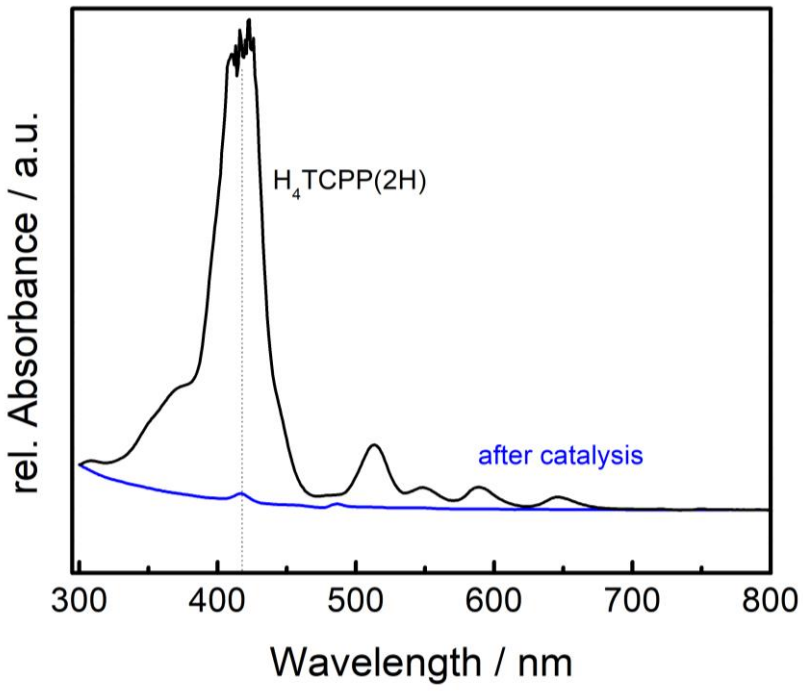

Figure 54. UV-Vis spectrum of the reaction solution after catalysis in comparison to porphyrin linker.

7.5.2 Infrared (IR)

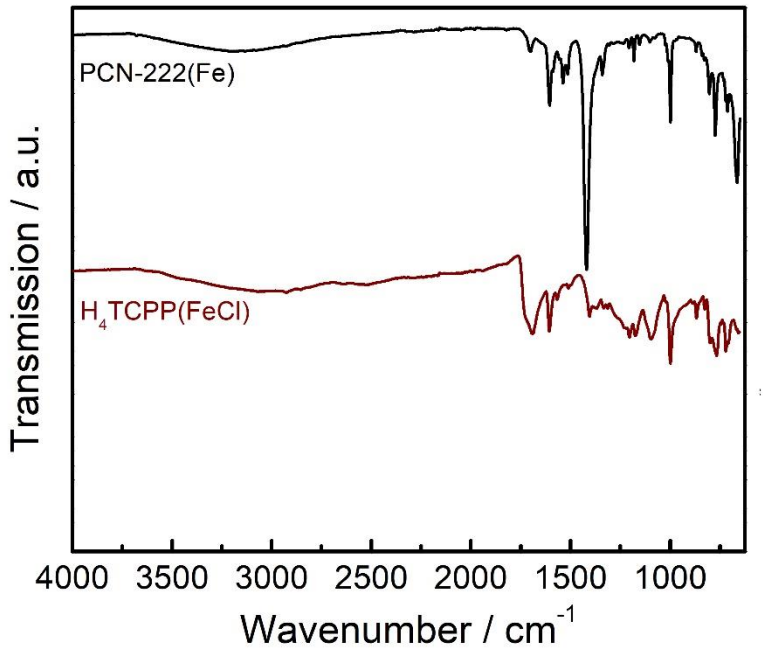

Figure 55. Infrared spectroscopy of PCN-222(Fe) in comparison to free H_4TCPP(FeCl) porphyrin linker.

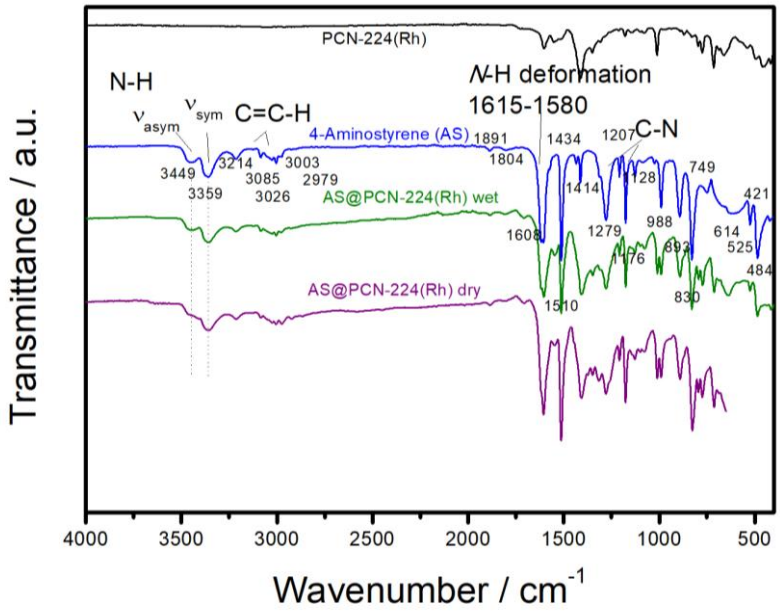

Figure 56. Infrared spectroscopy of PCN-224(Rh) (black), 4-aminostyrene (AS, blue), AS@PCN-224(Rh) wet (high concentration of AS) and AS@PCN-224(Rh) dry (low concentration of AS).

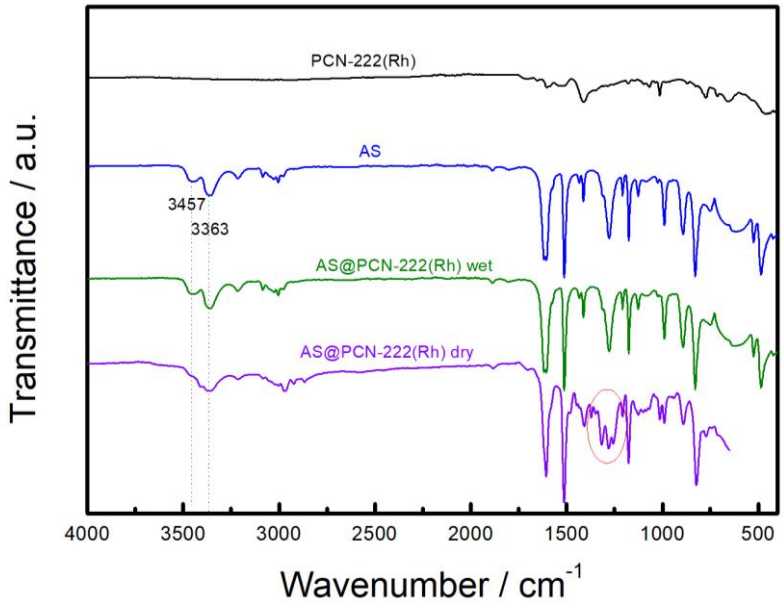

Figure 57. Infrared spectroscopy of PCN-222(Rh) (black), 4-aminostyrene (AS, blue), AS@PCN-222(Rh) wet (high concentration of AS) and AS@PCN-222(Rh) dry (low concentration of AS).

7.5.3 Thermogravimetric analysis (TGA)

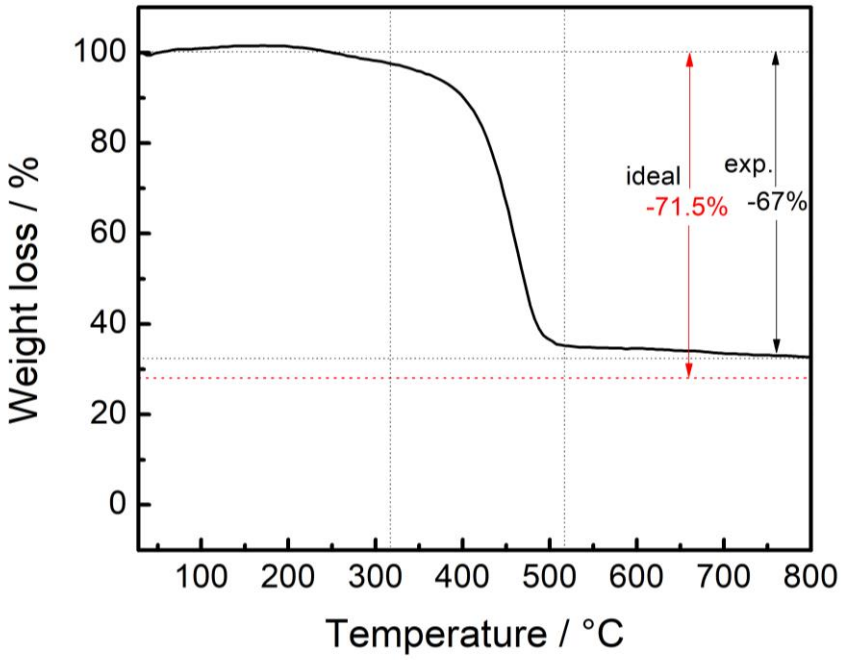

Figure 58. TGA of thermally pre-activated PCN-222 under synthetic air (80 % N_2, 20 % O_2). Illustration the expected mass loss of 'ideal' PCN-222 structure (red) in comparison to the experimentally observed mass loss, indicating the presence missing linker defects (4.5 %).

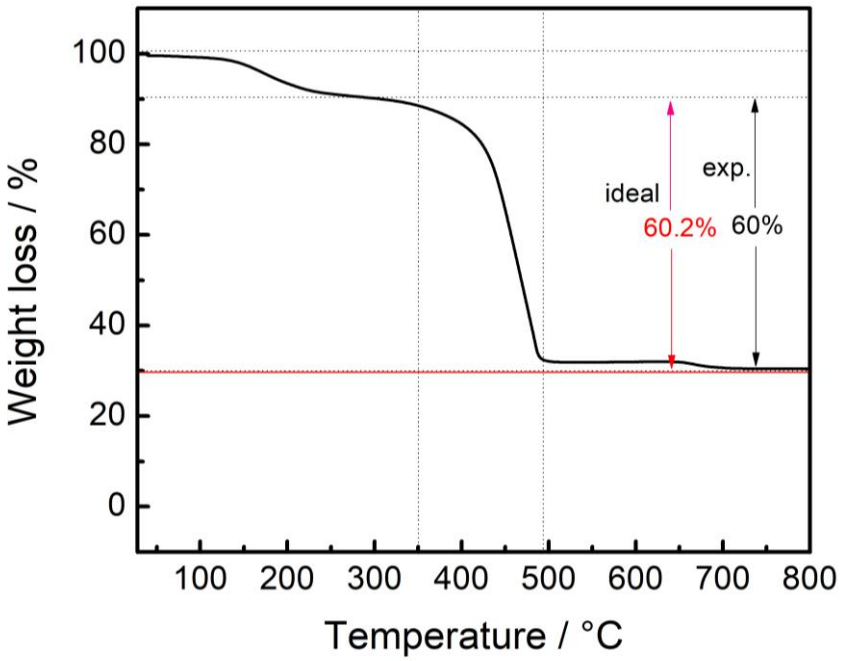

Figure 59. TGA of thermally pre-activated PCN-224 under synthetic air (80 % N_2, 20 % O_2). Illustration the expected mass loss of 'ideal' PCN-224 structure (red) in comparison to the experimentally observed mass loss, indicating the presence missing linker defects (0.2 %).

7.5.4 Powder X-ray Diffraction (PXRD)

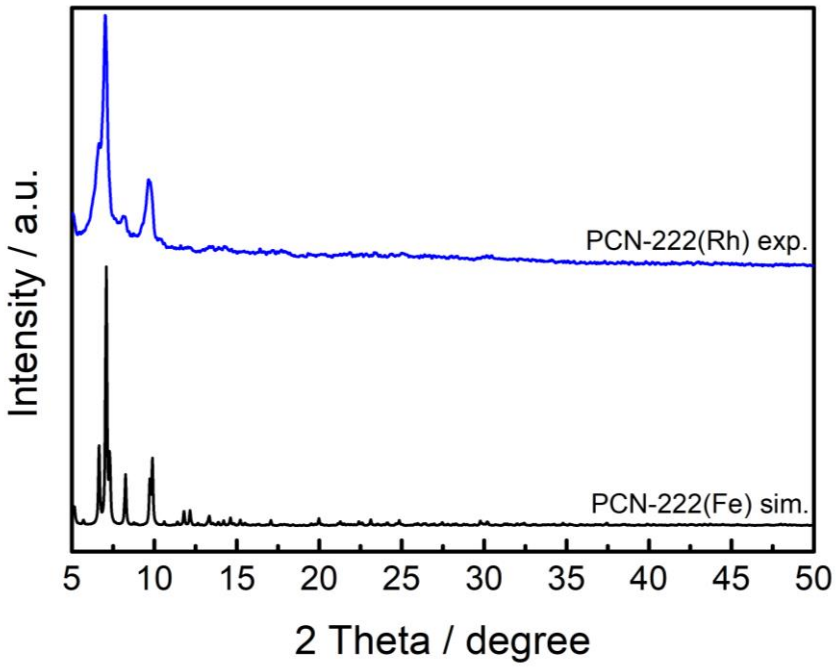

Figure 60. Experimental PXRD pattern of PCN-222(Rh) in comparison to simulated PCN-222(Fe).

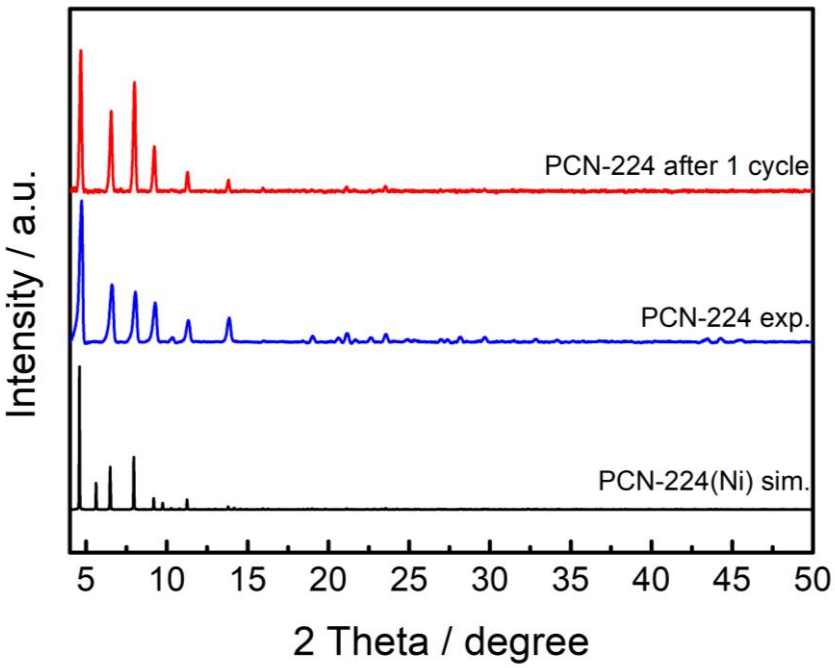

Figure 61. PXRD pattern of PCN-224 after one reaction cycle in comparison to experimental and simulated PCN-224.

7.5.5 Nuclear magnetic resonance (NMR)

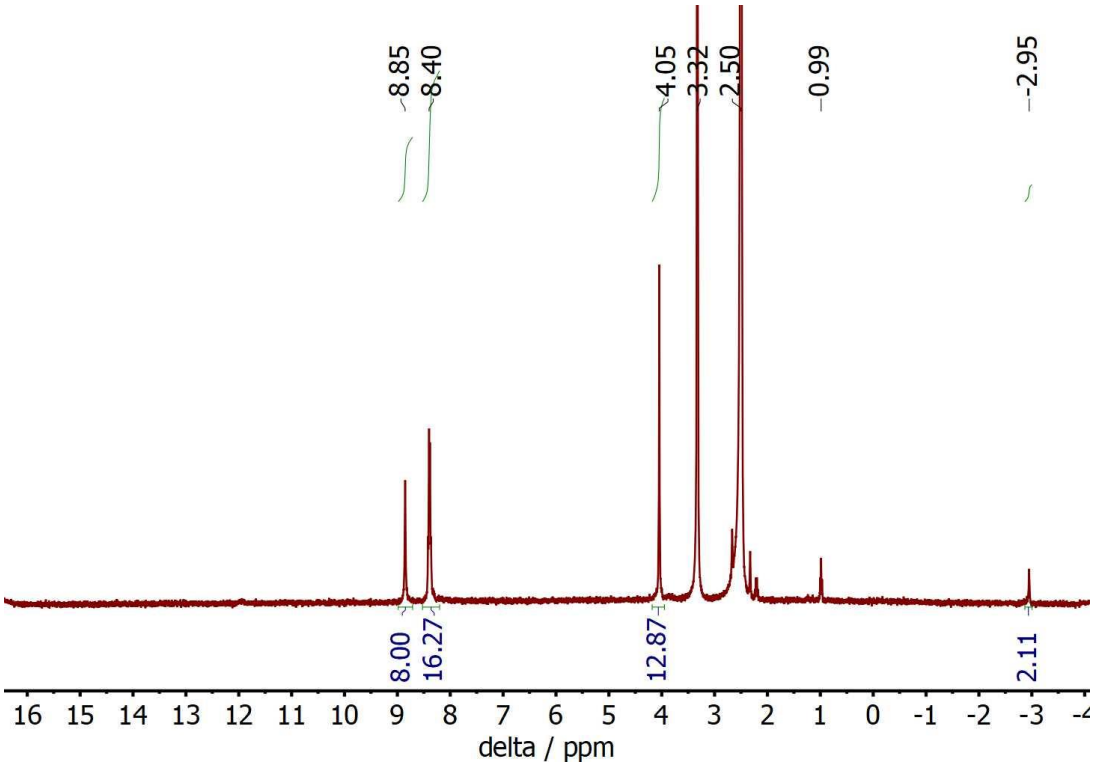

Figure 62. ^{1}H NMR of $H_4TPPCOOMe(2H)$ in DMSO-d_6.

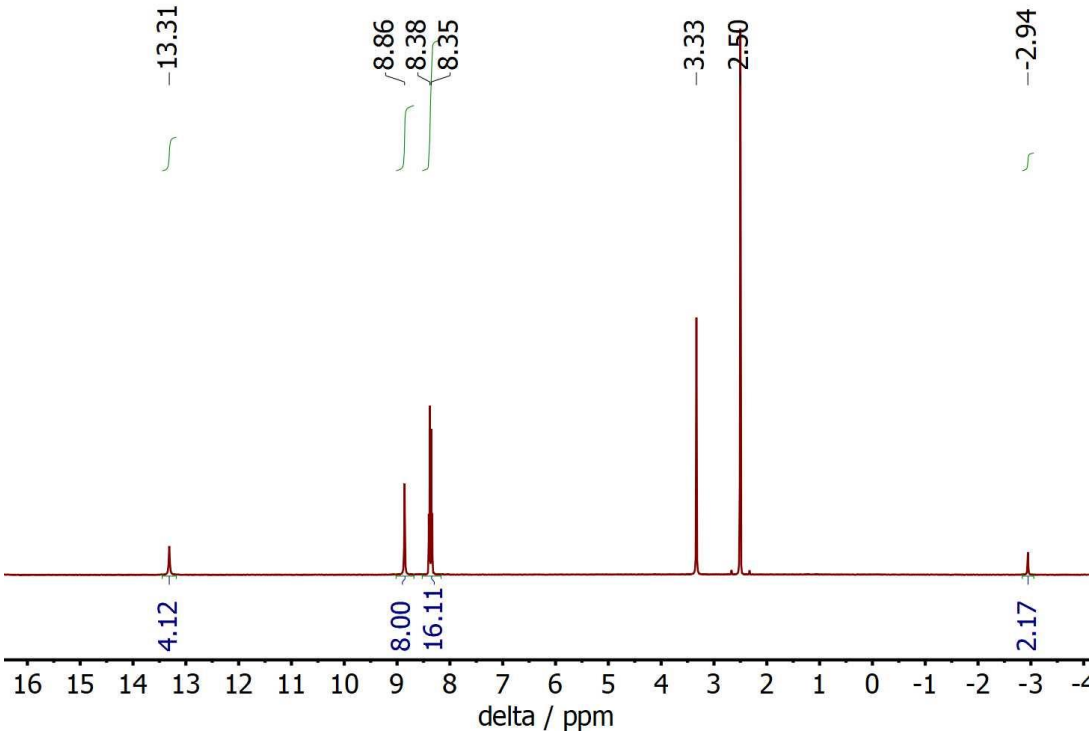

Figure 63. ^{1}H NMR of $H_4TCPP(2H)$ in DMSO-d_6.

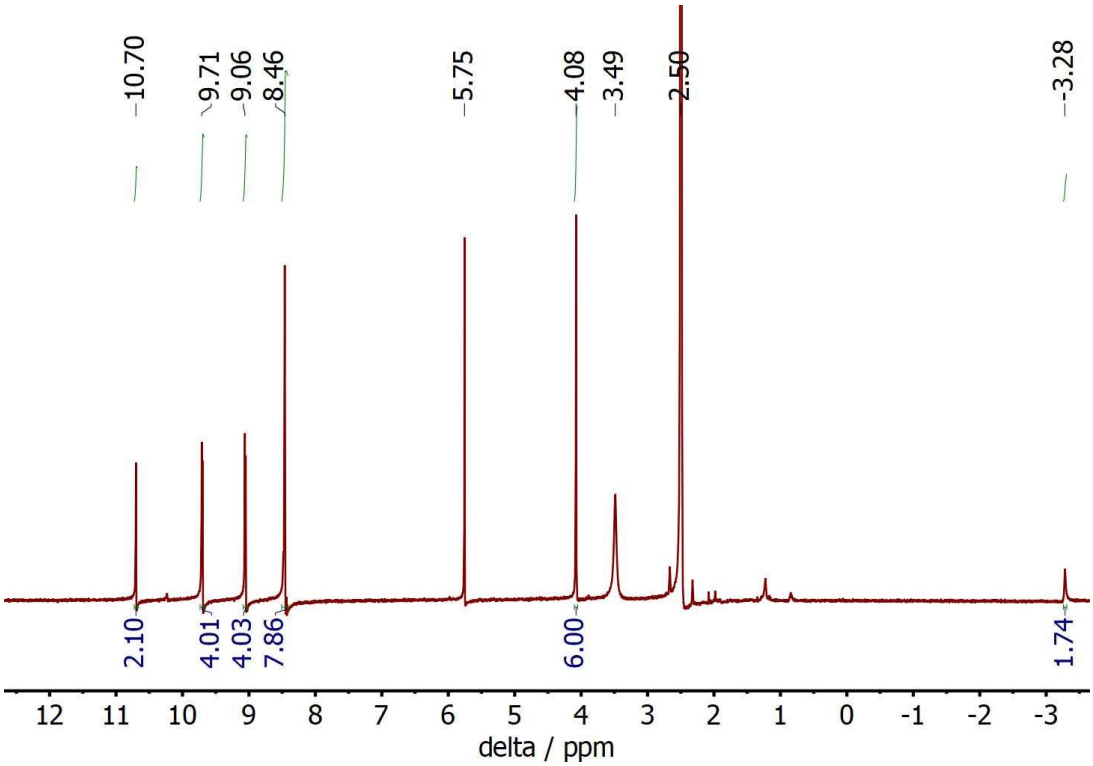

Figure 64. ^{1}H NMR of defect ligand ester in DMSO-d_6.

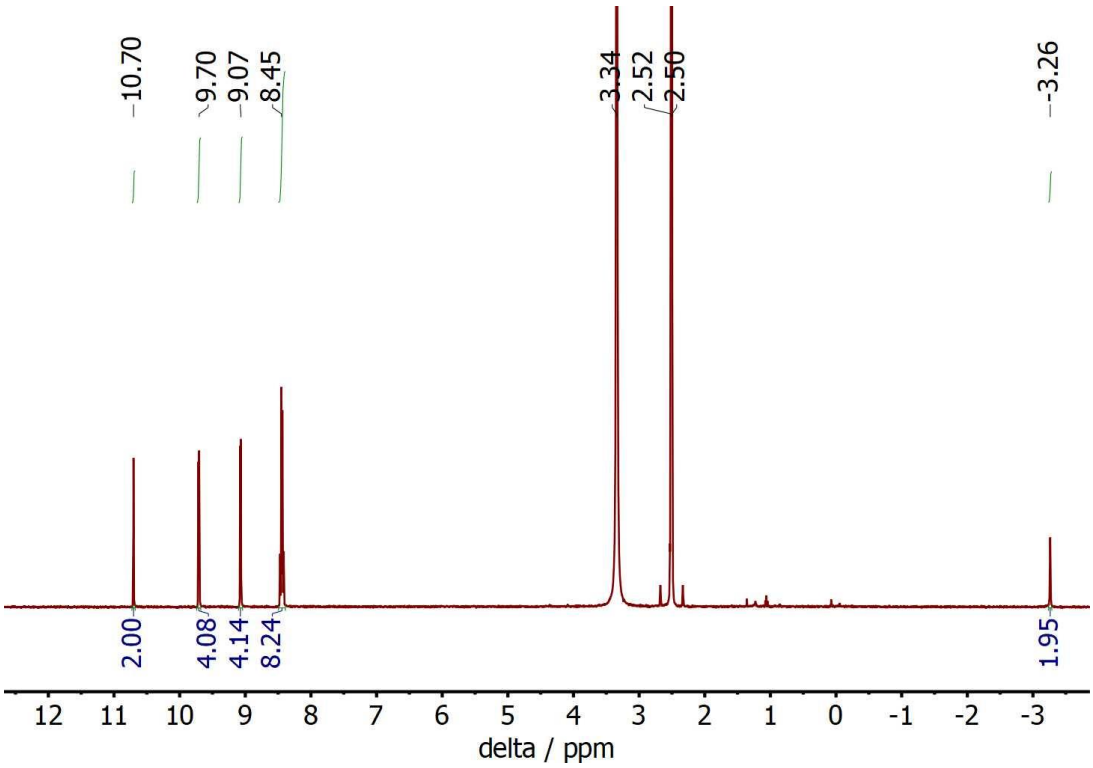

Figure 65. ^{1}H NMR of saponified defect ligand in DMSO-d_6.

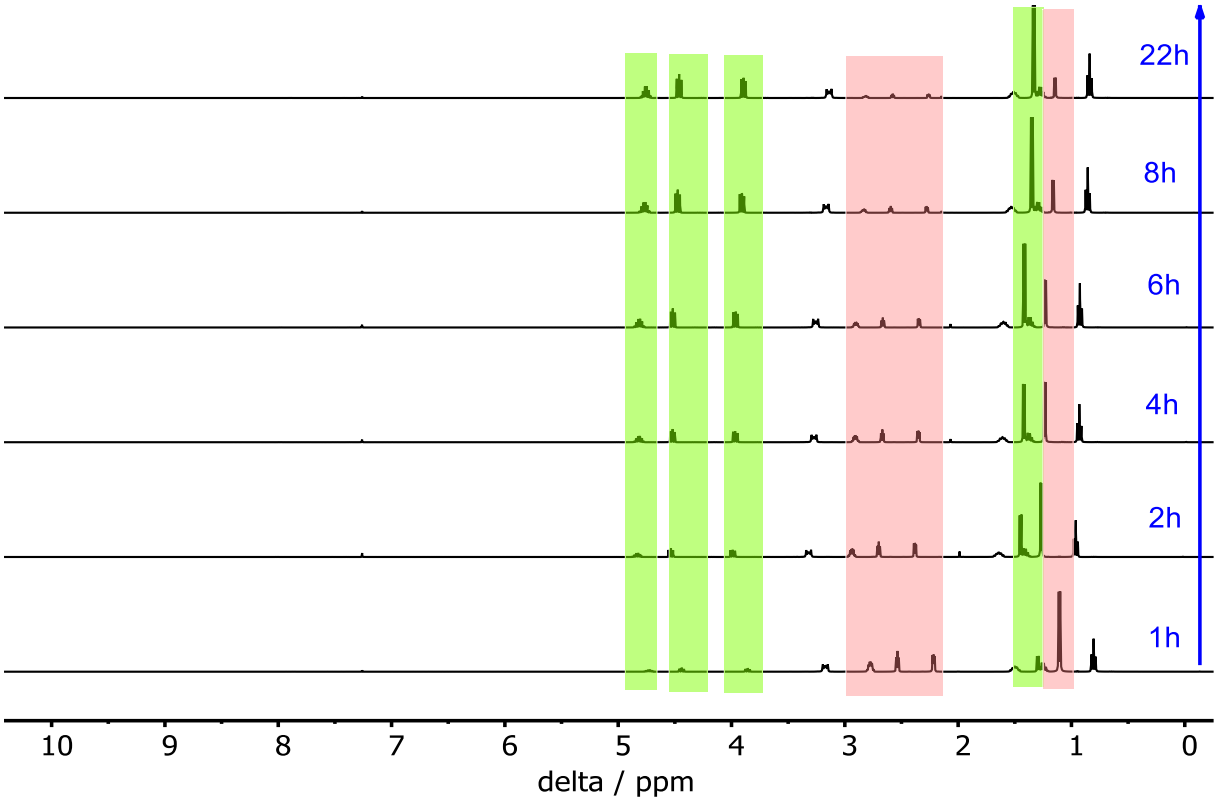

Figure 66. Conversion of propylene oxide (PO) to propylene carbonate (PC) is followed by ^{1}H NMR spectroscopy in $CDCl_3$. The signals which are assigned to PC are highlighted in green bars, while signals which are attributed to PO are depicted in red. Signals are slightly shifted due slightly different Bu_4NBr concentrations. This reaction was selected as an example using PCN-222(Mn) as catalyst.

7.5.6 Catalysis, Gas chromatography (GC)

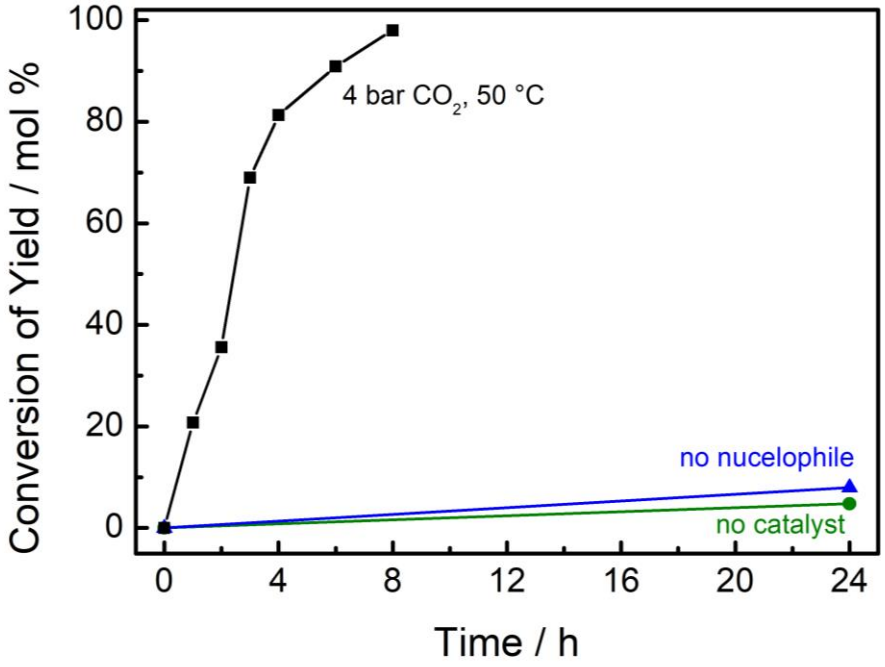

Figure 67. Yield-time curves in the CO_2 insertion into propylene epoxide under optimized conditions (p = 4 bar, T = 50 °C). The reaction requires both, nucleophile as well as catalyst.

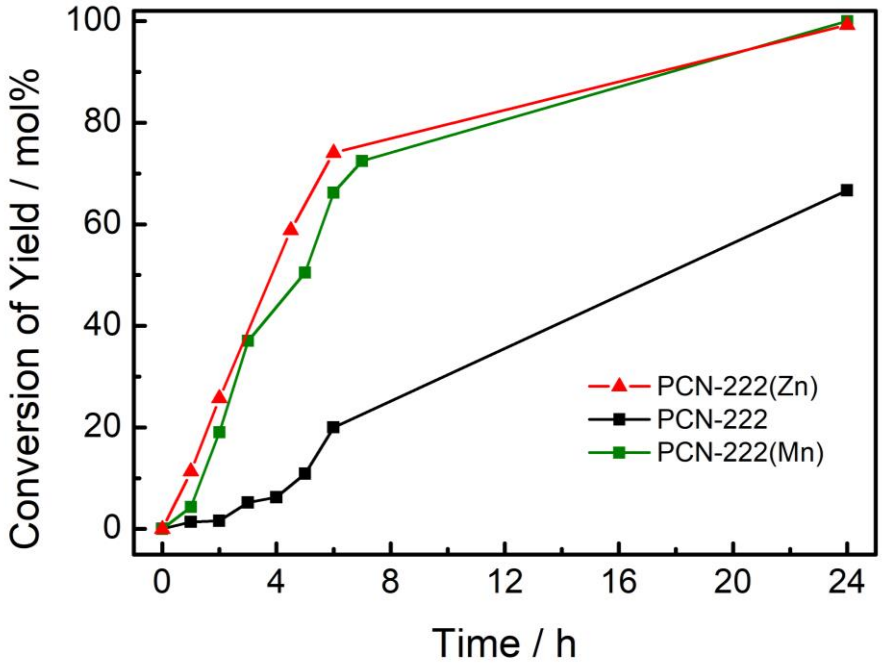

Figure 68. Conversion of yield of propylene carbonate under PCN-222 (black), PCN-222(Mn) (green) and PCN-222(Zn) catalysts (red).

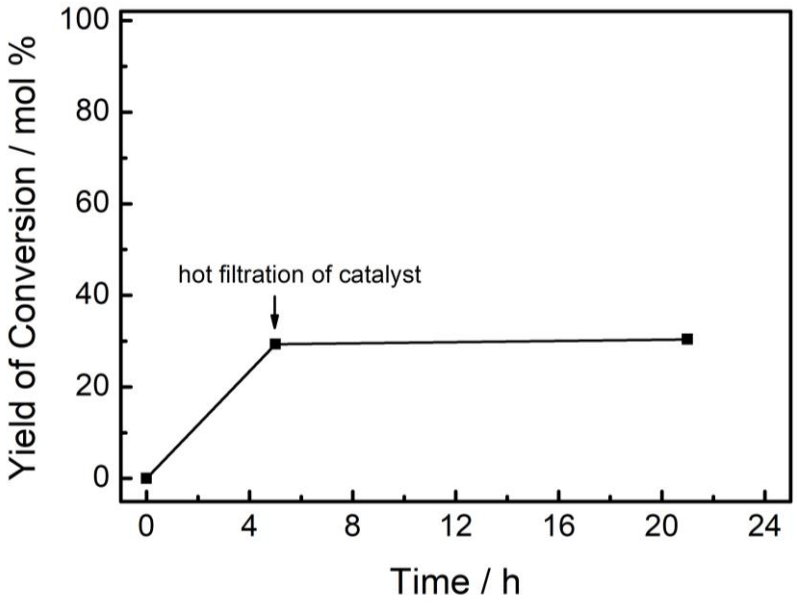

Figure 69. Hot filtration test of PCN-224 in the CO_2 insertion into propylene epoxide, whereby the catalyst was filtered off at 30% yield.

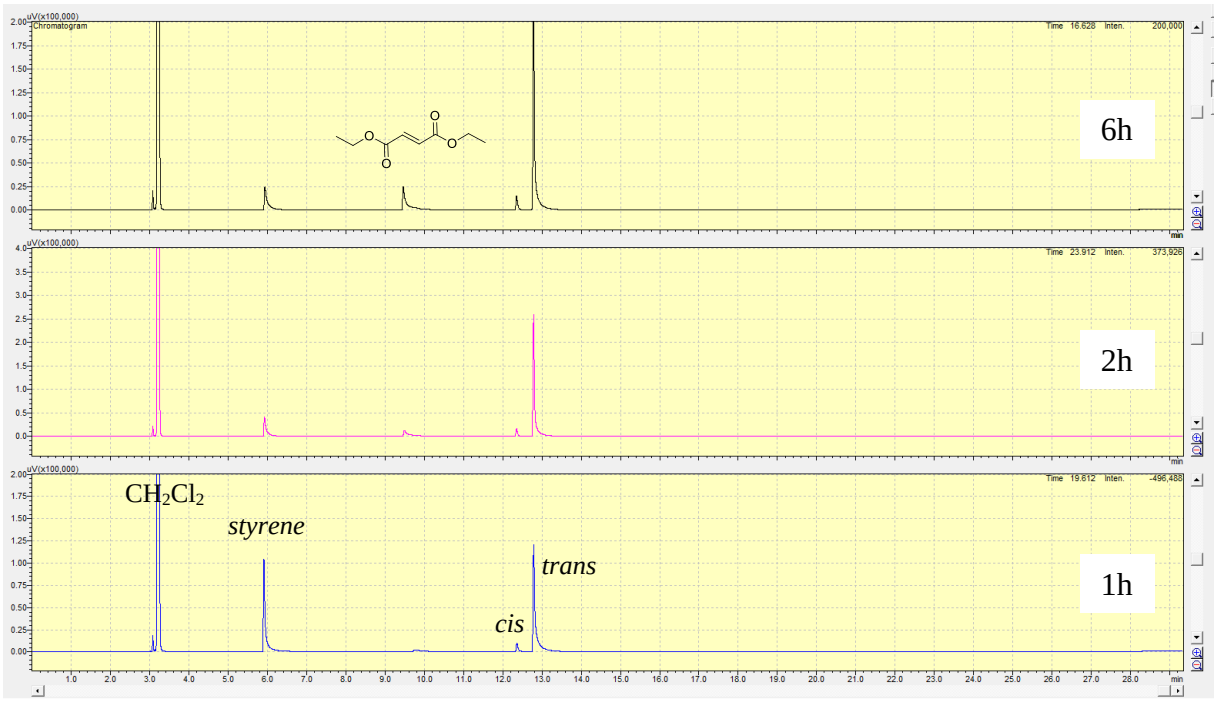

Figure 70. Gas chromatogram of the cyclopropanation reaction using styrene and ethyl diazoacetate (EDA) under PCN-224(Rh) catalyst. Evolution of the EDA dimerization product (r_t = 9.5 min) within increased reaction time is observed. In the reaction, 135 µL (1.1 mmol) EDA in 3 mL CH_2Cl_2 was added via a motorized syringe pump (speed = 0.5 mL/h) to a solution of olefin (0.8 mmol) in 3 mL CH_2Cl_2.

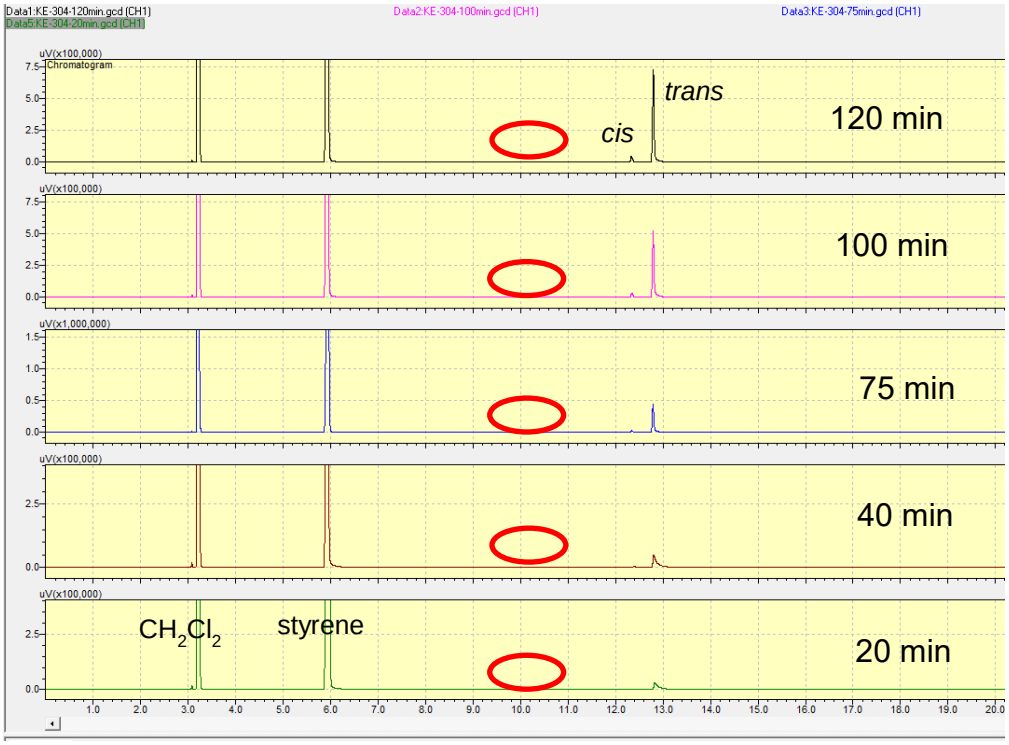

Figure 71. Gas chromatogram of the cyclopropanation reaction using styrene and ethyl diazoacetate (EDA) under PCN-224(Rh) catalyst. No formation of EDA coupling product is found under excess styrene conditions. Hereby, 135 µL (1.1 mmol) EDA diluted in 3 mL CH_2Cl_2 was added via a syringe pump (speed = 0.5 mL/h) to a suspension of catalyst in 2 mL styrene.

8 References

[1] H. Lu, X. P. Zhang, *Chem. Soc. Rev.* **2011**, *40*, 1899-1909.
[2] K. M. Smith, R. Guilard, *The Porphyrin Handbook*, Academic Press, San Diego, USA, **2000**‑**2003**.
[3] G. Richard Geier, T. Sasaki, *Tetrahedron* **1999**, *55*, 1859-1870.
[4] M. A. Schiavon, Y. Iamamoto, O. R. Nascimento, M. d. D. Assis, *J. Mol. Catal. A: Chem.* **2001**, *174*, 213-222.
[5] C.-J. Liu, W.-Y. Yu, S.-G. Li, C.-M. Che, *J. Org. Chem.* **1998**, *63*, 7364-7369.
[6] P. Battioni, R. Iwanejko, D. Mansuy, T. Mlodnicka, J. Poltowicz, F. Sanchez, *J. Mol. Catal. A: Chem.* **1996**, *109*, 91-98.
[7] Z. Li, C.-G. Xia, X.-M. Zhang, *J. Mol. Catal. A: Chem.* **2002**, *185*, 47-56.
[8] G. Simonneaux, P. Le Maux, Y. Ferrand, J. Rault-Berthelot, *Coord. Chem. Rev.* **2006**, *250*, 2212-2221.
[9] B. Meunier, *Chem. Rev.* **1992**, *92*, 1411-1456.
[10] W. Liu, J. T. Groves, *Acc. Chem. Res.* **2015**, *48*, 1727-1735.
[11] W. Liu, J. T. Groves, *J. Am. Chem. Soc.* **2010**, *132*, 12847-12849.
[12] C. Crestini, R. Saladino, P. Tagliatesta, T. Boschi, *Bioorg. Med. Chem.* **1999**, *7*, 1897-1905.
[13] C. Crestini, A. Pastorini, P. Tagliatesta, *J. Mol. Catal. A: Chem.* **2004**, *208*, 195-202.
[14] B. Meunier, A. Sorokin, *Acc. Chem. Res.* **1997**, *30*, 470-476.
[15] T. Aida, S. Inoue, *J. Am. Chem. Soc.* **1983**, *105*, 1304-1309.
[16] D. Bai, S. Duan, L. Hai, H. Jing, *ChemCatChem* **2012**, *4*, 1752-1758.
[17] T. Omura, R. Sato, *J Biol Chem* **1962**, *237*, PC1375-PC1376.
[18] S. Shaik, S. Cohen, Y. Wang, H. Chen, D. Kumar, W. Thiel, *Chem. Rev.* **2010**, *110*, 949-1017.
[19] J. T. Groves, W. J. Kruper, *J. Am. Chem. Soc.* **1979**, *101*, 7613-7615.
[20] E. Rose, B. Andrioletti, S. Zrig, M. Quelquejeu-Ethève, *Chem. Soc. Rev.* **2005**, *34*, 573-583.
[21] J. T. Groves, T. E. Nemo, R. S. Myers, *J. Am. Chem. Soc.* **1979**, *101*, 1032-1033.
[22] R. A. Sheldon, *Metalloporphyrins In Catalytic Oxidations*, New York, **1994**.
[23] J. T. Groves, W. J. Kruper, R. C. Haushalter, *J. Am. Chem. Soc.* **1980**, *102*, 6375-6377.
[24] C. L. Hill, B. C. Schardt, *J. Am. Chem. Soc.* **1980**, *102*, 6374-6375.
[25] C. K. Chang, F. Ebina, *J. Chem. Soc., Chem. Commun.* **1981**, 778-779.
[26] P. S. Traylor, D. Dolphin, T. G. Traylor, *J. Chem. Soc., Chem. Commun.* **1984**, 279-280.
[27] K. Gopalaiah, *Chem. Rev.* **2013**, *113*, 3248-3296.
[28] T. Shinji, S. Manabu, *Chem. Lett.* **1989**, *18*, 263-266.
[29] Z. Gross, N. Galili, L. Simkhovich, *Tetrahedron Lett.* **1999**, *40*, 1571-1574.
[30] E. Rose, M. Quelquejeu, R. P. Pandian, A. Lecas-Nawrocka, A. Vilar, G. Ricart, J. P. Collman, Z. Wang, A. Straumanis, *Polyhedron* **2000**, *19*, 581-586.
[31] Y. Chen, J. V. Ruppel, X. P. Zhang, *J. Am. Chem. Soc.* **2007**, *129*, 12074-12075.
[32] J. L. Maxwell, S. O'Malley, K. C. Brown, T. Kodadek, *Organometallics* **1992**, *11*, 645-652.
[33] S. O'Malley, T. Kodadek, *Organometallics* **1992**, *11*, 2299-2302.
[34] R. L. Halterman, S. T. Jan, *J. Org. Chem.* **1991**, *56*, 5253-5254.

[35] D. M. Carminati, D. Intrieri, A. Caselli, S. L. Gac, B. Boitrel, L. Toma, L. Legnani, E. Gallo, *Chem. Eur. J.* **2016**, *22*, 13599-13612.
[36] J. P. Collman, Z. Wang, A. Straumanis, M. Quelquejeu, E. Rose, *J. Am. Chem. Soc.* **1999**, *121*, 460-461.
[37] E. Rose, Q.-Z. Ren, B. Andrioletti, *Chem. Eur. J.* **2004**, *10*, 224-230.
[38] P. S. Coelho, E. M. Brustad, A. Kannan, F. H. Arnold, *Science* **2013**, *339*, 307-310.
[39] H. Lebel, J.-F. Marcoux, C. Molinaro, A. B. Charette, *Chem. Rev.* **2003**, *103*, 977-1050.
[40] G. Maas, *Chem. Soc. Rev.* **2004**, *33*, 183-190.
[41] *Carbocyclic Three-Membered Ring Compounds: Cyclopropanes, Transformations; Houblen-Weyl Methods of Organic Chemistry, Vol. E17c*, Stuttgart, Germany, **1997**.
[42] C. Ebner, E. M. Carreira, *Chem. Rev.* **2017**, *117*, 11651-11679.
[43] C. G. Hamaker, G. A. Mirafzal, L. K. Woo, *Organometallics* **2001**, *20*, 5171-5176.
[44] P. Tagliatesta, A. Pastorini, *J. Mol. Catal. A: Chem.* **2003**, *198*, 57-61.
[45] J. R. Wolf, C. G. Hamaker, J.-P. Djukic, T. Kodadek, L. K. Woo, *J. Am. Chem. Soc.* **1995**, *117*, 9194-9199.
[46] W. I. Dzik, X. Xu, X. P. Zhang, J. N. H. Reek, B. de Bruin, *J. Am. Chem. Soc.* **2010**, *132*, 10891-10902.
[47] D. Intrieri, A. Caselli, E. Gallo, *Eur. J. Inorg. Chem.* **2011**, *2011*, 5071-5081.
[48] H. J. Callot, C. Piechocki, *Tetrahedron Lett.* **1980**, *21*, 3489-3492.
[49] A. G. M. Barrett, D. C. Braddock, I. Lenoir, H. Tone, *J. Org. Chem.* **2001**, *66*, 8260-8263.
[50] M. Frauenkron, A. Berkessel, *Tetrahedron Lett.* **1997**, *38*, 7175-7176.
[51] J.-C. Wang, Y. Zhang, Z.-J. Xu, V. K.-Y. Lo, C.-M. Che, *ACS Catal.* **2013**, *3*, 1144-1148.
[52] D. A. Smith, D. N. Reynolds, L. K. Woo, *J. Am. Chem. Soc.* **1993**, *115*, 2511-2513.
[53] D. M. Carminati, D. Intrieri, S. Le Gac, T. Roisnel, B. Boitrel, L. Toma, L. Legnani, E. Gallo, *New J. Chem.* **2017**, *41*, 5950-5959.
[54] A. M. Appel, J. E. Bercaw, A. B. Bocarsly, H. Dobbek, D. L. DuBois, M. Dupuis, J. G. Ferry, E. Fujita, R. Hille, P. J. A. Kenis, C. A. Kerfeld, R. H. Morris, C. H. F. Peden, A. R. Portis, S. W. Ragsdale, T. B. Rauchfuss, J. N. H. Reek, L. C. Seefeldt, R. K. Thauer, G. L. Waldrop, *Chem. Rev.* **2013**, *113*, 6621-6658.
[55] S. Perathoner, G. Centi, *ChemSusChem* **2014**, *7*, 1274-1282.
[56] M. Cokoja, C. Bruckmeier, B. Rieger, W. A. Herrmann, F. E. Kühn, *Angew. Chem. Int. Ed.* **2011**, *50*, 8510-8537.
[57] F. Castro-Gómez, G. Salassa, A. W. Kleij, C. Bo, *Chem. Eur. J.* **2013**, *19*, 6289-6298.
[58] D. J. Darensbourg, *Inorg. Chem.* **2010**, *49*, 10765-10780.
[59] K. Yamaguchi, K. Ebitani, T. Yoshida, H. Yoshida, K. Kaneda, *J. Am. Chem. Soc.* **1999**, *121*, 4526-4527.
[60] H. Büttner, L. Longwitz, J. Steinbauer, C. Wulf, T. Werner, *Top. Curr. Chem.* **2017**, *375*, 50.
[61] C. Martín, G. Fiorani, A. W. Kleij, *ACS Catal.* **2015**, *5*, 1353-1370.
[62] J. W. Comerford, I. D. V. Ingram, M. North, X. Wu, *Green Chem.* **2015**, *17*, 1966-1987.
[63] B.-H. Xu, J.-Q. Wang, J. Sun, Y. Huang, J.-P. Zhang, X.-P. Zhang, S.-J. Zhang, *Green Chem.* **2015**, *17*, 108-122.
[64] M. H. Anthofer, M. E. Wilhelm, M. Cokoja, M. Drees, W. A. Herrmann, F. E. Kühn, *ChemCatChem* **2015**, *7*, 94-98.
[65] G. Fiorani, W. Guo, A. W. Kleij, *Green Chem.* **2015**, *17*, 1375-1389.
[66] T. Ema, Y. Miyazaki, S. Koyama, Y. Yano, T. Sakai, *Chem. Comm.* **2012**, *48*, 4489-4491.
[67] M.-Z. Wang, C.-Y. Zhou, M.-K. Wong, C.-M. Che, *Chem. Eur. J.* **2010**, *16*, 5723-5735.
[68] A. Berkessel, E. Ertürk, C. Laporte, *Adv. Synth. Catal.* **2006**, *348*, 223-228.

[69] A. Wang, J. Li, T. Zhang, *Nature Reviews Chemistry* **2018**, *2*, 65-81.
[70] B. F. Abrahams, B. F. Hoskins, R. Robson, *J. Am. Chem. Soc.* **1991**, *113*, 3606-3607.
[71] B. F. Abrahams, B. F. Hoskins, D. M. Michail, R. Robson, *Nature* **1994**, *369*, 727.
[72] S. Kitagawa, R. Kitaura, S.-i. Noro, *Angew. Chem. Int. Ed.* **2004**, *43*, 2334-2375.
[73] V. L. Rechac, F. G. Cirujano, A. Corma, F. X. Llabrés i Xamena, *Eur. J. Inorg. Chem.* **2016**, *2016*, 4512-4516.
[74] D. W. Lewis, D. J. Willock, C. R. A. Catlow, J. M. Thomas, G. J. Hutchings, *Nature* **1996**, *382*, 604-606.
[75] IUPAC, Cambridge, UK **2005**.
[76] B. P. Block, J. Simkin, L. R. Ocone, *J. Am. Chem. Soc.* **1962**, *84*, 1749-1750.
[77] R. Batten Stuart, R. Champness Neil, X.-M. Chen, J. Garcia-Martinez, S. Kitagawa, L. Öhrström, M. O'Keeffe, M. Paik Suh, J. Reedijk, in *Pure and Applied Chemistry, Vol. 85*, **2013**, p. 1715.
[78] K. Susumu, K. Mitsuru, *Bull. Chem. Soc. Jpn.* **1998**, *71*, 1739-1753.
[79] C. Berge, *Proc. Natl. Acad. Sci.* **1957**, *43*, 842-844.
[80] C. Rösler, Dissertation thesis, Ruhr-Universität Bochum (Germany), **2016**.
[81] H. Li, M. Eddaoudi, M. O'Keeffe, O. M. Yaghi, *Nature* **1999**, *402*, 276-279.
[82] J. Lee, O. K. Farha, J. Roberts, K. A. Scheidt, S. T. Nguyen, J. T. Hupp, *Chem. Soc. Rev.* **2009**, *38*, 1450-1459.
[83] A. Corma, H. García, F. X. Llabrés i Xamena, *Chem. Rev.* **2010**, *110*, 4606-4655.
[84] A. Venkatasubramanian, J.-H. Lee, V. Stavila, A. Robinson, M. D. Allendorf, P. J. Hesketh, *Sens Actuators B Chem* **2012**, *168*, 256-262.
[85] L. V. Meyer, F. Schönfeld, K. Müller-Buschbaum, *Chem. Comm.* **2014**, *50*, 8093-8108.
[86] L. E. Kreno, K. Leong, O. K. Farha, M. Allendorf, R. P. Van Duyne, J. T. Hupp, *Chem. Rev.* **2012**, *112*, 1105-1125.
[87] C. G. Silva, A. Corma, H. García, *J. Mater. Chem.* **2010**, *20*, 3141-3156.
[88] H.-C. Zhou, J. R. Long, O. M. Yaghi, *Chem. Rev.* **2012**, *112*, 673-674.
[89] H. Furukawa, K. E. Cordova, M. O'Keeffe, O. M. Yaghi, *Science* **2013**, *341*.
[90] J. Liu, P. K. Thallapally, B. P. McGrail, D. R. Brown, J. Liu, *Chem. Soc. Rev.* **2012**, *41*, 2308-2322.
[91] S. Kaskel, *The Chemistry of Metal-Organic Frameworks*, Wiley-VCH, Weinheim.
[92] S. Horike, S. Shimomura, S. Kitagawa, *Nat. Chem.* **2009**, *1*, 695.
[93] S. S.-Y. Chui, S. M.-F. Lo, J. P. H. Charmant, A. G. Orpen, I. D. Williams, *Science* **1999**, *283*, 1148-1150.
[94] G. Férey, M. Latroche, C. Serre, F. Millange, T. Loiseau, A. Percheron-Guégan, *Chem. Comm.* **2003**, 2976-2977.
[95] N. N. Greenwood, A. Earnshaw, *Chemie der Elemente*, VCH, Weinheim, **1988**.
[96] J. H. Cavka, S. Jakobsen, U. Olsbye, N. Guillou, C. Lamberti, S. Bordiga, K. P. Lillerud, *J. Am. Chem. Soc.* **2008**, *130*, 13850-13851.
[97] M. Kim, S. M. Cohen, *CrystEngComm* **2012**, *14*, 4096-4104.
[98] Y. Bai, Y. Dou, L.-H. Xie, W. Rutledge, J.-R. Li, H.-C. Zhou, *Chem. Soc. Rev.* **2016**, *45*, 2327-2367.
[99] H. Wang, X. Dong, J. Lin, S. J. Teat, S. Jensen, J. Cure, E. V. Alexandrov, Q. Xia, K. Tan, Q. Wang, D. H. Olson, D. M. Proserpio, Y. J. Chabal, T. Thonhauser, J. Sun, Y. Han, J. Li, *Nat. Commun.* **2018**, *9*, 1745.
[100] R. G. Pearson, *J. Am. Chem. Soc.* **1963**, *85*, 3533-3539.
[101] Z. Guo, B. Chen, *Dalton Trans.* **2015**, *44*, 14574-14583.
[102] S. S.-Y. Chui, S. M.-F. Lo, J. P. H. Charmant, A. G. Orpen, I. D. Williams, *Science* **1999**, *283*, 1148-1150.
[103] H. Li, M. Eddaoudi, M. O'Keeffe, O. M. Yaghi, *Nature* **1999**, *402*, 276.

[104] S. Surblé, C. Serre, C. Mellot-Draznieks, F. Millange, G. Férey, *Chem. Comm.* **2006**, 284-286.
[105] L. Valenzano, B. Civalleri, S. Chavan, S. Bordiga, M. H. Nilsen, S. Jakobsen, K. P. Lillerud, C. Lamberti, *Chem. Mater.* **2011**, *23*, 1700-1718.
[106] I. Luz, C. Rösler, K. Epp, F. X. Llabrés i Xamena, R. A. Fischer, *Eur. J. Inorg. Chem.* **2015**, 3904-3912.
[107] J. B. DeCoste, G. W. Peterson, H. Jasuja, T. G. Glover, Y.-g. Huang, K. S. Walton, *J. Mater. Chem. A* **2013**, *1*, 5642-5650.
[108] G. C. Shearer, S. Forselv, S. Chavan, S. Bordiga, K. Mathisen, M. Bjørgen, S. Svelle, K. P. Lillerud, *Top. Catal.* **2013**, *56*, 770-782.
[109] J. E. Mondloch, M. J. Katz, N. Planas, D. Semrouni, L. Gagliardi, J. T. Hupp, O. K. Farha, *Chem. Comm.* **2014**, *50*, 8944-8946.
[110] M. Eddaoudi, J. Kim, N. Rosi, D. Vodak, J. Wachter, M. O'Keeffe, O. M. Yaghi, *Science* **2002**, *295*, 469-472.
[111] M. Li, D. Li, M. O'Keeffe, O. M. Yaghi, *Chem. Rev.* **2014**, *114*, 1343-1370.
[112] J. Jiang, F. Gándara, Y.-B. Zhang, K. Na, O. M. Yaghi, W. G. Klemperer, *J. Am. Chem. Soc.* **2014**, *136*, 12844-12847.
[113] E. Plessers, G. Fu, C. Tan, D. De Vos, M. Roeffaers, *Catalysts* **2016**, *6*, 104.
[114] D. Feng, K. Wang, J. Su, T.-F. Liu, J. Park, Z. Wei, M. Bosch, A. Yakovenko, X. Zou, H.-C. Zhou, *Angew. Chem. Int. Ed.* **2015**, *54*, 149-154.
[115] S. Nakagaki, G. K. Ferreira, G. M. Ucoski, K. A. Dias de Freitas Castro, *Molecules* **2013**, *18*, 7279-7308.
[116] S. Huh, S.-J. Kim, Y. Kim, *CrystEngComm* **2016**, *18*, 345-368.
[117] M. E. Kosal, J.-H. Chou, S. R. Wilson, K. S. Suslick, *Nat. Mater.* **2002**, *1*, 118.
[118] K. S. Suslick, P. Bhyrappa, J. H. Chou, M. E. Kosal, S. Nakagaki, D. W. Smithenry, S. R. Wilson, *Acc. Chem. Res.* **2005**, *38*, 283-291.
[119] C. V. K. Sharma, G. A. Broker, J. G. Huddleston, J. W. Baldwin, R. M. Metzger, R. D. Rogers, *J. Am. Chem. Soc.* **1999**, *121*, 1137-1144.
[120] M. Shmilovits, M. Vinodu, I. Goldberg, *Cryst. Growth Des.* **2004**, *4*, 633-638.
[121] D. Hagrman, P. J. Hagrman, J. Zubieta, *Angew. Chem. Int. Ed.* **1999**, *38*, 3165-3168.
[122] S. George, S. Lipstman, I. Goldberg, *Cryst. Growth Des.* **2006**, *6*, 2651-2654.
[123] T. Ohmura, A. Usuki, K. Fukumori, T. Ohta, M. Ito, K. Tatsumi, *Inorg. Chem.* **2006**, *45*, 7988-7990.
[124] X.-S. Wang, M. Chrzanowski, W.-Y. Gao, L. Wojtas, Y.-S. Chen, M. J. Zaworotko, S. Ma, *Catal. Sci.* **2012**, *3*, 2823-2827.
[125] E.-Y. Choi, P. M. Barron, R. W. Novotney, C. Hu, Y.-U. K. Kwon, W. Choe, *CrystEngComm* **2008**, *10*, 824-826.
[126] B. J. Burnett, P. M. Barron, W. Choe, *CrystEngComm* **2012**, *14*, 3839-3846.
[127] E. Kühn, V. Bulach, M. W. Hosseini, *Chem. Comm.* **2008**, 5104-5106.
[128] N. U. Day, C. C. Wamser, M. G. Walter, *Polym Int* **2015**, *64*, 833-857.
[129] O. K. Farha, A. M. Shultz, A. A. Sarjeant, S. T. Nguyen, J. T. Hupp, *J. Am. Chem. Soc.* **2011**, *133*, 5652-5655.
[130] L. Meng, Q. Cheng, C. Kim, W.-Y. Gao, L. Wojtas, Y.-S. Chen, M. J. Zaworotko, X. P. Zhang, S. Ma, *Angew. Chem. Int. Ed.* **2012**, *51*, 10082-10085.
[131] X.-L. Yang, M.-H. Xie, C. Zou, Y. He, B. Chen, M. O'Keeffe, C.-D. Wu, *J. Am. Chem. Soc.* **2012**, *134*, 10638-10645.
[132] W.-Y. Gao, M. Chrzanowski, S. Ma, *Chem. Soc. Rev.* **2014**, *43*, 5841-5866.
[133] A. M. Shultz, O. K. Farha, J. T. Hupp, S. T. Nguyen, *J. Am. Chem. Soc.* **2009**, *131*, 4204-4205.
[134] W.-Y. Gao, L. Wojtas, S. Ma, *Chem. Comm.* **2014**, *50*, 5316-5318.
[135] J. Li, Y. Ren, C. Qi, H. Jiang, *Chem. Comm.* **2017**, *53*, 8223-8226.

[136] W. Jiang, J. Yang, Y.-Y. Liu, S.-Y. Song, J.-F. Ma, *Inorg. Chem.* **2017**, *56*, 3036-3043.
[137] W. Morris, B. Volosskiy, S. Demir, F. Gándara, P. L. McGrier, H. Furukawa, D. Cascio, J. F. Stoddart, O. M. Yaghi, *Inorg. Chem.* **2012**, *51*, 6443-6445.
[138] D. Feng, Z.-Y. Gu, J.-R. Li, H.-L. Jiang, Z. Wei, H.-C. Zhou, *Angew. Chem. Int. Ed.* **2012**, *51*, 10307-10310.
[139] D. Feng, W.-C. Chung, Z. Wei, Z.-Y. Gu, H.-L. Jiang, Y.-P. Chen, D. J. Darensbourg, H.-C. Zhou, *J. Am. Chem. Soc.* **2013**, *135*, 17105-17110.
[140] K. Epp, A. L. Semrau, M. Cokoja, R. A. Fischer, *ChemCatChem* **2018**, *10*, 3506-3512.
[141] Y. Chen, T. Hoang, S. Ma, *Inorg. Chem.* **2012**, *51*, 12600-12602.
[142] J. W. Brown, Q. T. Nguyen, T. Otto, N. N. Jarenwattananon, S. Glöggler, L.-S. Bouchard, *Catal. Commun.* **2015**, *59*, 50-54.
[143] J. W. Maina, C. Pozo-Gonzalo, L. Kong, J. Schutz, M. Hill, L. F. Dumee, *Mater Horiz.* **2017**, *4*, 345-361.
[144] M. H. Beyzavi, N. A. Vermeulen, K. Zhang, M. So, C.-W. Kung, J. T. Hupp, O. K. Farha, *ChemPlusChem* **2016**, *81*, 708-713.
[145] M. H. Beyzavi, N. A. Vermeulen, A. J. Howarth, S. Tussupbayev, A. B. League, N. M. Schweitzer, J. R. Gallagher, A. E. Platero-Prats, N. Hafezi, A. A. Sarjeant, J. T. Miller, K. W. Chapman, J. F. Stoddart, C. J. Cramer, J. T. Hupp, O. K. Farha, *J. Am. Chem. Soc.* **2015**, *137*, 13624-13631.
[146] J. A. Smegal, C. L. Hill, *J. Am. Chem. Soc.* **1983**, *105*, 3515-3521.
[147] in *PATAI'S Chemistry of Functional Groups*.
[148] Y. Bai, Y. Dou, L.-H. Xie, W. Rutledge, J.-R. Li, H.-C. Zhou, *Chem. Soc. Rev.* **2016**, *45*, 2327-2367.
[149] D. Farrusseng, S. Aguado, C. Pinel, *Angew. Chem. Int. Ed.* **2009**, *48*, 7502-7513.
[150] F. G. Cirujano, A. Corma, F. X. Llabrés i Xamena, *Chem. Eng. Sci.* **2015**, *124*, 52-60.
[151] H. Wu, Y. S. Chua, V. Krungleviciute, M. Tyagi, P. Chen, T. Yildirim, W. Zhou, *J. Am. Chem. Soc.* **2013**, *135*, 10525-10532.
[152] Z. Hu, D. Zhao, *CrystEngComm* **2017**, *19*, 4066-4081.
[153] G. C. Shearer, S. Chavan, S. Bordiga, S. Svelle, U. Olsbye, K. P. Lillerud, *Chem. Mater.* **2016**, *28*, 3749-3761.
[154] F. Vermoortele, B. Bueken, G. Le Bars, B. Van de Voorde, M. Vandichel, K. Houthoofd, A. Vimont, M. Daturi, M. Waroquier, V. Van Speybroeck, C. Kirschhock, D. E. De Vos, *J. Am. Chem. Soc.* **2013**, *135*, 11465-11468.
[155] S. Dissegna, R. Hardian, K. Epp, G. Kieslich, M.-V. Coulet, P. Llewellyn, R. A. Fischer, *CrystEngComm* **2017**, *19*, 4137-4141.
[156] S. Dissegna, K. Epp, W. R. Heinz, G. Kieslich, R. A. Fischer, *Adv Mater* **2018**, *30*, e1704501.
[157] H. Furukawa, F. Gándara, Y.-B. Zhang, J. Jiang, W. L. Queen, M. R. Hudson, O. M. Yaghi, *J. Am. Chem. Soc.* **2014**, *136*, 4369-4381.
[158] J. E. Mondloch, W. Bury, D. Fairen-Jimenez, S. Kwon, E. J. DeMarco, M. H. Weston, A. A. Sarjeant, S. T. Nguyen, P. C. Stair, R. Q. Snurr, O. K. Farha, J. T. Hupp, *J. Am. Chem. Soc.* **2013**, *135*, 10294-10297.
[159] K. M. Choi, H. M. Jeong, J. H. Park, Y.-B. Zhang, J. K. Kang, O. M. Yaghi, *ACS Nano* **2014**, *8*, 7451-7457.
[160] Y. Liu, R. C. Klet, J. T. Hupp, O. Farha, *Chem. Comm.* **2016**, *52*, 7806-7809.
[161] J. Zheng, M. Wu, F. Jiang, W. Su, M. Hong, *Catal. Sci.* **2015**, *6*, 3466-3470.
[162] H.-Q. Xu, J. Hu, D. Wang, Z. Li, Q. Zhang, Y. Luo, S.-H. Yu, H.-L. Jiang, *J. Am. Chem. Soc.* **2015**, *137*, 13440-13443.
[163] F. X. Llabres i Xamena, J. Gascon, in *Metal Organic Frameworks as Heterogeneous Catalysts*, The Royal Society of Chemistry, **2013**, pp. 1-5.

[164] W. Xu, Q. Ding, P. Sang, J. Xu, Z. Shi, L. Zhao, Y. Chi, W. Guo, *J. Phys. Chem. C* **2015**, *119*, 21943-21951.
[165] D. Feng, Z.-Y. Gu, J.-R. Li, H.-L. Jiang, Z. Wei, H.-C. Zhou, *Angewandte Chemie* **2012**, *124*, 10453-10456.
[166] M. Hesse, H. Meier, B. Zeeh, *Spektroskopische Methoden in der organischen Chemie*, Georg Thieme Verlag KG, Stuttgart, **2005**.
[167] G. Kickelbick, U. Schubert, *Chem. Ber.* **1997**, *130*, 473-478.
[168] Y. Gao, F. R. Kogler, H. Peterlik, U. Schubert, *J. Mater. Chem.* **2006**, *16*, 3268-3276.
[169] M. Puchberger, F. R. Kogler, M. Jupa, S. Gross, H. Fric, G. Kickelbick, U. Schubert, *Eur. J. Inorg. Chem.* **2006**, *2006*, 3283-3293.
[170] R. Noyori, *Angew. Chem. Int. Ed.* **2002**, *41*, 2008-2022.
[171] S. F. Kirsch, *Angew. Chem. Int. Ed.* **2009**, *48*, 2450-2451.
[172] A. Miyashita, A. Yasuda, H. Takaya, K. Toriumi, T. Ito, T. Souchi, R. Noyori, *J. Am. Chem. Soc.* **1980**, *102*, 7932-7934.
[173] T. Katsuki, K. B. Sharpless, *J. Am. Chem. Soc.* **1980**, *102*, 5974-5976.
[174] K. Manna, T. Zhang, W. Lin, *J. Am. Chem. Soc.* **2014**, *136*, 6566-6569.
[175] J. S. Seo, D. Whang, H. Lee, S. I. Jun, J. Oh, Y. J. Jeon, K. Kim, *Nature* **2000**, *404*, 982.
[176] A. Gheorghe, M. A. Tepaske, S. Tanase, *Inorg. Chem. Front.* **2018**, *5*, 1512-1523.
[177] M. Yoon, R. Srirambalaji, K. Kim, *Chem. Rev.* **2012**, *112*, 1196-1231.
[178] S. H. A. M. Leenders, R. Gramage-Doria, B. de Bruin, J. N. H. Reek, *Chem. Soc. Rev.* **2015**, *44*, 433-448.
[179] A. M. Castilla, W. J. Ramsay, J. R. Nitschke, *Acc. Chem. Res.* **2014**, *47*, 2063-2073.
[180] J. C. Jansen, E. J. Creyghton, S. L. Njo, H. van Koningsveld, H. van Bekkum, *Catal. Today* **1997**, *38*, 205-212.
[181] A. Corma, M. E. Domine, L. Nemeth, S. Valencia, *J. Am. Chem. Soc.* **2002**, *124*, 3194-3195.
[182] C. Li, H. Zhang, D. Jiang, Q. Yang, *Chem. Comm.* **2007**, 547-558.
[183] S. H. Kim, C. K. Shin, J. H. Seok, C. Y. Lee, G. J. Kim, in *Stud. Surf. Sci. Catal., Vol. 165*, **2007**, pp. 745-748.
[184] A. Corma, M. Iglesias, F. X. L. i. Xamena, F. Sánchez, *Chem. Eur. J.* **2010**, *16*, 9789-9795.
[185] F. G. Cirujano, F. X. Llabrés i Xamena, A. Corma, *Dalton Trans.* **2012**, *41*, 4249-4254.
[186] H. H. Mautschke, F. Drache, I. Senkovska, S. Kaskel, F. X. Llabrés i Xamena, *Catal. Sci. Technol.* **2018**, *8*, 3610-3616.
[187] R. E. Morris, X. Bu, *Nat. Chem.* **2010**, *2*, 353.
[188] T. Sawano, H. Yamamoto, *J. Org. Chem.* **2018**, *83*, 4889-4904.
[189] L. Huang, Y. Chen, G.-Y. Gao, X. P. Zhang, *J. Org. Chem.* **2003**, *68*, 8179-8184.
[190] S. Fantauzzi, E. Gallo, E. Rose, N. Raoul, A. Caselli, S. Issa, F. Ragaini, S. Cenini, *Organometallics* **2008**, *27*, 6143-6151.
[191] S. Zhu, J. V. Ruppel, H. Lu, L. Wojtas, X. P. Zhang, *J. Am. Chem. Soc.* **2008**, *130*, 5042-5043.
[192] H. J. Callot, F. Metz, C. Piechocki, *Tetrahedron* **1982**, *38*, 2365-2369.
[193] M. P. Doyle, W. R. Winchester, J. A. A. Hoorn, V. Lynch, S. H. Simonsen, R. Ghosh, *J. Am. Chem. Soc.* **1993**, *115*, 9968-9978.
[194] J. Liu, Y.-Z. Fan, X. Li, Z. Wei, Y.-W. Xu, L. Zhang, C.-Y. Su, *Appl. Catal., B* **2018**, *231*, 173-181.
[195] X. Jing, C. He, L. Zhao, C. Duan, *Acc. Chem. Res.* **2019**, *52*, 100-109.
[196] J. D. Bass, S. L. Anderson, A. Katz, *Angew. Chem. Int. Ed.* **2003**, *42*, 5219-5222.
[197] J. L. Bolliger, in *Effects of Nanoconfinement on Catalysis* (Ed.: R. Poli), Springer International Publishing, Cham, **2017**, pp. 17-48.

[198] L. R. Collins, M. van Gastel, F. Neese, A. Fürstner, *J. Am. Chem. Soc.* **2018**, *140*, 13042-13055.
[199] T. Zhang, Y. Shi, S. Zhang, C. Jia, C. He, C. Duan, *New J. Chem.* **2018**, *42*, 18448-18457.
[200] R. J. H. Gregory, *Chem. Rev.* **1999**, *99*, 3649-3682.
[201] M. North, D. L. Usanov, C. Young, *Chem. Rev.* **2008**, *108*, 5146-5226.
[202] D. A. Evans, L. K. Truesdale, G. L. Carroll, *J. Chem. Soc., Chem. Commun.* **1973**, 55-56.
[203] T. S. Omura, R., *J. Biol. Chem.* **1962**, *237*, 1375‑1376.
[204] M. Zhao, S. Ou, C.-D. Wu, *Acc. Chem. Res.* **2014**, *47*, 1199-1207.
[205] S. Nakagaki, G. Ferreira, G. Ucoski, K. Dias de Freitas Castro, *Molecules* **2013**, *18*, 7279.
[206] H.-F. Yao, Y. Yang, H. Liu, F.-G. Xi, E.-Q. Gao, *J. Mol. Catal. A: Chem.* **2014**, *394*, 57-65.
[207] J. R. Monnier, *Appl. Catal., A* **2001**, *221*, 73-91.
[208] D. Feng, Z. Y. Gu, J. R. Li, H. L. Jiang, Z. Wei, H. C. Zhou, *Angew. Chem. Int. Ed. Engl.* **2012**, *51*, 10307-10310.
[209] J. S. Manka, D. S. Lawrence, *Tetrahedron Lett.* **1989**, *30*, 6989-6992.

9 Appendix

9.1 List of publications

Peer-reviewed journal publications on which this thesis is based:

1. **K. Epp**, A. L. Semrau, M. Cokoja, R. A. Fischer, *ChemCatChem* **2018**, 10, 3506 – 3512. *'Dual Site Lewis-Acid Metal-Organic Framework Catalysts for CO_2 Fixation: Counteracting Effects of Node Connectivity, Defects and Linker Metalation'*. DOI: 10.1002/cctc.201800336

Manuscripts under preparation:

K. Epp, B. Bueken, B. J. Hofmann, M. Cokoja, D. De Vos, R. A. Fischer. *'Network topology and cavity confinement-controlled diastereoselectivity in cyclopropanation reactions catalyzed by porphyrin-based MOFs'.*

Review article:

S. Dissegna, **K. Epp**, W. R. Heinz, G. Kieslich, R. A. Fischer, *Adv. Mater.* **2018**, *30*, e1704501. *'Defective Metal-Organic Frameworks'.* DOI: 10.1002/adma.201704501

Contributions to peer-reviewed journal publications outside the scope of this thesis:

1. I. Luz, C. Rösler, **K. Epp**, F. X. Llabrés i Xamena, R. A. Fischer, *Eur. J. Inorg. Chem.* **2015**, 3904–3912. *'Pd@UiO-66-Type MOFs Prepared by Chemical Vapor Infiltration as Shape-Selective Hydrogenation Catalysts'.* DOI: 10.1002/ejic.201500299

2. W. Zhang, O. Kozachuk, R. Medishetty, A. Schneemann, R. Wagner, K. Khaletskaya, **K. Epp**, R. A. Fischer, *Eur. J. Inorg. Chem.* **2015**, 3913–3920. *'Controlled SBU Approaches to Isoreticular Metal-Organic Framework Ruthenium-Analogues of HKUST-1'.* DOI: 10.1002/ejic.201500478

3. W. Zhang, M. Kauer, O. Halbherr, **K. Epp**, P. Guo, M. I. Gonzalez, D. J. Xiao, C. Wiktor, F. X. LIabrés i Xamena, C. Wöll, Y. Wang, M. Muhler, R. A. Fischer, *Chem. Eur. J.* **2016**, 22, 14297–14307. *'Ruthenium Metal–Organic Frameworks with Different Defect Types: Influence on Porosity, Sorption, and Catalytic Properties'.* DOI: 10.1002/chem.201602641

4. W. Zhang, K. Freitag, S. Wannapaiboon, C. Schneider, **K. Epp**, G. Kieslich, R. A. Fischer, *Inorg. Chem.* **2016**, 55, 24, 12492–12495. *'Elaboration of a Highly Porous $Ru^{II,II}$ Analogue of HKUST-1*'. DOI: 10.1021/acs.inorgchem.6b02038

5. W. Zhang, M. Kauer, P. Guo, S. Kunze, S. Cwik, M. Muhler, Y. Wang, **K. Epp**, G. Kieslich, R. A. Fischer, *Eur. J. Inorg. Chem.* **2017**, 925–931. *'Impact of Synthesis Parameters on the Formation of Defects in HKUST-1'.* DOI: 10.1002/ejic.201601239

6. S. Dissegna, R. Hardian, **K. Epp**, G. K., M.-V.Coulet, P. Llewellyn, R. A. Fischer, *CrystEngComm **2017**, 19*, 4137–4141. *'Using Water Adsorption Measurements to access the Chemistry of defects in the Metal–Organic Framework UiO-66'.* DOI: 10.1039/c7ce00224f

7. S. Wannapaiboon, A. Schneemann, I. Hante, M. Tu, **K. Epp**, A. L. Semrau, C. Sternemann, M. Paulus, S. J. Baxter, G. Kieslich, R. A. Fischer, *Nat. Comm.* **2019**, 10, 346. *'Control of Structural Flexibility of Layered-Pillared Metal-Organic Frameworks Anchored at Surfaces'.* DOI: 10.1038/s41467-018-08285

9.2 Oral presentations

K. Epp, Werner R. Heinz, B. Bueken, M. Cokoja, D. De Vos, R. A. Fischer
5th International Conference on Metal-Organic Frameworks "MOF2018", Auckland, USA, December 2018. (Poster)

K. Epp, F. X. Llabrés i Xamena, R. A. Fischer
4th International Conference on Metal-Organic Frameworks "MOF2016", Long Beach, USA, September 2016. (Poster)

K. Epp, F. X. Llabrés i Xamena, O. Kozachuk, R. A. Fischer
49th annual meeting of the German Catalytic Society (GeCats), Weimar, Germany, March 2016. (Poster)

K. Epp, S. Dissegna, F. X. Llabres i Xamena, M. Cokoja, R. A. Fischer
Catalysis Research Center (CRC) joint meeting, Raitenhaslach, Germany, November 2016. (Poster)